

**AN ATLAS OF THE ARCTIC AND THE ANTARCTIC
SEA ICE TRENDS (1999-2009) - DERIVED FROM
QUIKSCAT SCATTEROMETER DATA**



Sandip R. Oza, R. K. K. Singh, N. K. Vyas and Abhijit Sarkar

**Oceanic Sciences Division
Atmospheric and Oceanic Sciences Group (AOSG/EPSA)
Space Applications Centre (ISRO)
Ahmedabad 380 015**

March 2012

DOCUMENT CONTROL AND DATA SHEET

- 1. Report No.** : SAC/EPSA/AOSG/OSD/SR/04/2012
- 2. Publication Date** : March 2012
- 3. Title** : An atlas of the Arctic and the Antarctic sea ice trends (1999-2009) - derived from QUIKSCAT scatterometer data
- 4. Type of Report** : Scientific Report
- 5. Pages and Figures** : 88 (43)
- 6. No. of References** : 71
- 7. Author(s)** : Sandip R. Oza, R. K. K. Singh, N. K. Vyas and Abhijit Sarkar
- 8. Originating Unit** : OSD/AOSG/EPSA, Space Applications Centre, (ISRO), Ahmedabad-380 015
- 9. Abstract** : This report summarizes the recent changes that have taken place in the sea ice extent over the hemispheric level as well as at 1x1 degree grid cell level using QuikSCAT Ku-band scatterometer data (1999-2009).
- 10. Key Words** : Polar region, Arctic, Antarctic, Sea-ice extent, growth cycle, remote sensing, scatterometer
- 11. Security Classification :** Unrestricted
- 12. Distribution Statement :** General

EXECUTIVE SUMMARY

Sea ice plays an important role in the Earth's climate system. The changes observed in Sea Ice Extent (SIE) over the polar regions in the recent past are alarming. The present Atlas focuses on the monthly trends observed for the sea ice cover at $1^\circ \times 1^\circ$ grid using QuikSCAT Ku-band scatterometer data for a decade (August 1999 - July 2009).

The interesting outcomes of the study for the Arctic and Antarctic as a whole and for various smaller geographic regions have been highlighted in the Atlas.

Noteworthy observations of the study are

- (i) recent decline in summer sea ice extent in the Arctic is of the order of 0.16 M Sq km per year with reference to the average summer sea ice extent between 1999 to 2008,
- (ii) a significant negative trend up to 15% per year in the Chukchi and East Siberian seas in the summer minimum extent of sea ice cover. However, a negative trend in the winter-maximum is observed in Barents Sea, which is a distinct pattern,
- (iii) A drastic increase of 12-months running average SIE from 2007 to 2008 observed in both the hemispheres

The results presented in the Atlas are also important considering the seamless continuity of Ku-band scatterometer data through the India's Oceansat-2 scatterometer (OSCAT) launched in November 2009. The two sensors are quite similar, with only minor differences in frequency of operation and incidence angles.

ACKNOWLEDGEMENTS

Authors place their sincere gratitude to Dr. R. R. Navalgund, Director, Space Applications Centre (SAC, ISRO) for his constant encouragement and direction that accelerated the polar science activities in SAC.

We are deeply grateful to Shri Kiran Kumar, Associate Director, SAC for his continued interest and support in the retrieval of sea ice from scatterometer data. Authors sincerely thank Dr. J. S. Parihar, Deputy Director, EPSA, SAC for his valuable suggestions and guidance provided for the polar ice studies using long term scatterometer data set and bringing out a book of comprehensive atlas.

Authors gratefully acknowledge Dr. P. S. Desai, Former Chief Scientist, SAC, Dr. Anjana Desai, Former Head, Department of Geography, Gujarat University and Dr. Sushma Panigrahy, GD, ABHG/EPSA, who reviewed the atlas and provided their suggestions to significantly improve the scientific and graphical contents of the atlas. Authors acknowledge their special indebtedness to Dr. Pradip K. Pal, GD, AOSG/EPSA for his deep and sustaining support, without which this work could not have been completed in time.

The guidance provided by Dr. B. S. Gohil, Head, GRD, AOSG and Dr. Raj Kumar, Head, OSD, AOSG during the entire course of processing work is deeply appreciated. The support provided by Shri I. C. Matieda, Head, DWD, EPSA and his team is thankfully acknowledged.

First two authors would like to express their grateful thanks to Dr. Rasik Ravindran, Director, NCAOR (MoES), Goa, for providing an incredible breadth of opportunity for the participation in the Indian Scientific Expedition to Antarctica (InSEA) that helped us in analyzing the sea ice trends. Precious InSEA photographs provided by Shri Dipak A. Maroo are also thankfully acknowledged.

We acknowledge that QuikSCAT sigma-0 data is obtained from the NASA sponsored Scatterometer Climate Record Pathfinder at Brigham Young University through the courtesy of David G. Long.

CONTENTS

Chapter 1: Introduction	1
1.1 Importance of sea ice	1
1.2 Recent changes observed in sea ice extents	3
1.3 Remote sensing for the assessment of sea ice properties	4
1.4 History of polar ice activities at SAC(ISRO)	5
Chapter 2: Satellite data and sea ice identification technique	12
2.1 Scatterometer basics	12
2.2 Scatterometer data	15
2.3 Physics behind the detection of Ocean and Ice	16
2.3.1 Retrieval of ocean wind	16
2.3.2 Sea Ice detection	18
2.3.3 Ambiguity in Ice-Ocean discrimination	21
2.4 Derivation of Sea ice cover	22
2.5 Generation of sea ice fraction grid at 1 degree cell size	24
2.6 Generation of grid-cell-wise images of regression statistic	25
2.7 Computation of sea ice area in the Arctic and the Antarctic	26
Chapter 3: Arctic Sea ice trends	30
3.1 Physiography of the Arctic	30
3.2 Comparison with NSIDC sea ice extent	31
3.3 Analysis of inter-annual variations	34
3.4 Grid-wise sea ice trends of maximum and minimum sea ice cover	36
Chapter 4: Antarctic sea ice trends	50
4.1 Physiography of the Antarctic Polar region	50
4.2 Analysis of inter-annual variations	50
4.3 Grid-wise sea ice trends of maximum and minimum sea ice cover:	53
Chapter 5: Inter-comparison of hemispheric sea-ice patterns	67
5.1 Inter-annual variations in sea ice extent	67
5.2 Sea ice growth cycle	68
5.3 Correlation between the Arctic and the Antarctic Sea Ice Extents	68
5.4 Trends of annual average sea ice extents	70
Chapter 6: Summary of findings and future scope	72
6.1 Important findings	72
6.2 Future scope	75
REFERENCES	78
Annexure-1 Acronyms	84
Annexure-1 Sea ice Glossary	85

LIST OF FIGURES

1. Fig. 1.1: Different stages of the formation of sea ice. (a) Grease ice (b) Grease ice aligned in the direction of katabatic winds (c) Early stage of the formation of Pancake ice (d) Pancake ice (e) Interlocking of Nilas (f) Observing the Slush formed over the fast ice around Antarctic continentPage-3
2. Figure 1.2 Seasonal variations in ice extent for different sectors as well as for the entire Antarctic Southern Polar Ocean regions derived for the period June 1999 to May 2001 (Vyas et al., 2003)Page-7
3. Figure 1.3 : Antarctic sea ice cover derived from Oceansat-1 MSMR 18 GHz brightness temperature data; (a) summer sea ice cover and (b) winter sea ice cover.....Page-8
4. Figure 1.4 : Arctic sea ice cover derived from Oceansat-1 MSMR 18 GHz brightness temperature data; (a) summer sea ice cover and (b) winter sea ice cover.....Page-8
5. Figure 2.1: Ku-band backscatter image of January 15, 2000 (a) Horizontally polarized component (b) Vertically polarized component.....Page-17
6. Figure 2.2: Monthly climatological maximum sea ice cover shown by green color with dark green boundary (Image bounds: Longitudes: 180° W to +180° E; Latitudes: 90° N to 90° S; each grid cell: 15 ° x 15 °)Page-28
7. Figure 2.3: Sea ice and ocean identification using the near-real time scatterometer data. Identified ocean area (with cyan color) shows the changes occurred in the parts of Arctic/Antarctic from the monthly climatological maximum sea-ice cover (1978-2002). Significant changes are observed in (1) East Greenland Sea, (2) Barents Sea, (3) Chukchi Sea, (4) East Siberian Sea, (5) Okhotsk Sea, (6) Bellinghausen and Amundsen Seas and (7) Ross Sea.....Page-29
8. Figure 2.4: Area under 1x1 degree grid-cell at different latitudes.....Page-29
9. Figure. 3.1 Arctic Polar region and the surroundings.....Page-32
10. Figure 3.2: Comparison of QuikSCAT derived summer minimum SIE for the Arctic (at SAC/ISRO) using STD method with the PMR based NSIDC SIE data. The main findings to be noted are (i) the similar trend/pattern of the two curves, and (ii) the larger SIE consistently shown by the QuikSCAT dataPage-33
11. Figure 3.3 : Monthly SIE statistics (2000-2008) of the Arctic (a) Monthly SIE for some of the study years (b) Average monthly SIE with upper and lower limit

of one SD. (The following may be noted: (i) the larger variability of the summer minimum compared to winter maximum, and (ii) minimum variability in June and November)	Page-35
12. Figure 3.4: Trend observed in summer minimum and winter maximum SIE in the Arctic. Locations identified with numbers are (1) Chukchi, (2) Okhotsk, (3) East Siberian, (4) Laptev, (5) Barents, (6) East Greenland.....	Page-36
13. A-1: Month-wise Sea ice trends in the Arctic – October.....	Page-38
14. A-2: Month-wise Sea ice trends in the Arctic – November	Page-39
15. A-3: Month-wise Sea ice trends in the Arctic – December.....	Page-40
16. A-4: Month-wise Sea ice trends in the Arctic – January.....	Page-41
17. A-5: Month-wise Sea ice trends in the Arctic – February.....	Page-42
18. A-6: Month-wise Sea ice trends in the Arctic – March.....	Page-43
19. A-7: Month-wise Sea ice trends in the Arctic – April.....	Page-44
20. A-8: Month-wise Sea ice trends in the Arctic – May	Page-45
21. A-9: Month-wise Sea ice trends in the Arctic – June	Page-46
22. A-10: Month-wise Sea ice trends in the Arctic – July.....	Page-47
23. A-11: Month-wise Sea ice trends in the Arctic – August	Page-48
24. A-12: Month-wise Sea ice trends in the Arctic – September.....	Page-49
25. Figure. 4.1 Antarctic polar region and the surroundings.....	Page-51
26. Figure 4.2: Monthly SIE statistics (2000-2008) of the Antarctic (a) Monthly SIE for some of the extreme melting years and one normal study year (b) Average monthly SIE for the entire study period with upper and lower limit of one SD. The following may be noted: (i) the larger variability of the summer minimum compared to winter maximum, (ii) minimum variability in June and November), (iii) summer variability (1.5 M km^2) less than Arctic (2.0 M km^2), and (iv) minimum variability in July and November.....	Page-52
27. Figure 4.3: Trend observed in summer minimum and winter maximum SIE in the Antarctic. Locations identified with numbers are (7) Weddell, (8) Indian Ocean sector, (9) Ross, (10) Amundsen, (11) Bellingshausen.....	Page-53
28. B-1: Month-wise Sea ice trends in the Antarctic – March.....	Page-55
29. B-2: Month-wise Sea ice trends in the Antarctic – April.....	Page-56
30. B-3: Month-wise Sea ice trends in the Antarctic – May.....	Page-57
31. B-4: Month-wise Sea ice trends in the Antarctic – June.....	Page-58
32. B-5: Month-wise Sea ice trends in the Antarctic – July	Page-59
33. B-6: Month-wise Sea ice trends in the Antarctic – August.....	Page-60

34. B-7: Month-wise Sea ice trends in the Antarctic – September	Page-61
35. B-8: Month-wise Sea ice trends in the Antarctic – October	Page-62
36. B-9: Month-wise Sea ice trends in the Antarctic – November	Page-63
37. B-10: Month-wise Sea ice trends in the Antarctic – December	Page-64
38. B-11: Month-wise Sea ice trends in the Antarctic – January.....	Page-65
39. B-12: Month-wise Sea ice trends in the Antarctic – February	Page-66
40. Figure 5.1: Month-wise Coefficient of variation observed in SIE during the period from 1999-2008. Low variability in winter and high variability in the summer months of corresponding summer months may be noted.....	Page-69
41. Figure 5.2: Sea Ice Growth profiles (Note that the build up of ice is fast and decay is slow in the Arctic. This is just the opposite in the Antarctic).....	Page-69
42. Figure 5.3: Anti-correlation between Arctic and Antarctic SIE. Note that the relationship is non-linear.....	Page-70
43. Figure 5.4: 12-month running average sea ice extent. Note that the slope of the curve for the Antarctic is an order of magnitude smaller compared to the Arctic, although the signs are opposite.....	Page-71
44. Figure 6.1: The sea ice decay observed from OCEANSAT-2 OSCAT in the Antarctic from November to March due to summer melting of sea ice cover.....	Page-77

LIST OF TABLES

1. Table 2.1: Specifications of known space-borne scatterometers.....page-14
2. Table 3.1: Summary of the grid-wise trend observed in the Arctic.....page-37
3. Table 4.1: Summary of the grid-wise trend observed in the Antarctic.....Page-54

CHAPTER-1

1.0 INTRODUCTION

1.1 Importance of Sea ice

Sea ice is one of the most seasonally-varying geophysical features on Earth. It covers 7% of the Earth's surface at the minimum and 13% at the maximum level. In simple words sea ice can be considered as any form of ice that is found at sea and has originated from the freezing of sea water. One of the most important properties of sea ice is that it is less dense than sea water and therefore it floats over ocean surface.

Sea Ice is having a profound effect on the ocean and atmosphere. It modulates the normal exchange of heat and mass between the atmosphere and the ocean by insulating sea surface from atmosphere.

The albedo of sea ice is much higher, by a factor of ten, than that of open ocean water. This give rise to the ice-albedo feed-back processes (Thomas and Dickmann, 2003), a perturbation in the surface energy balance resulting in a decrease in ice extent due to warming may propagate and amplify since the reduction in ice extent in turn increases the amount of solar energy absorbed by the system (Curry et al., 1995).

One can consider sea ice as a thin blanket covering the ocean surface. This blanket controls the fluxes of heat, moisture and momentum across the ocean-atmosphere interface. It is now believed that recent frequent episodes of heavy snowfall and freezing winters in parts of Europe, such as in 2005, 2009 and 2010, can be traced to higher evaporation or heat source, in the form of 0° C

ocean-water underneath polar colder air, exposed by Arctic's receding sea ice surface. Hence, such snowfall can be considered as a part of the hydrological cycle.

In addition, sea ice cover it is also controlled by the ocean-atmosphere forcing. Because of its lower thickness, it is highly vulnerable and even small change within the ocean-atmosphere is able to introduce significant change in the thickness and extents of the sea ice.

Hence, sea ice affects the atmosphere through lowered rate of evaporation as well as strong ice albedo-feedback mechanism and also affects, ocean through the release of brine/fresh water during its growth/melting cycle. Since the total time duration of the growth and the melting is of the order of one year, the ice cover effectively integrates the climate signal over this short period and acts as an indicator of climate (Rees, 2005).

There are various types of sea ice, according to its stage of development. First-year Ice is the Sea ice of not more than one winter's growth, developing from young ice, with a thickness of 30 cm or greater. The old (multi-year) Ice is defined as sea ice that has survived at least one summer's melt. Its topographic features generally are smoother than those of first-year ice. The examples of sea ice types based on its stages are shown in figure 1.1. However, due to the harsh climate and the remoteness of the polar oceans sea ice features are among the least understood regions of the planet. The thin sea-ice layer over the ocean surface just accounts for the 0.1% of the Earth's permanent ice volume but covers the 70% of the ice aerial extent.

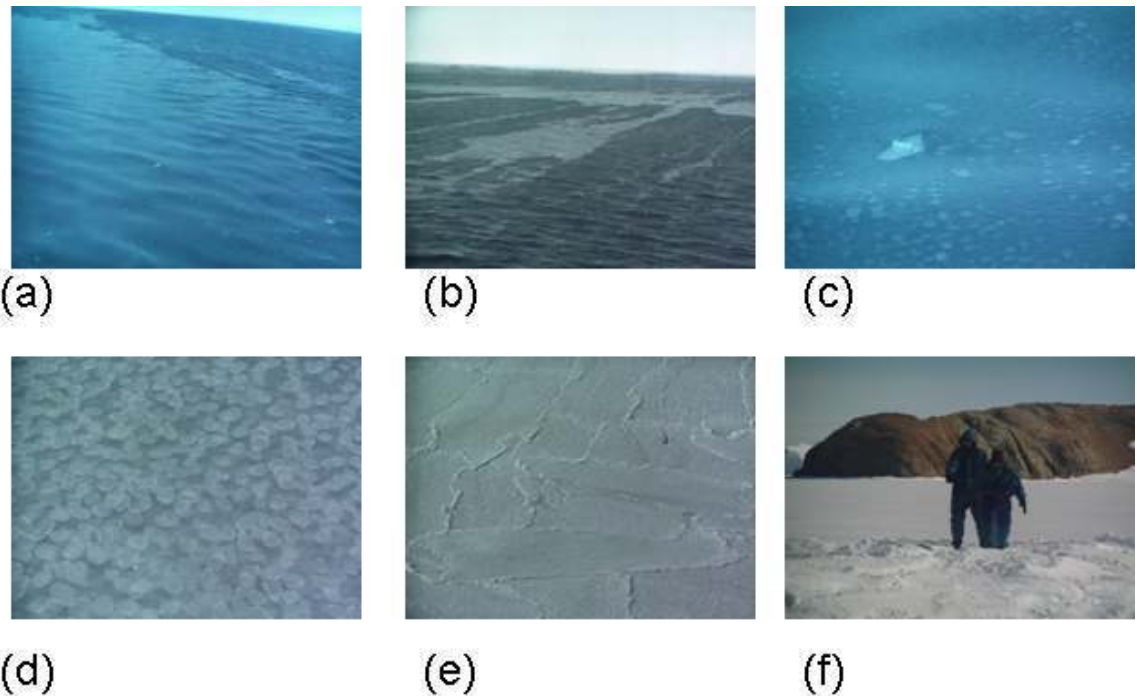


Fig. 1.1: Different stages of the formation of sea ice. (a) Grease ice (b) Grease ice aligned in the direction of katabatic winds (c) Early stage of the formation of Pancake ice (d) Pancake ice (e) Interlocking of Nilas (f) Observing the Slush formed over the fast ice around Antarctic continent

1.2 Recent changes observed in sea ice extents

Turner et al. (2007) indicated that some of the largest environmental changes have taken place in the polar regions. In the Antarctic, where a slight positive trend in sea-ice extent is apparent during 1978-1996, different atmospheric and oceanic processes tend to stabilize the present state of the seasonal ice cover (Eicken and Lemke, 2001). Arctic sea ice, on the other hand, appears more susceptible to climatic changes, with a decrease in ice extent from 1978-1996.

As pointed out by Turner et al. (2007), a synthesis of observational evidence and present understanding leads to the conclusion that the polar changes in the past several decades are attributable to a combination of circulation-driven changes, augmented by the effect of local feedback processes and increased greenhouse gas concentrations. They emphasized that even in the absence of a complete understanding of ongoing and projected environmental changes, it will be necessary to address the limits of adaptive capacity of the local systems. Only with climate models and satellite observations we will ultimately obtain adequate estimate of the polar sea-ice mass-balance, but much hard work remains to be done (Laxon et al., 2003).

1.3 Remote sensing for the assessment of sea ice properties

Investigations of vast sea ice area, distributed in remote and hostile environment is possible only through the application of remote sensing technology. Microwave remote sensing is playing a major role in polar ice studies, due to its all weather and day-night sensing capability, which is not possible through the sensing capabilities of sensors operating at other frequencies. A number of studies have been carried out for the assessment of sea ice concentration using passive microwave remote sensing techniques (Bhandari et al., 2005; Campbell, 1973; Cavalieri et al., 1984; 1991; Smith, 1996; Meier, 2005; Spreen et al., 2007; Vyas et al., 2003). Studies have also been carried out using active microwave sensors, viz. SAR and scatterometer for sea ice cover monitoring, however, higher spatial resolution of SAR limits its application to localized areas. Due to relatively larger swath and high revisit period over polar region, scatterometer has an advantage over SAR for the

regional and global monitoring, especially for climate related applications (Long et al., 2001).

1.4 History of polar ice activities at SAC (ISRO)

Polar science activities at SAC started way back in 1974 with the research work on upper atmospheric thermal structure and atmospheric circulation over Antarctica (Sehra, 1976a; 1976b). The work was based on the analysis of data collected during the 17th Soviet Antarctic Expedition (1971-73). Bedrock elevation studies were later on carried out over Queen Maud Land, East Antarctica using the data collected during the 4th Indian Scientific Expedition to Antarctica (InSEA) in 1984-85 (Bhattacharya and Majumdar, 1987).

The activities on remote sensing of polar ice at SAC were conceptualized during the planning phase of ISRO's Oceansat-1 utilization programme in 1998. The studies of polar ice characteristics were initiated using the brightness temperature data from space-borne SMMR and SSM/I passive microwave radiometers. The activities received a boost after the launch of Oceansat-1 carrying the Multi-channel Scanning Microwave Radiometer (MSMR) onboard, in May 1999. Oceansat-1 was placed in a near circular, polar sun-synchronous orbit at an altitude of 720 km. The MSMR was operating at four frequencies (6.6, 10.65, 18 and 21 GHz), each having both the vertical (V) and the horizontal (H) polarizations.

Using the passive microwave data from SSM/I, Majumdar and Mohanty (2000) delineated the changes in snow cover in and around Antarctica. By this time MSMR data became available and Vyas and Dash (2000) have

demonstrated that MSMR has high potential for the study of the polar ice features. The large scale Antarctic features captured by MSMR were investigated and reported by Vyas et al. (2001). The observed brightness temperature (Tb) of open water was much lower than that of sea ice due to the significant difference in the emissivity of these two surface features. This provides the basis for differentiation of sea ice from open water. The Tb over ice-covered area was found to vary over a wide range, allowing estimation of different levels of sea-ice concentrations. Vyas et al. (2001) and Dash et al. (2001) have demonstrated the capability of MSMR for mapping the sea-ice distribution over the Antarctic Circumpolar Sea, as well as, for capturing the land-ice signatures of some of the known geomorphological features on the continent of Antarctica. Bhandari et al. (2002) further discussed the results obtained from microwave remote sensing of sea ice in the Antarctic region from MSMR.

The above-mentioned studies have proven the capability of MSMR acquired data to provide the quantitative estimation of sea ice characteristics. As discussed by Vyas et al. (2003), MSMR estimates of sea ice extents over important regions of the Weddell Sea and the Ross Sea, as well as over the entire Antarctic region clearly bring out the nature of seasonal and secular variations (figure 1.2). They have observed a weak but consistent increasing trend of approximately 0.043 M sq. km of sea ice per year for the entire Antarctic southern polar region. The brightness temperature variations within the sea ice zone in the Arctic and the Antarctic are shown in figure 1.3 (Kumar, 2005).

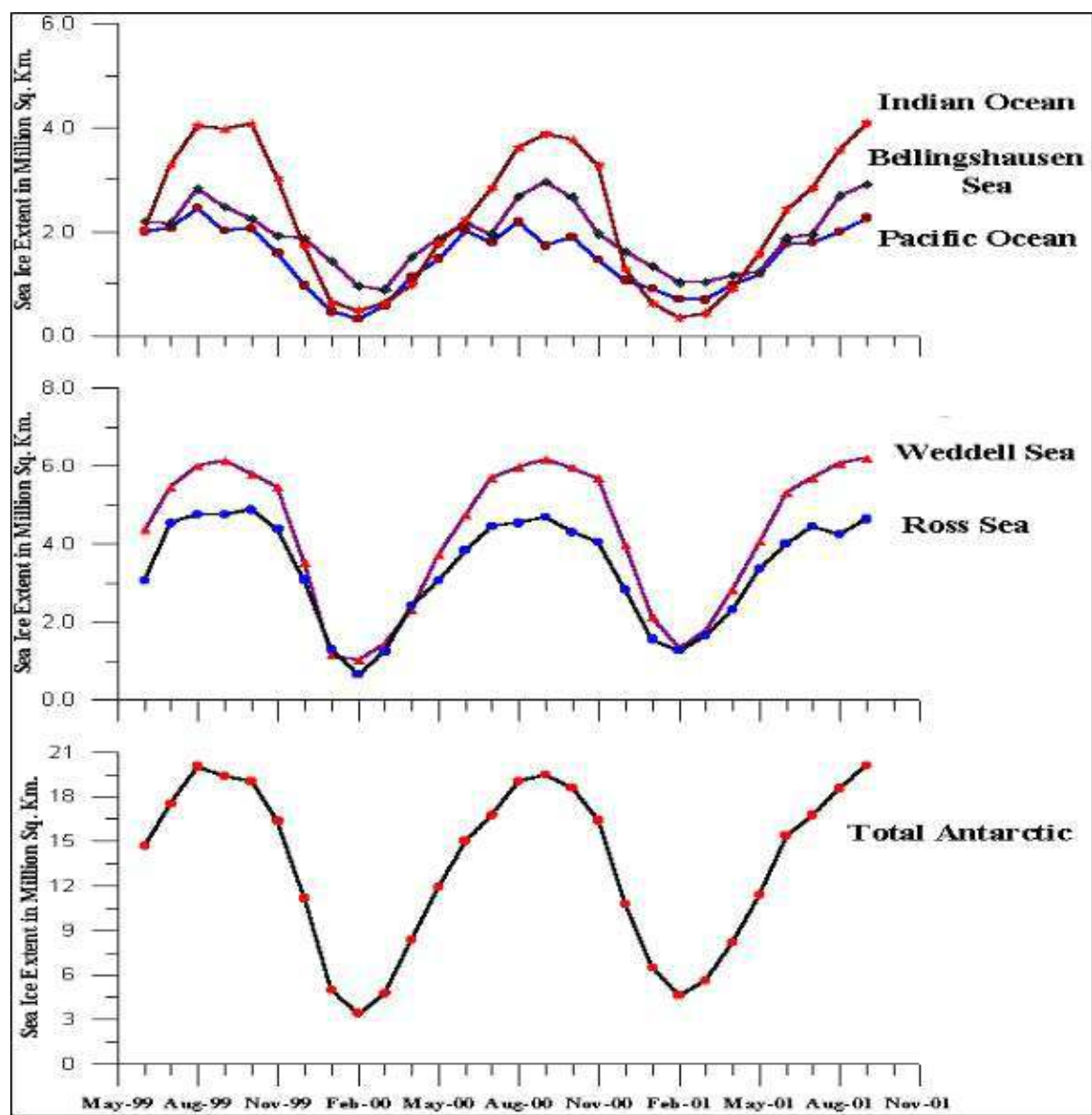


Figure 1.2 Seasonal variations in ice extent for different sectors as well as for the entire Antarctic Southern Polar Ocean regions derived for the period June 1999 to May 2001 (Vyas et al., 2003)

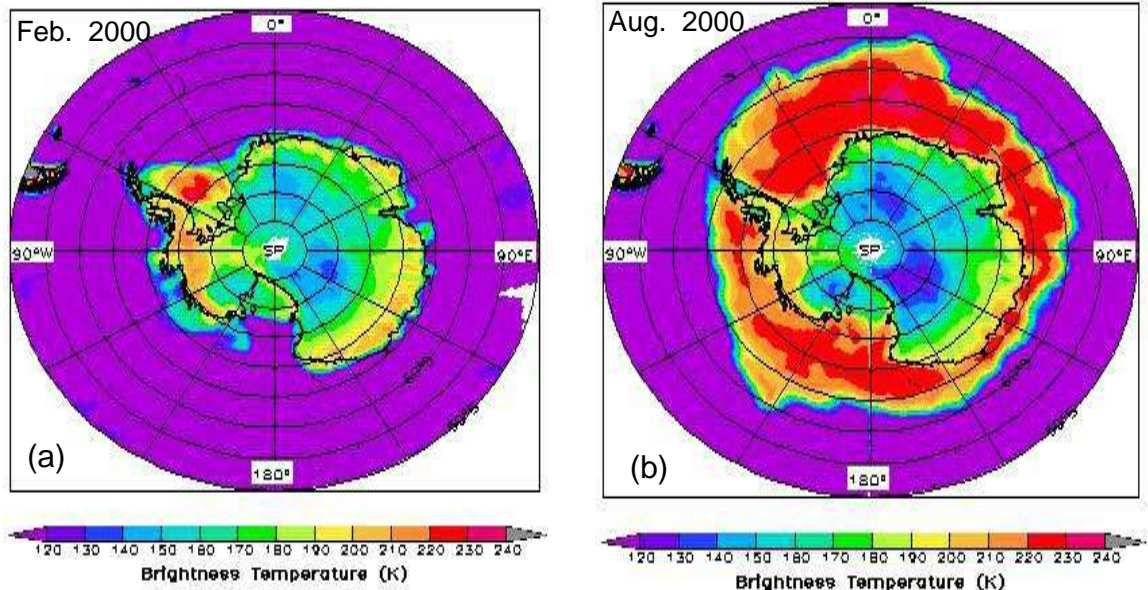


Figure 1.3: Antarctic sea ice cover derived from Oceansat-1 MSMR 18 GHz brightness temperature data; (a) summer sea ice cover and (b) winter sea ice cover

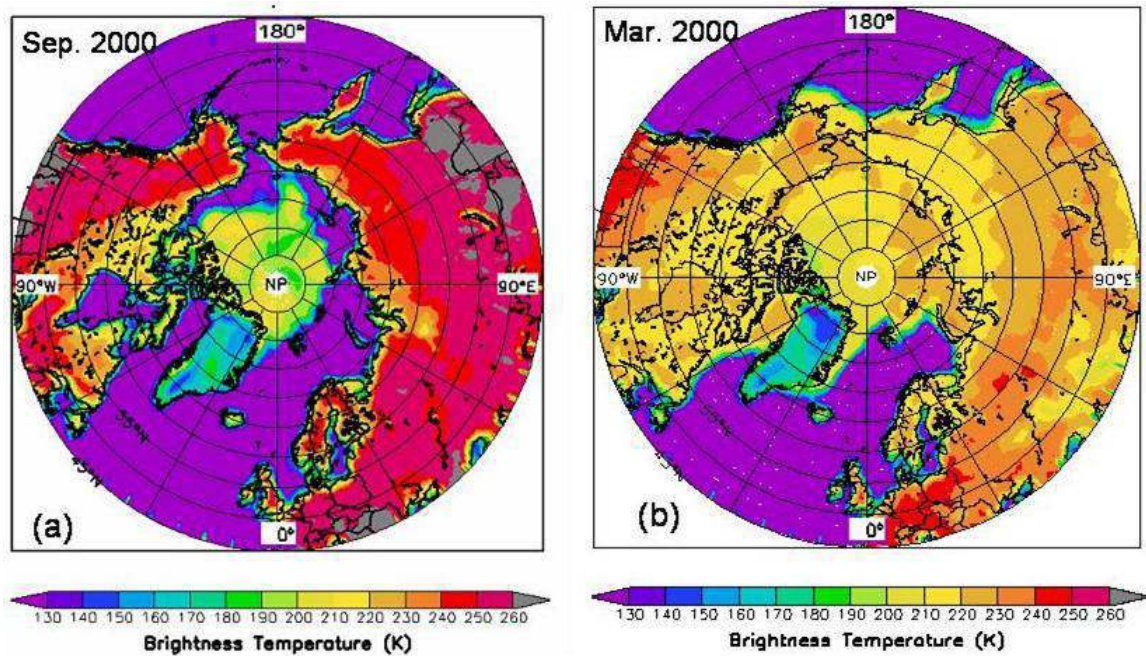


Figure 1.4: Arctic sea ice cover derived from Oceansat-1 MSMR 18 GHz brightness temperature data; (a) summer sea ice cover and (b) winter sea ice cover

The development of MSMR based sea ice concentration algorithm and its application to the Antarctic sea ice regions were reported by Bhandari et al. (2005). Sreenivasan and Majumdar (2006) have studied the temporal variation patterns of sea ice surrounding Antarctica using SSM/I data during its depletion phase (November 2001 to January 2002). They have observed that overall extents under all ice concentration categories during different months over the study period have decreased considerably in comparison to the sea ice concentration categories during 1978–87 period. DEMs over parts of Antarctica were generated by Bhattacharya et al. (2006) using SEASAT altimeter data and the probable implications of DEM in studying ice sheet/glacier movements were also discussed. Seasonal variations of the sea ice cover in the Northern as well as in the Southern polar regions were investigated and discussed by Sharma et al. (2009).

SAC has also conducted test and evaluation of indigenously developed low-cost, multi-band, ground-truth radiometers at Antarctica during 26th InSEA (2006-07). Measurements, for test and evaluation, were carried out in terms of following parameters: a) spectral reflectance measurement of ice and fresh snow surfaces, b) terrestrial solar spectral irradiance: direct and global components (Manjul et al., 2010). SAC has also supported InSEA activities by installing an Earth Station at Indian Antarctic station “Maitri” during 27th InSEA (2007-08).

Considering the importance of scatterometer based observations in the study of polar ice and ISRO's plan of launching a Ku-band scatterometer, studies were initiated to explore the potential of QuikSCAT Ku-band

scatterometer for the sea ice edge detection (Bhandari et al., 2006; Bhandari and Khare, 2009). Recently, Oza et al. (2011c) have developed spatio-temporal coherence based technique for the improved identification of sea ice from scatterometer data. Recent results on sea ice trends have been reported by Oza et al. (2010). An interesting analysis of the melting onset dates is presented in Oza et al. (2011a).

The experience gained during the decade long activities (1999-2009) have given an impetus for the widening of the scope of polar ice activities. This led to the (i) investigation of inter-annual variations of surface melting derived from QuikSCAT over Amery Ice-shelf (Oza et al., 2011b) based on the experience gained during 28th and 29th InSEA (2009-10) and (ii) development of the AMSR-E based technique for the estimation of sea ice thickness (Singh et al., 2011).

SAC has, jointly with National Centre for Antarctic and Oceanic Research (NCAOR), carried out extensive studies and published an atlas of Antarctic Sea Ice using data from Oceansat-1 MSMR data (Vyas et al., 2004). The atlas of sea ice maps has served as a useful reference source for the researchers in India and abroad. This atlas has provided an insight into the monthly variations of sea ice cover in the southern polar region. The present atlas moves one step further by providing the maps of Sea Ice trends observed in last decade, the topic attracting broad scientific and societal attention in the context of climate change. Majority of the remote sensing studies carried out to investigate sea ice trends have been concentrated either on the Arctic/Antarctic level, as a whole, or at sector level. Majority of the grid-level trend studies are based

mainly on model results and very few studies have actually made use of satellite data.

The present study reports the trends observed in sea ice fraction at 1x1 degree grid cell level using QuikSCAT scatterometer decade-long data. Separate trends have been derived for each month of the year and discussed in detail. The atlas also discusses significant trends observed in Sea Ice Extent (SIE) over the Arctic and the Antarctic in the recent past.

This scatterometer based study is important in the context of Oceansat-2 OSCAT scatterometer launched by India in September 2009 with almost similar specifications as QuikSCAT scatterometer and is the only available Ku-band scatterometer at present.

CHAPTER-2

2.0 SATELLITE DATA AND SEA ICE IDENTIFICATION TECHNIQUE

2.1 Scatterometer Basics:

Space-borne scatterometers are active microwave instruments for measuring the Normalized Radar Cross Section, also known as backscattering co-efficient (σ_0) of the Earth's surface. A scatterometer transmits radar pulses and receives backscattered energy, the intensity of which depends on the roughness and dielectric properties of a particular target. Surface properties and geometry that affect backscatter from ice, snow, water, soil and vegetation include surface roughness, moisture content, leaf size and density, branch orientation, and preferential alignment of surface scatterers. Dielectric properties are affected by the material present and physical characteristics of the effective scattering medium or its layer (snow grain size, brine concentration in sea ice, salinity in water and canopy leaf density of vegetation) as well as by the state of sea water. As scatterometers can be very accurately calibrated, generally, to less than a few tenths of a decibel (dB), seasonal and inter-annual differences that result in changes as low as 1-2 dB may be confidently examined.

Thus, Scatterometer is a calibrated Radar specifically designed to measure accurately the scattering co-efficient (σ_0). Scatterometer transmits microwave pulses and the backscattered intensity and the round trip time are measured. The intensity gives a measure of the scattering co-efficient and the

time information gives the target location. The scattering co-efficient (σ_0) is related to other instrument parameters as follows (Ulaby et al., 1986a):

$$\sigma_0 = \{(4\pi)^3 \times R^4 / (G^2 \times \lambda^2)\} \times (P_r/P_t)$$

Where,

σ_0 = Backscattering co-efficient.

G = The Gain of Antenna.

λ = Wavelength

R = Range

P_t = Transmitted Power

P_r = Received Power

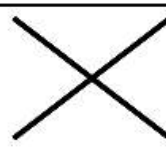
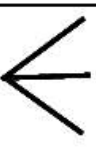
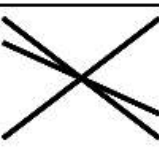
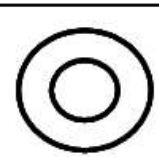
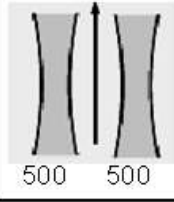
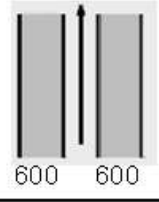
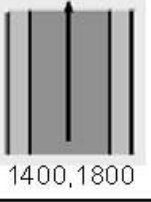
It may be noted that σ_0 is proportional to the ratio of the received power and the transmitted power, and so, only this ratio need to be measured for relative calibration, provided the range is known accurately.

The SeaWinds instrument was launched on a dedicated polar satellite QuikSCAT in 1999. QuikSCAT SeaWinds, also known as simply “QuikSCAT” or QSCAT, is a conically scanning pencil-beam system. With pencil-beam systems, angle measurement normally achieves the resolution (Wu et al., 1994). Pencil-beam scatterometer instrument generally consists of two off-nadir beams, inner and outer. Their beams are realized by having two offset feeds along with a parabolic reflector, which is mechanically spun about the yaw axis of the satellite. Both the satellite motion and the conical scanning take place simultaneously. Hence, each point in the inner swath is viewed twice by the inner beam and similarly twice by the outer beam. QSCAT is the first conically scanning satellite – borne scatterometer featuring a pencil-beam Radar.

QSCAT has a one meter parabolic reflector antenna rotating at 18 revolutions per minute, scanning the two pencil-beam footprint paths in a

circular pattern at incidence angles 46° and 54°, respectively for inner (H-pol.) and outer (V-Pol.) beams. QSCAT is placed in the orbit at 803 km above the Equator with 98.616° inclination. The recurrent period of 4 days (57 orbits) makes the orbital period of about 101 minutes (14.25 orbits per day).

Table 2.1: Specifications of known space-borne scatterometers

	SASS on Seasat-A	AMI on ERS-1/2	NSCAT on ADEOS1	SeaWinds on QuikSCAT
Azimuths				
Altitude (km)	810	780	805	803
Inclination	106°	98.52°	98.7°	98.616°
Polarization	V-H, V-H	V Only	V, V-H, V	V-Outer, H-Inner
Beam Resolution	Fixed Doppler	Range Gate	Variable Doppler	Pencil-Beam
Sci. Modes	Many	SAR, Wind	Wind Only	Wind/Hi-Res.
Resolution	50/100 km	25/50 km	25/50 km	25 km/6x25 km
Swath	 500 500	 500	 600 600	 1400,1800
Incidence Angle	0° - 70°	18° - 59°	17° - 60°	46° and 54°
Daily Coverage	Variable	< 41%	78 %	>90 %
Date	6/1978 - 10/1978	ERS-1: 8/1991 – 5/1996 & ERS-2: 3/1996 – 1/2001	8/1996-6/1997	6/1999 to 11/2009

The instrument collects data over ocean, land, and ice in a continuous, 1800 km wide swath centered on spacecraft's nadir subtrack, making approximately 1.1 million ocean surface wind measurements and covering 90% of Earth's surface each day. The comparison of specifications of various space-borne scatterometers is made in table 2.1. It is to be noted that OSCAT on board Oceansat-2 launched by India in September 2009 has specifications almost similar to those of QuikSCAT with minor difference in incidence angles.

2.2 Scatterometer data

Ku-band scatterometer daily composite data (at 0.2 degree resolution) from "QuikSCAT" have been utilized. The data for the outer beam is vertically polarized and the inner beam is horizontally polarized. The global rectangular lat/long gridded data (Long, 2000) for the period from August 1999 to July 2009 was used in the study. The grid resolution is 0.2° lat/long grid-cell or about 22.5 km at the equator. The images are temporal averages over one day period of all the σ_0 measurements whose centers fall within each image pixel area (0.2° x 0.2° lat/long grid). Sample images are shown in figure 2.1. It is seen from the figure that over a day, majority of northern and southern polar region gets filled by the satellite observations.

We intend to derive the decadal average trend for each month of the year separately. In this context, there are 10 data points for each calendar month, one for each of the 10 years. QuikSCAT daily backscatter data for four consecutive days around the middle of each month were utilized to derive the sea ice cover.

2.3 Physics behind the detection of Ocean and ice:

2.3.1 Retrieval of Ocean wind

Retrieval of the surface wind information (speed and direction) is the most important application of a space-borne scatterometer. For sea water, penetration depth δ_p , decreases from 1cm at 1 GHz to 1 mm at 16 GHz (Ulaby et al., 1986b). Hence, the dominant mechanism of scattering from sea water is surface scattering. The idea of retrieval of ocean surface winds from scatterometer was based on the assumption that these surface ripples are in equilibrium with the local wind stress. The following points describe the physics behind this retrieval:

- Ocean backscatter at both V and H polarizations are equal at nadir and decrease with increasing incidence angle and the V-pol backscatter becomes stronger than H-pol. This behavior is explained by the physical optics (Kirchhoff) approximation near nadir, and Bragg (resonant) scattering theory at larger incidence angles.
- The roughness generated by the local wind is responsible for the backscatter of incident energy and is measured in terms of radar backscattering coefficient by scatterometer (Gohil, 1992). Changes in wind velocity cause changes in surface roughness, which in turn modify the σ_0 of the ocean and hence magnitude of backscattered power (Sarkar, 2003).
- The backscatter coefficient increases with wind speed at incidence angles greater than 20° (Jones et al., 1978). The backscatter from the ocean increases with wind speed up to a point of saturation, namely a

point beyond which ocean roughness no longer changes due to increasing wind speed.

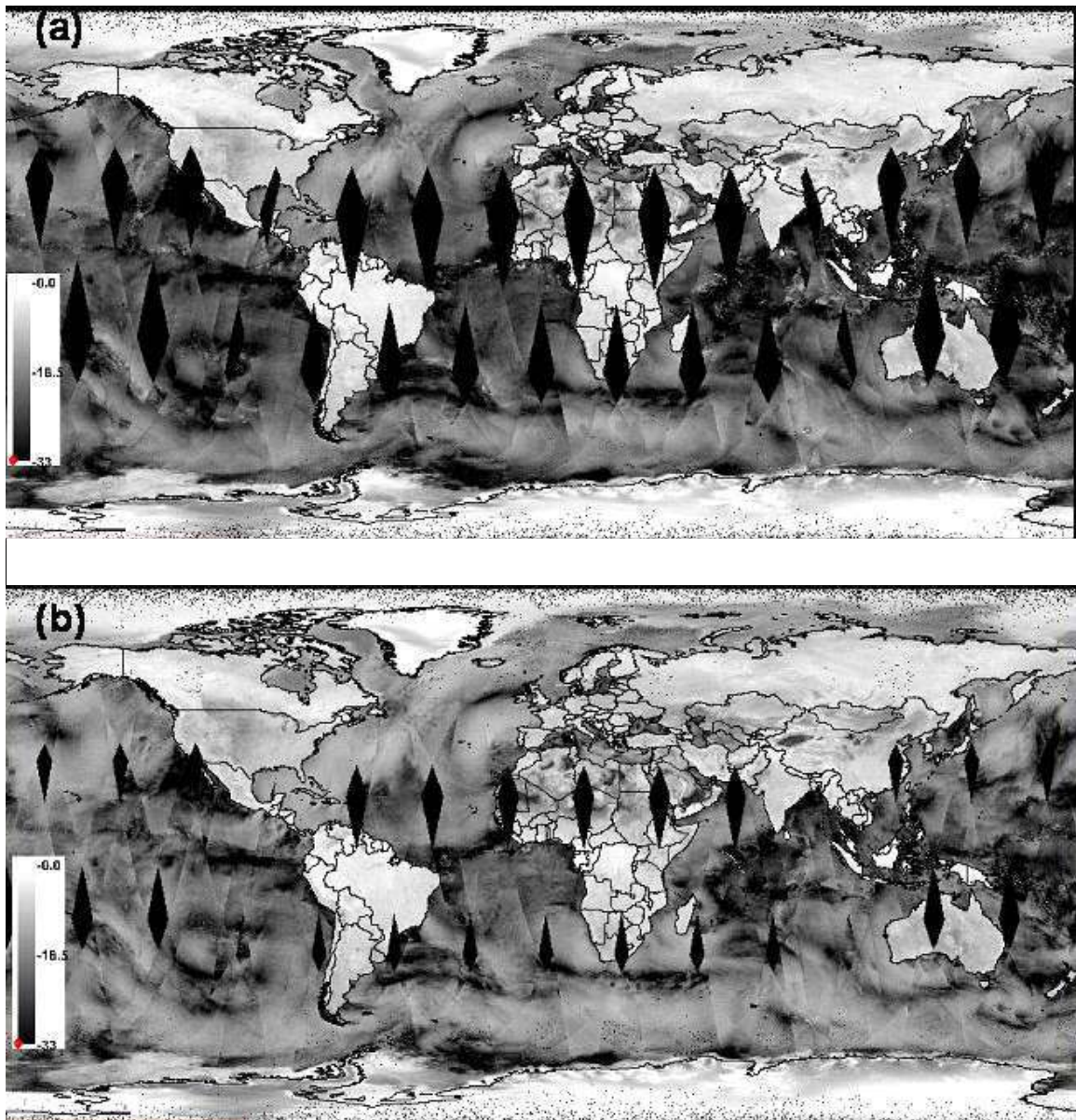


Figure 2.1: Ku-band backscatter image of January 15, 2000 (a) Horizontally polarized component (b) Vertically polarized component

- Jones et al. (1978) have also demonstrated the anisotropic characteristics of the scattering. The backscatter depends not only on the magnitude of the wind stress but also on the wind direction relative

to the direction of the radar beam. The wind direction sensitivity of σ_0 varies periodically with angle between the plane of incidence and wind direction with peak around 60° angle (Sarkar and Kumar, 1985).

Hence, the key to determining the wind direction and speed from scatterometer is the anisotropic behavior of the surface roughness over ocean, since the crests and troughs of the surface wave field tend to align themselves perpendicularly to the wind direction (Rees, 2006). The capability of measuring both wind speed and direction is the major uniqueness of the scatterometer. Developments of algorithms for the wind vector retrieval from SASS scatterometer were demonstrated by many researchers (Jones et al., 1982; Pandey, 1987; Sarkar and Kumar, 1986). Gohil and Pandey (1985) have demonstrated an algorithm based on the fact that all the dual polarized noise-free σ_0 measurements, taken in any azimuth direction, should provide the same wind speed in the true direction of wind. The past decade has seen continuous improvement in the algorithms, coverage and resolution of scatterometer derived ocean surface winds (Gohil et al., 2008; 2010; Stoffelen and Portabella, 2006).

2.3.2 Sea ice detection

In contrast to ocean backscatter, which is a result of surface interaction processes only, sea ice backscatter at Ku-band also arises from volume interactions deeper in the ice layer. Sea ice consists of freshwater ice, brine, and air bubbles. Because of this, sea ice exhibits a complicated dielectric behavior. Over the frequency range of 1-40 GHz the relative permittivity of sea ice falls in the relatively narrow range of 2.5 to 8 (Ulaby et al., 1986b). In

contrast, the dielectric loss factor ϵ'' covers a wide range of values from less than 0.01 to more than 1.0. In general ϵ'' decreases with increasing temperature, increases with increasing salinity and is typically 3 to 10 times larger for FY ice than for MY ice (because the salinity of FY ice is typically 5 times that of MY ice).

As given by Ulaby et al. (1986a), the penetration depth for a natural material (except water) with $\epsilon''/\epsilon' < 1$,

$$\text{Penetration depth } \delta_p = (\lambda (\epsilon')^{0.5} / (2\pi \epsilon''))$$

Hence, depth of penetration increases with decreasing dielectric loss factor ϵ'' . This indicates that penetration depth for MY ice would be much higher than FY ice. Typically at -10° C temperature and 15 GHz frequency, depth of penetration is in the range of 0.01-0.1 m for FY ice and 0.1-0.2 m for MY ice (Ulaby et al., 1986a).

As the salinity increases, penetration depth decreases due to the increase in dielectric loss factor (ϵ''). As studied by Hallikainen and Winebrenner (1992), the relationship between dielectric constant (real part ϵ' and imaginary part ϵ'') and relative fractional brine volume (FBV) at 10 GHz is as given below:

$$\epsilon' = 3.0 + 0.012 * \text{FBV} \text{ and } \epsilon'' = 0.0 + 0.010 * \text{FBV} \text{ for FBV} \leq 70\% \text{ at 10GHz}$$

In addition to this, the salinity, size, shape, and number densities of brine inclusions and air bubbles in the ice layer are strongly influenced by the temperature during ice growth and desalination (Yueh et al., 1997). This results into distinct polarization, intensity and directional radiation properties of ice that allow its effective identification against an ocean background. Important points from the previous research works are summarized below.

- The level of sea ice backscatter observed during the winter months is very stable, ranging from -5 to -21 dB for the H-pol component at 46 deg incidence and from -7 to -23 dB for the V-pol component at 54 deg incidence. The backscatter levels of summer multi-year ice range from -10 to -20 dB for both, H- and V-pol. components.
- Sea ice backscatter is azimuthally isotropic (Early and Long, 1997), whereas the azimuthal modulation of ocean backscatter can reach up to 6-7 dB. This indicates that there is a strong ice-ocean discrimination power encoded in azimuthal variability. It is interesting to note that the isotropic behavior of sea ice is also in contrast to the anisotropic (azimuth-angle dependent) backscatter behaviors of some parts of Antarctic ice sheet that correlate well with the formation of wind-induced snow features like 'Sastrugis' (Young and Hyland, 1998).
- Scattering from a complex medium like sea ice involves both volume and surface scattering mechanisms. As discussed earlier, air bubbles, brine pockets, and snow grains are sources of volume scattering. In dense new ice the brine pockets are assumed to be the source of volume scattering, whereas in older less dense and less saline ice types (e.g. multi-year ice), gas bubbles are the source of volume scattering. Because these volume scatterers are randomly oriented and almost spherical, the vertically and horizontally polarized normalized radar cross sections, σ_{vhh} and σ_{vhv} , are thus similar (Yueh et al., 1997).
- Surface scattering is contributed by the rough surfaces of ice ridges, sea ice and snow cover at all length scales. In general, the surface roughness of

sea ice, except thin ice, is comparable with or much larger than the wavelength (~ 2 cm) of Ku-band (Tucker et al., 1992).

➤ This means that the geometric optics scattering from surface facets facing the scatterometer may become significant even at large incidence angles. Consequently, the levels of Ku-band σ_{OHH} and σ_{OVV} will be similar for most sea ice surfaces. From the above described characteristics of volume and surface scattering, we anticipate that the co-polarization ratio ($\sigma_{\text{OVV}}/\sigma_{\text{OHH}}$) is close to unity for sea ice at Ku-band, regardless of which scattering mechanism dominates. Similarly, APR, the Active Polarization Ratio ($(\sigma_{\text{OHH}} - \sigma_{\text{OVV}})/(\sigma_{\text{OHH}} + \sigma_{\text{OVV}})$), is close to zero.

➤ Hence, as against the ocean (surface) scattering, which is characterized by steep backscatter gradients relative to the incidence angle and substantial polarization ratio, scattering from sea ice yields smaller gradients and near unity polarization ratio.c

2.3.3 Ambiguity in Ice-ocean discrimination

The APR for Bragg scattering increases with increasing incidence angles and may reach as high as 10 dB at 60° incidence angle at low winds. The APR of sea surface backscatter is smaller at higher wind speeds. This might be due to the increasing coverage of breaking waves and foam with increasing wind speed. It has been suggested that breaking waves significantly increase the level of σ_{OHH} at high incidence angles beyond what is predicted from the Bragg scattering mechanism (Smirnov and Zavorotny, 1995). An increase in σ_{OHH} due to breaking waves translates into a reduction of the APR of ocean backscatter, and consequently, reduces the APR contrast of sea ice and open water.

Thus, previous research work indicates that the backscatter levels from sea ice overlap with the range of backscatter from open water at high wind conditions. This clearly makes it difficult to distinguish sea ice and open water using only backscatter levels. Yueh et al. (1997) have demonstrated the use of specific range of σ_0 measurements and co-polarization ratio ($\sigma_{\text{ow}}/\sigma_{\text{oHH}}$) for the identification of sea ice. Co-polarization ratio takes care of the ice-ocean ambiguity.

Remund and Long (1999) developed an ice-ocean discrimination algorithm for NSCAT that used polarization difference ($\sigma_{\text{ow}} - \sigma_{\text{oHH}}$), the vertically polarized incidence dependency and both, σ_{oHH} and σ_{ow} , and standard deviation images to automatically detect the ice edge. The method has been improved by Haarpaintner et al. (2004). They have developed a more accurate method to take care of the ice-ocean ambiguity by incorporating effective Active Polarization Ratio APR of 3x3 pixel window. They also utilized the previous day knowledge of sea ice for the removal of ambiguity. Oza et al. (2011c) have further improved the Haarpaintner et al. (2004) algorithm by incorporating the spatio-temporal coherence criteria for accurate identification of sea ice.

2.4 Derivation of Sea ice cover

Oza et al. (2011c) have developed a method to resolve the ice-ocean ambiguity by using the time-scale of the ice/ocean processes and the continuity based spatial information about sea ice. The ocean surface wind fields, generally, exhibit variability over a time scale of a few hours to a few days. The sea-ice cover exhibits variability over a time scale of a few days to a few weeks. In general, the time scales of the two processes are different. This

suggests that the ocean and sea ice pixels can be better distinguished in spatio-temporal domain. Wind fields are most likely to vary significantly over 3-4 days, hence the data of previous 4 days are optimum for the identification of sea ice pixels with reasonable accuracy. The overall accuracy achieved by them is of the order of 95 per cent, considering both the hemispheres. They have adapted a set of hierarchical classification rules to identify the sea-ice and ocean classes, which are given below. Here thresholds for the σ_{OH} , σ_{ov} and Standard Deviation (SD) were taken from Haarpaintner et al. (2004). The APR described below refers to the Active Polarization Ratio defined as $(\sigma_{\text{OHH}} - \sigma_{\text{OVV}})/(\sigma_{\text{OHH}} + \sigma_{\text{OVV}})$. A pixel will be classified as sea ice if all the following criteria are met:

- i. $\sigma_{\text{OHH}} > -25$ dB in winter and > -28 dB in summer
- ii. $\sigma_{\text{OVV}} > -25$ dB in winter and > -28 dB in summer
- iii. $\text{APR} < \text{APR}_0$ for winter and summer; $\text{APR}_0 = -0.025$, same as that used by Oza et al. (2011c)
- iv. 4-Day Standard deviation (SD_0) < 4 dB in winter and < 5 dB in summer; where SD_0 is the SD of σ_{OHH} or σ_{OVV} , whichever is higher
- v. Condition for temporal coherence: Condition (i) to (iv) should be satisfied at least for the median number of daily data-images (at least for 3 days out of 4 consecutive days)
- vi. Condition for spatial coherence: At least, Median number of pixels, or more, in the moving window should be sea-ice (at least 5 pixels out of 3x3 set of neighboring pixels)

The last two criteria together are Spatio-temporal coherence criteria. The 4-days daily backscatter images (H & V) were utilized to check the spatio-temporal coherence. This Spatio-Temporal sea ice Discrimination algorithm is henceforth abbreviated as STD algorithm hereafter. The STD criteria minimize the probability of wrong identification of ice or ocean pixels.

The STD criterion also minimizes the error introduced by the effect of rain on scatterometer σ_0 measurements. Rain attenuates the radar signal passing through to the surface, adds backscatter from droplets and perturbs the surface due to droplet impact and rain-induced wind drafts (Draper and Long, 2004). Generally, $0.2^\circ \times 0.2^\circ$ area is larger than rain field area. Since, rain is a dynamic phenomenon; its impact will be minimized in the daily product. The remaining contributions at pixel level will be further minimized by the STD algorithm, since it checks the coherence for 3x3 pixels for four days and thereby eliminating the noisy pixels.

In case, the daily data images correspond to the beginning or to the end of a month, the month in which majority of the four input images falls was considered for climatological monthly sea-ice extent mask (figure 2.2). Non-polar area was removed using this mask to overcome the problem of false detection in and around tropical and temperate (or mid-latitude) oceans, and to avoid unnecessary computation for non-polar regions.

2.5 Generation of sea ice fraction grid at 1 degree cell size

The variations occurring at the larger area level, as compared to 25 or 50 km pixel resolution are playing a significant role in the physical processes occurring between the sea ice and the Ocean/Atmosphere. Here, a study has

been made to investigate the variations observed at 1x1 degree level using scatterometer data. The fractions of pixels falling in each geographical 1 x 1 degree grid-cell were computed for the generation of Sea Ice Fraction (SIF) image for each month during the study period. This fraction is conceptually different from the sea ice concentration which is being derived operationally using AMSR-E or SSM/I Passive Microwave Radiometer (PMR) data. PMR data is providing the information on the percentage of sea ice within the footprint of the sensor.

However, the derived SIF image will provide the information on the fraction of sea ice dominated pixels within a 1x1 degree grid cell. The long term changes in such SIF, if any, can be considered as an indicator of climate change, over the corresponding geographic region.

A comparison of derived sea-ice image with the climatological monthly maximum sea-ice extent image is shown in figure 2.3.

2.6 Generation of grid-cell-wise images of regression statistic

The 1x1 degree grid-cells of SIF images for each month during the period of 2000 to 2009, (total of 10 images for each month) were utilized to develop the grid-cell wise linear relationship in the form of

Here A_t is the trend coefficient and indicates the per-year rate of change in SIF during the study period for the grid cell and A_0 is the constant term, representing the SIF value at the beginning of the study period.

Finally, a stack of five layers has been generated. These layers are grid-cell wise trend-coefficient, constant term, R-square, F-Ratio and a mask of grid-cells

that shows the significant F-ratio. This mask will indicate that the relationship developed is statistically significant and there is no reason to doubt the validity of regression coefficients, even if the physical process responsible for it is not well understood. If for a grid-cell the F-ratio is not significant, it will indicate the existence of statistically weak correlation between the inter-annual variations in SIF.

2.7 Computation of sea ice area in the Arctic and the Antarctic

The sea ice area (SIA) of each 1x1 degree grid-cell was computed by multiplying the SIF of that grid cell with the geographical area of the same. The geographical area (A_g) of each cell was computed using the trigonometric rules as given below. On the spherical surfaces of the Earth, take a small element of area with:

- (i) One side along a latitude circle with length $R \cos\theta d\phi$
- (ii) The other side along a longitude circle with length $R d\theta$
- (iii) Let the element be small enough, so that it can be approximated by a rectangle.

Here, R is the radius of the Earth, θ is the latitude and ϕ is the longitude. Here, $d\theta$ and $d\phi$ represent infinitesimally small arc lengths along the latitude and the longitude lines encompassing to the infinitesimally small rectangular area.

Now, by integrating the above equation, the area of any larger element encompassed within a definite latitude/longitude zone, with the corners (θ_1, ϕ_1) and (θ_2, ϕ_2) , can be written as:

$$\text{Area of the grid cell } (A_g) = R^2 [\sin \theta_2 - \sin \theta_1] [\phi_2 - \phi_1] \dots \dots \dots (2)$$

Here, all the angles are in radian units. Figure 2.4 shows the variations in the area (A_g) under 1x1 degree grid-cell at different latitudes.

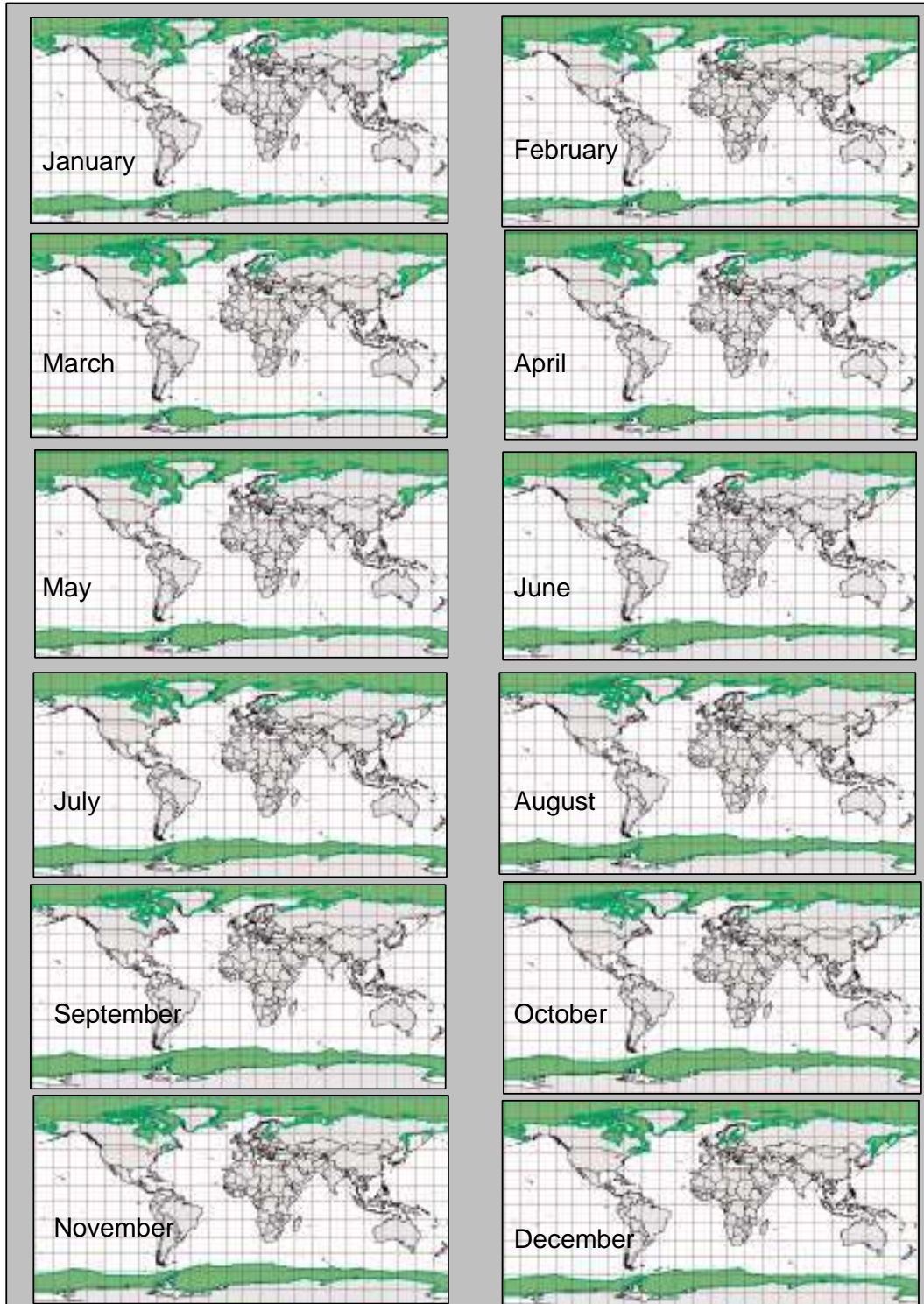


Figure 2.2: Monthly climatological maximum sea ice cover shown by green color with dark green boundary (Image bounds: Longitudes: 180° W to +180° E; Latitudes: 90° N to 90° S; each grid cell: 15 ° x 15 °)

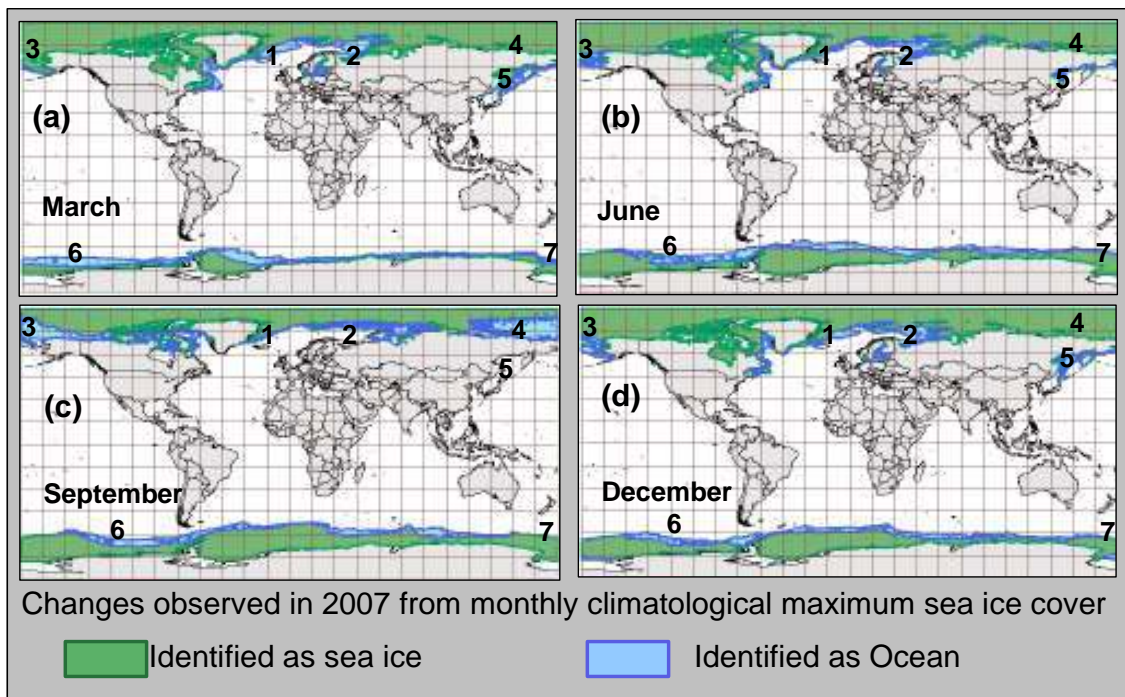


Figure 2.3: Sea ice and ocean identification using the near-real time scatterometer data. Identified ocean area (with cyan color) shows the changes occurred in the parts of Arctic/Antarctic from the monthly climatological maximum sea-ice cover (1978-2002). Significant changes are observed in (1) East Greenland Sea, (2) Barents Sea, (3) Chukchi Sea, (4) East Siberian Sea, (5) Okhotsk Sea, (6) Bellinghausen and Amundsen Seas and (7) Ross Sea.

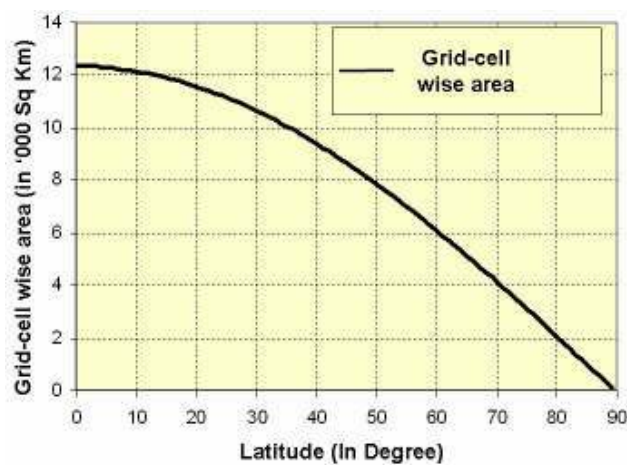


Figure 2.4: Area under 1x1 degree grid-cell at different latitudes

CHAPTER-3

3.0 ARCTIC SEA ICE TRENDS

3.1 Physiography of the Arctic

The figure 3.1 shows the Arctic polar region and the surrounding areas prepared using ArcGlobe module of ARCGIS. In the Northern Hemisphere, Arctic Polar Region covers the southern limit of terrestrial Tundra, the Arctic Ocean and the Sub-arctic Seas and the atmosphere to the north of the region of the Polar Front. The Arctic Ocean is a deep basin centered on the North Pole and surrounded by land and narrow outlets (Bering Strait, Davis Strait, Fram Strait, Norwegian Sea and Greenland Sea etc.) in to the Atlantic and the Pacific oceans.

The ice in the Arctic Ocean can survive for a long time due to the big oceanic gyre present in the Arctic Ocean, which will allow ice to grow and increase in its thickness. Ice will rotate for years due to this gyre until it leaves the basin through one of the straits/outlets.

In the Arctic there are two main large scale wind driven drift components. The first is the Beaufort gyre, a clockwise rotation around the North Pole which results from an average high pressure system that creates the winds in the region. The second is the transpolar drift, where ice moves from the Siberian coast across the Arctic basin to the north coast of Greenland. This allows the flow of ice in to the North Atlantic through the Fram strait between Greenland

and Svalbard. Arctic sea-ice extent varies between 8 and 15 M sq km during the annual cycle (Eicken and Lemke, 2001).

3.2 Comparison with NSIDC sea ice extent

It is observed (figure 3.2) that in all the years during the study period, the scatterometer derived sea ice extent, based on STD algorithm, is on an average 10 per cent higher than the passive microwave radiometer (PMR) derived NSIDC data in the month of September. However, it may be noted that both the curves follow the same trend/pattern. This shows that the SIE values obtained by the STD algorithm are in close agreement with NSIDC SIE values, but for a positive bias, which can be explained on the basis of difference in the processes recorded by the scatterometers and the PMRs.

The summer melting in the Arctic will be at its maximum in September month. Summer is the time when sea ice breaks into individual ice floes, particularly in the marginal sea-ice zone, which is also saturated with wet snow/ice layer due to the ongoing peak summer melting process. The snow cover and the rough edges of the floes provide very high backscatter (σ_0) because of the strong reflected radar signal back from the surface. This makes the partially melted sea ice distinguishable from water, more easily.

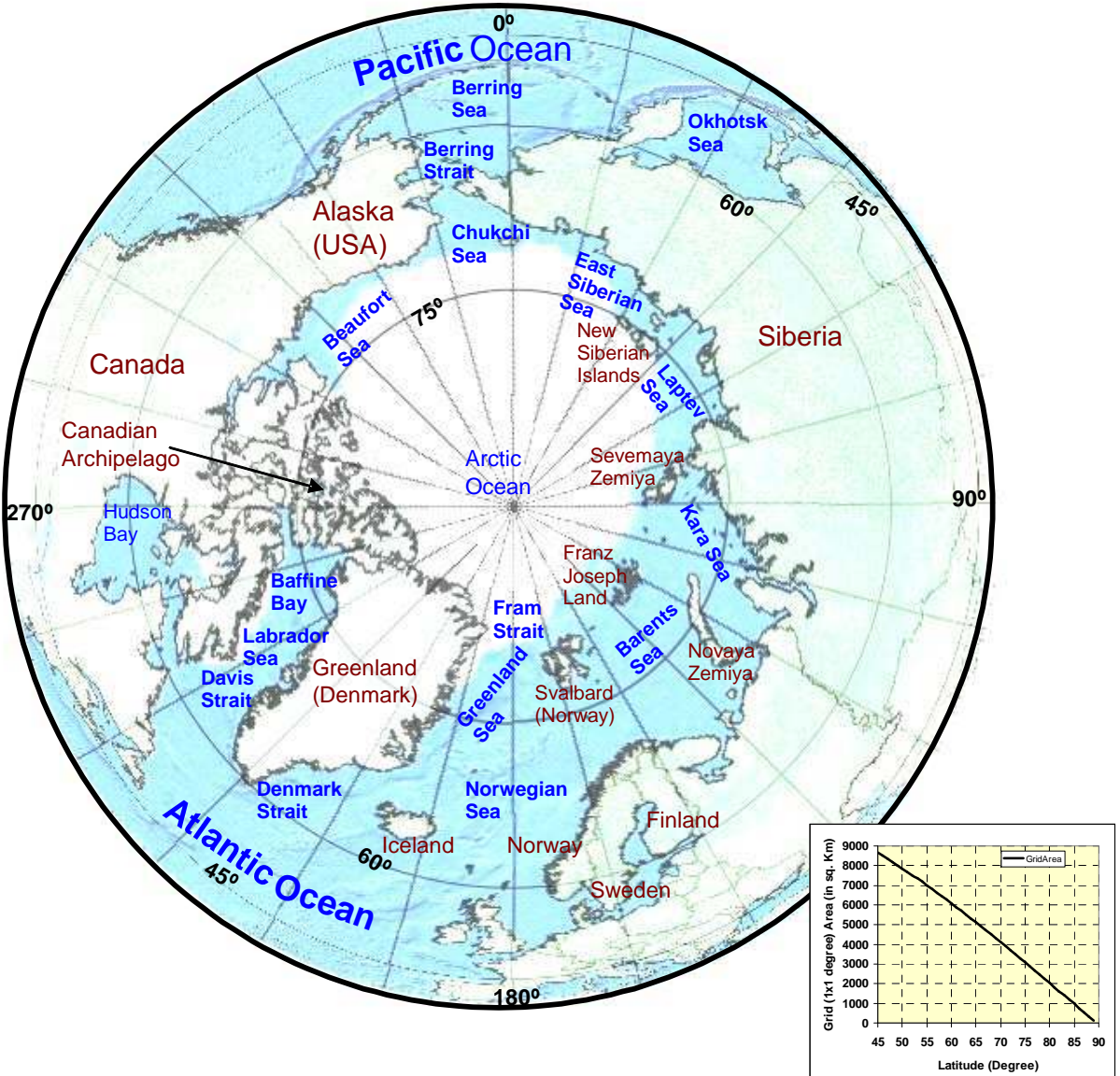


Figure. 3.1 Arctic Polar region and the surroundings

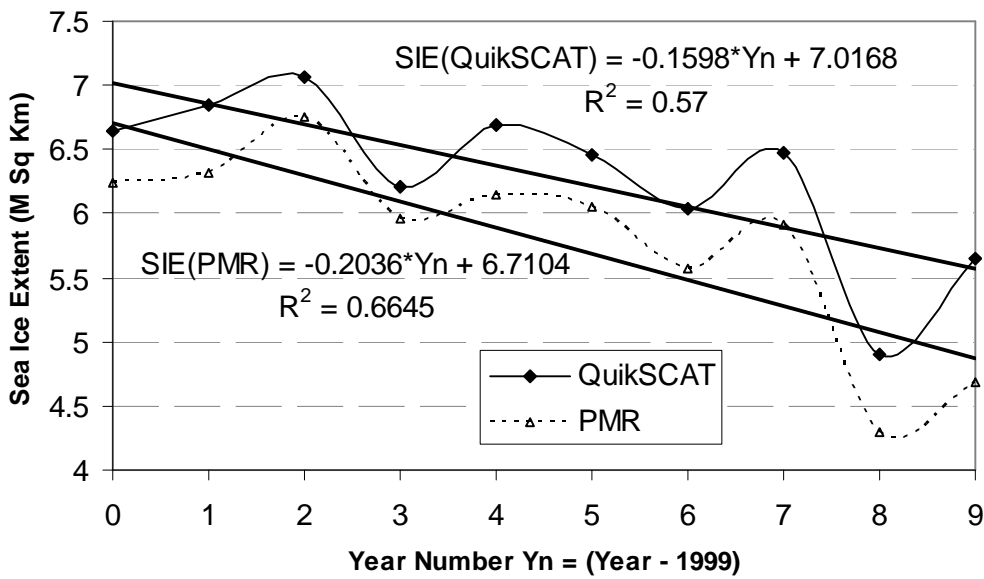


Figure 3.2: Comparison of QuikSCAT derived summer minimum SIE for the Arctic (at SAC/ISRO) using STD method with the PMR based NSIDC SIE data. The main findings to be noted are (i) the similar trend/pattern of the two curves, and (ii) the larger SIE consistently shown by the QuikSCAT data.

On the contrary, brightness temperature of the ice covered by wet snow or slush during the summer, as observed by PMR is generally low making the sea ice less distinct from open water on passive microwave imagery. Therefore the PMR data tends to underestimate SIE compared to scatterometer data during the summer period. This underestimation by PMR compared to Scatterometer can be of the order of 14% (Tedesco et al., 2008).

As observed from figure 3.2, the summer sea ice extent is reduced from 6.65 M sq km in 1999 to 5.64 M sq km in 2008. This gives an average decline of the order of 2.54% (0.16 M Sq km) per year in the summer sea ice extent (September month) from 1999 to 2008, considering the inter-annual variations.

For the same period the decline as per PMR based NSIDC data is of the order of 3.52 % (0.20 M Sq km) per year. The earlier rate of NSIDC-data based decline from 1979 to 1998 is of the order of 0.04 M Sq km per year. Hence, the

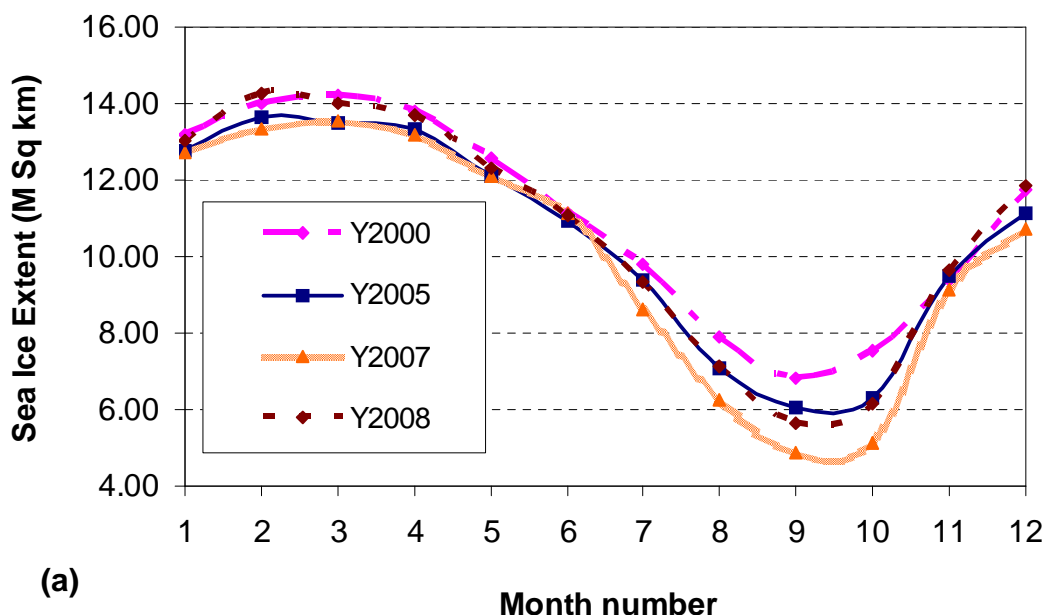
recent rate of decline is five times faster than the earlier long time rate of decline.

3.3 Analysis of inter-annual variations

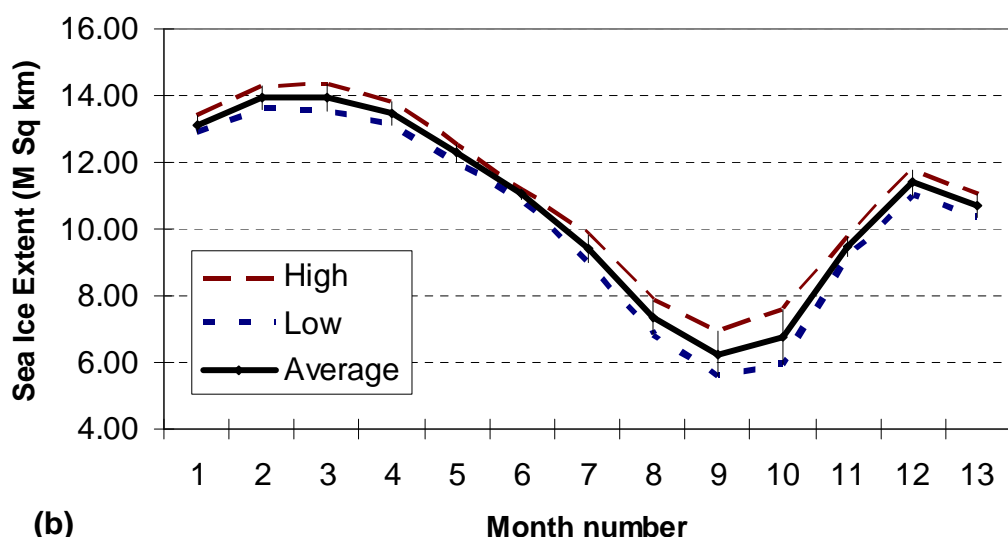
The study period includes full calendar years only from 2000 to 2008. During these years, the year 2007 has recorded the minimum sea ice extent ever since 1979 in the Arctic. The year 2008 is the second minimum followed by 2005, the third minimum. The monthly variations of SIE during these three years are compared with the year 2000 (figure 3.3a), which is a normal year.

It is observed that year-to-year variations are higher during the summer period as compared to the winter period. Surprisingly, they are almost negligible in the months of June and November.

Figure 3.3b shows average sea ice for different months from 1999-2008. Upper and lower limits of 1 Standard Deviation (SD) are also shown. Higher SD in summer as compared to winter and negligible SD in the months of June and November can be easily noticed. Lower SD during the month of March as compared to the same in September indicates that the winter maximum sea ice extent has not changed drastically as compared to the summer minimum.



(a)



(b)

Figure 3.3 : Monthly SIE statistics (2000-2008) of the Arctic (a) Monthly SIE for some of the study years (b) Average monthly SIE with upper and lower limit of one SD. (The following may be noted: (i) the larger variability of the summer minimum computed to winter maximum, and (ii) minimum variability in June and November)

3.4 Grid-wise sea ice trends of maximum and minimum sea ice cover

The grid-wise pattern of recent trends obtained from the derived 1x1 degree SIF data for the summer minimum and the winter maximum are shown in the figure 3.4. In the Arctic, a significant negative trend up to 15% per year in the Chukchi and East Siberian seas is visible in the summer minimum extent.

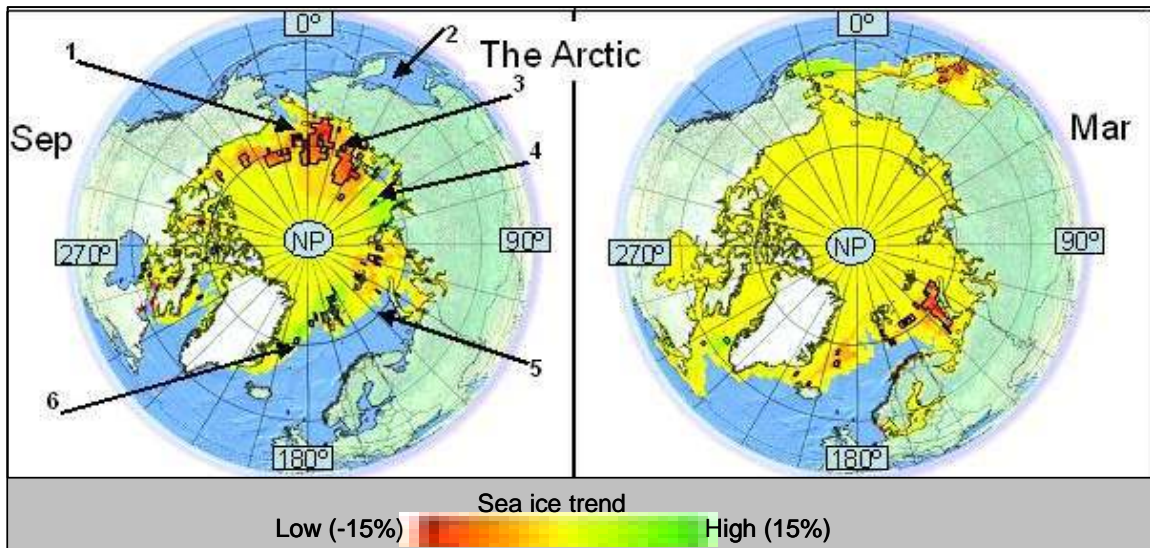


Figure 3.4: Trend observed in summer minimum and winter maximum SIE in the Arctic. Locations identified with numbers are (1) Chukchi, (2) Okhotsk, (3) East Siberian, (4) Laptev, (5) Barents, (6) East Greenland

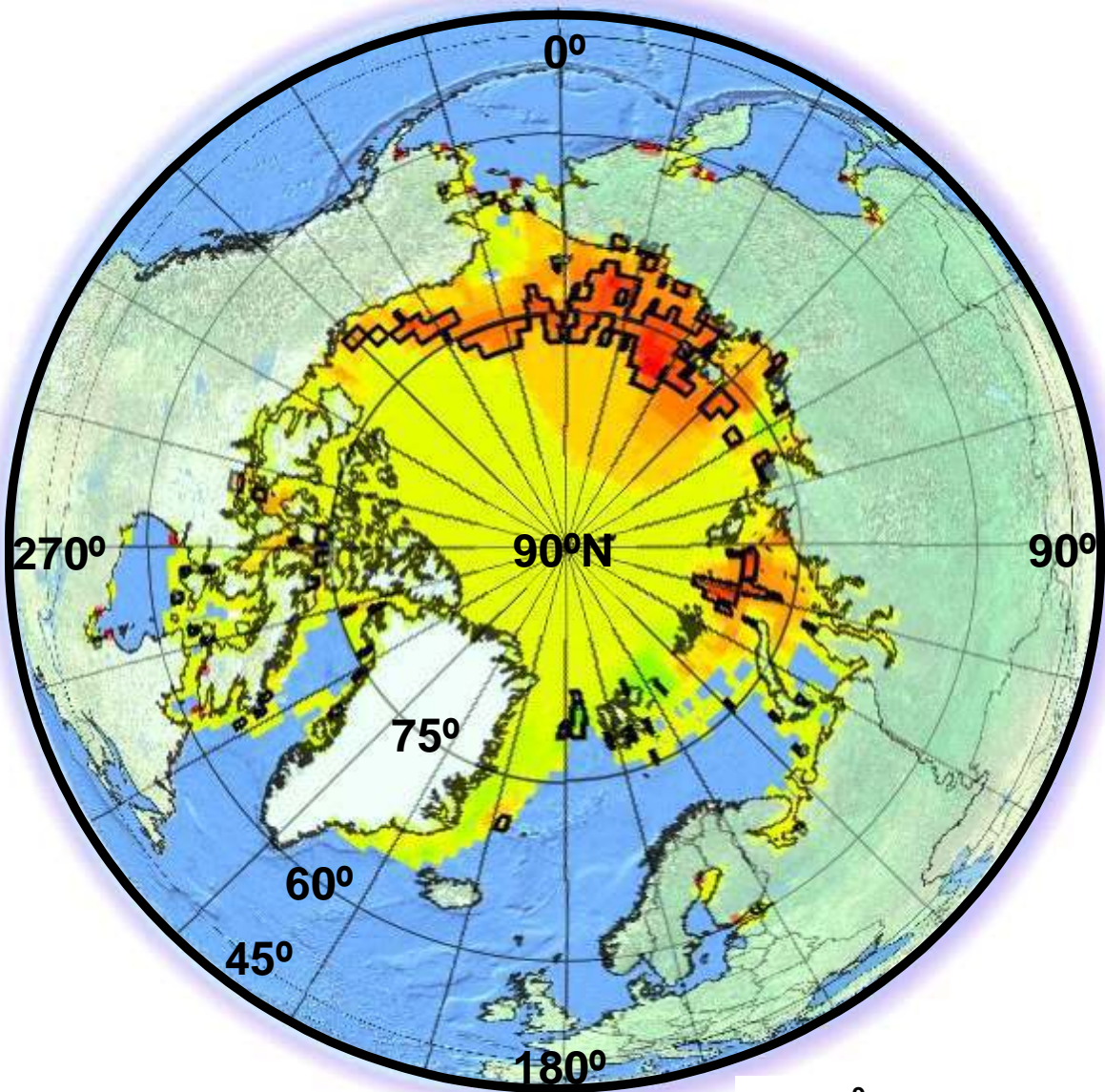
A weak positive trend is also visible in the Laptev and East Greenland seas. However, negative trend in winter-maximum in Barents Sea is a distinct pattern. The positive trend in the Bearing Sea and negative trend in Okhotsk Sea are also visible in the winter-maximum image. Month-wise trends observed in the Arctic are shown in color plates A1 to A12, and observations are summarized in table 3.1. Black colored Polygons in the sea ice region indicate grids showing statistically significant trends at 95% confidence interval.

Table 3.1: Summary of the grid-wise trend observed in the Arctic

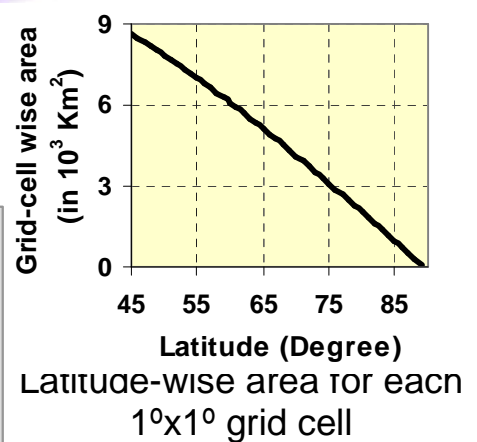
Region	Name	Jan	Feb	Mar	Apr	May	Jun	Jul	Aug	Sep	Oct	Nov	Dec
Central Arctic		-	+	+	+	-	+/-	+	+	+	+	+	-
Barents Sea	--S	- S	--S	-S	--S	--	+/- S	-	+	+/-	+/-	+/-	- S
Kara Sea		-	+	+	+	-	-	+/- S	--S	+ S	--	+/- S	-
Laptev Sea		-	+	+	+	-	-	+	+	+	+	+	-
East Siberian Sea		-	+	+	+	-	-	+	--S	--S	--	+ S	-
Chukchi Sea		-	+	+	+	-	- S	+/-	--S	--S	+/-	--S	--
Bering Sea	
Bering Strait		-	++	++ S	++ S	++ S	-	.	.	.	+	+/-	-
Beaufort Sea		-	+	+	+	-	-	- -	-S	- S	--	+ S	-
Baffin Bay		-	+	+	+	-	+/-	++	+	+	-/.	+	-
Labrador Sea		-	+		+	-	-	+	+/- S	+	.	++	-
Davis Strait	--S	+	++ S	++ S	++ S	-	-	+ S	+	.	.	-S	+/-
Denmark Sea		-	++ S	+	++	- S	-	- S	+	.	.	+	-
Greenland Sea		-	+	+	- S	--S	+/- S	+	+	+	++	++S	+/- S
Fram Strait		-	+	+	+	-	-	+	+	+	+	+S	-
Hudson Bay		-	+	+	+	-	-	+	+	.	.	.	+/- S
Okhotsk Sea	- S	- S	- S	- S	- S	- S	- S

Explanation of symbols used: Strong Negative trend (--), Weak Negative (-), No definite trend (.), Weak Positive (+), Strong Positive (++) , Statistically Significant (S).

A-1: Month-wise Sea Ice Trends in the Arctic - October

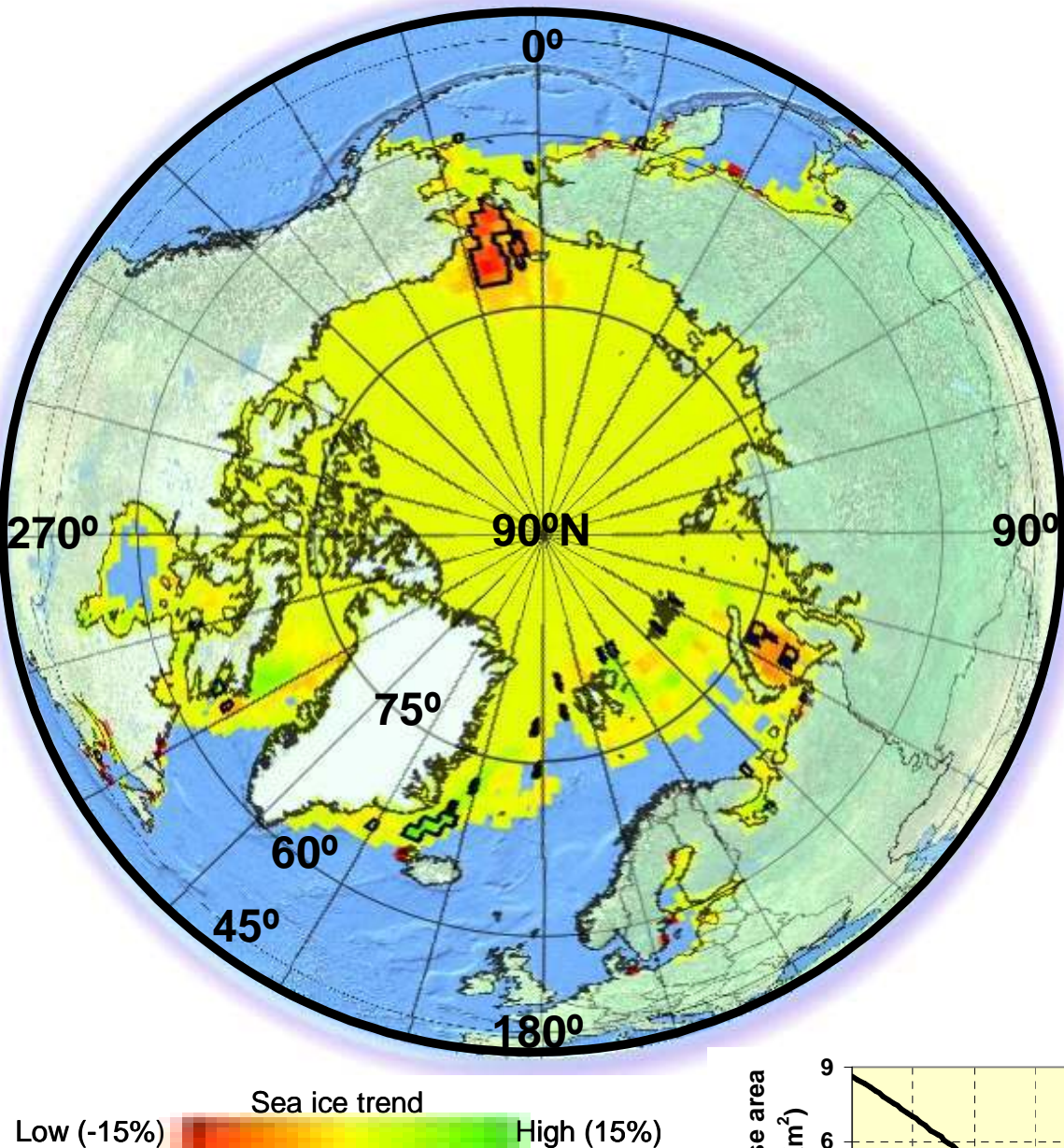


- Statistically significant negative trend is evident in the large area over Beaufort, Chukchi, East Siberian and Laptev Seas
- The area showing negative trend is higher than that in September month, whereas in November month it is limited to Chukchi Sea (see respective plates)

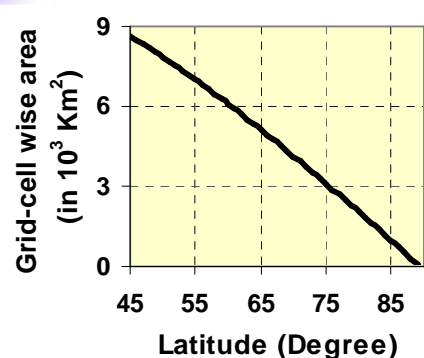


A-1

A-2: Month-wise Sea Ice Trends in the Arctic - November

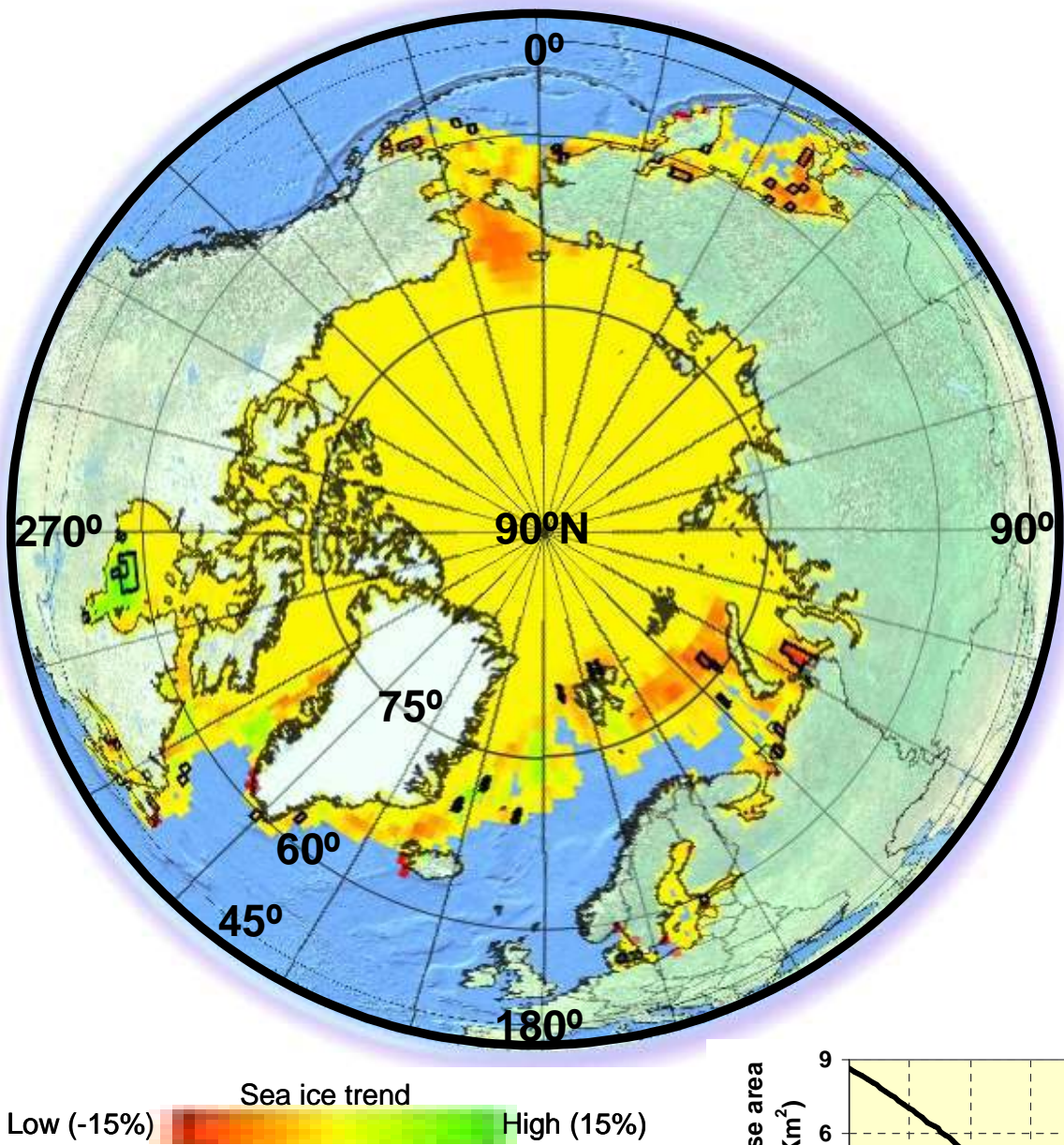


- Statistically significant negative trend is evident in the chukchi Sea, towards Bearing Stratit. Area between Greenland and Iceland is showing positive trend.
- The area showing negative trend is much lower than that in the month of October. The trend values are higher than these in the month of December (see respective plates).
- Also, in large parts of the Arctic, a weak positive trend prevails (though not statistically significant)

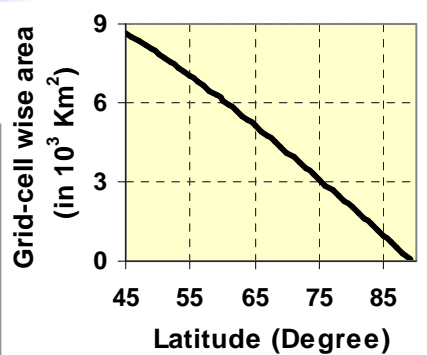


A-2

A-3: Month-wise Sea Ice Trends in the Arctic – December

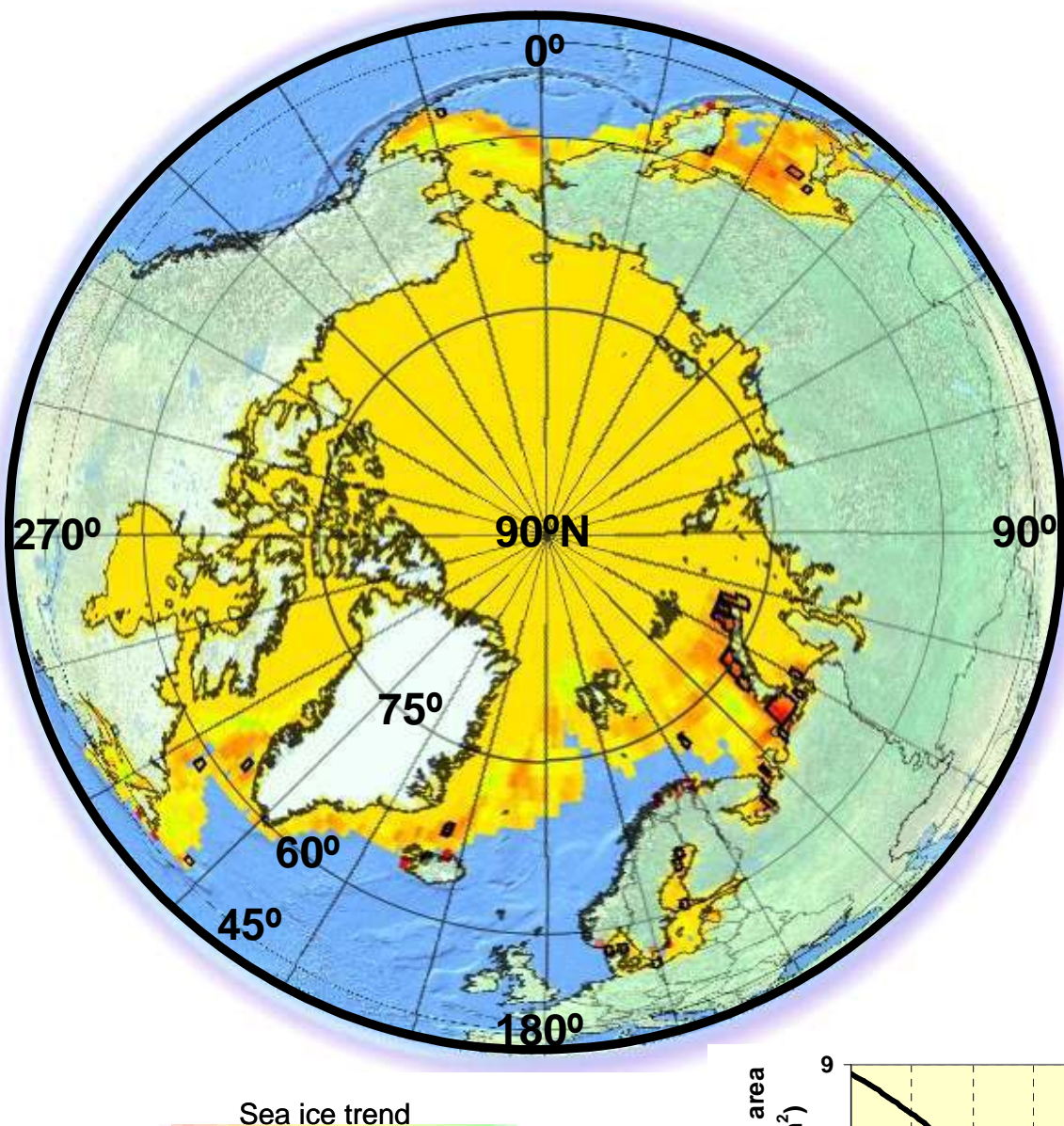


- Statistically significant trend is not visible, however weak negative trend is evident in the Chukchi sea and in parts of Kara and Barents Seas. The previous month (November) was showing significant negative trend in this area.
- The pattern of statistically weak trend continues in the subsequent (January) month (see respective plates).
- Also, in large parts of the Arctic, the weak positive trend of November changes over to a weak negative trend in December (though not statistically significant)

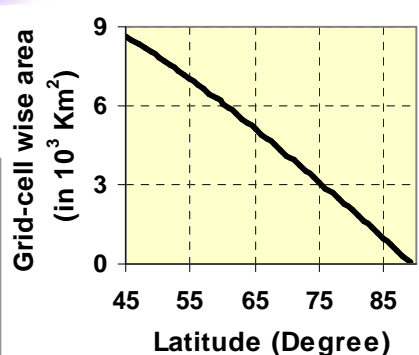


A-3

A-4: Month-wise Sea Ice Trends in the Arctic - January

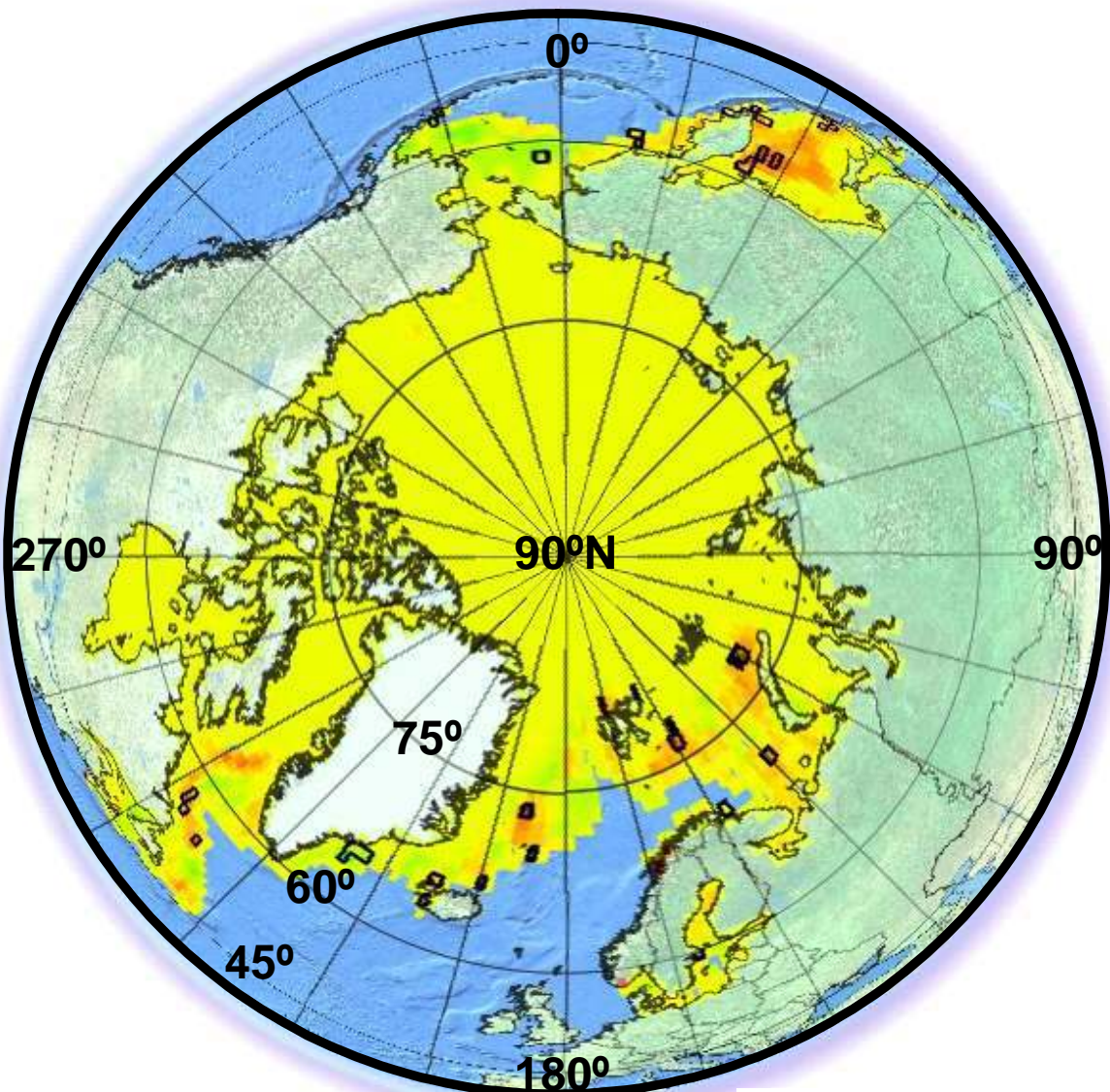


- As observed in the previous (December) month, statistically weak trend is observed in the Arctic.
- In large parts of the Arctic, the weak negative trend of December gets slightly strengthens in January.
- The statistically weak positive trend is evident in the subsequent (February) month in the Bering Sea. (see respective plates).

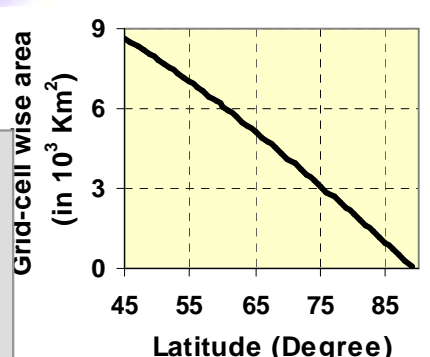


A-4

A-5: Month-Wise Sea Ice Trends in the Arctic – February

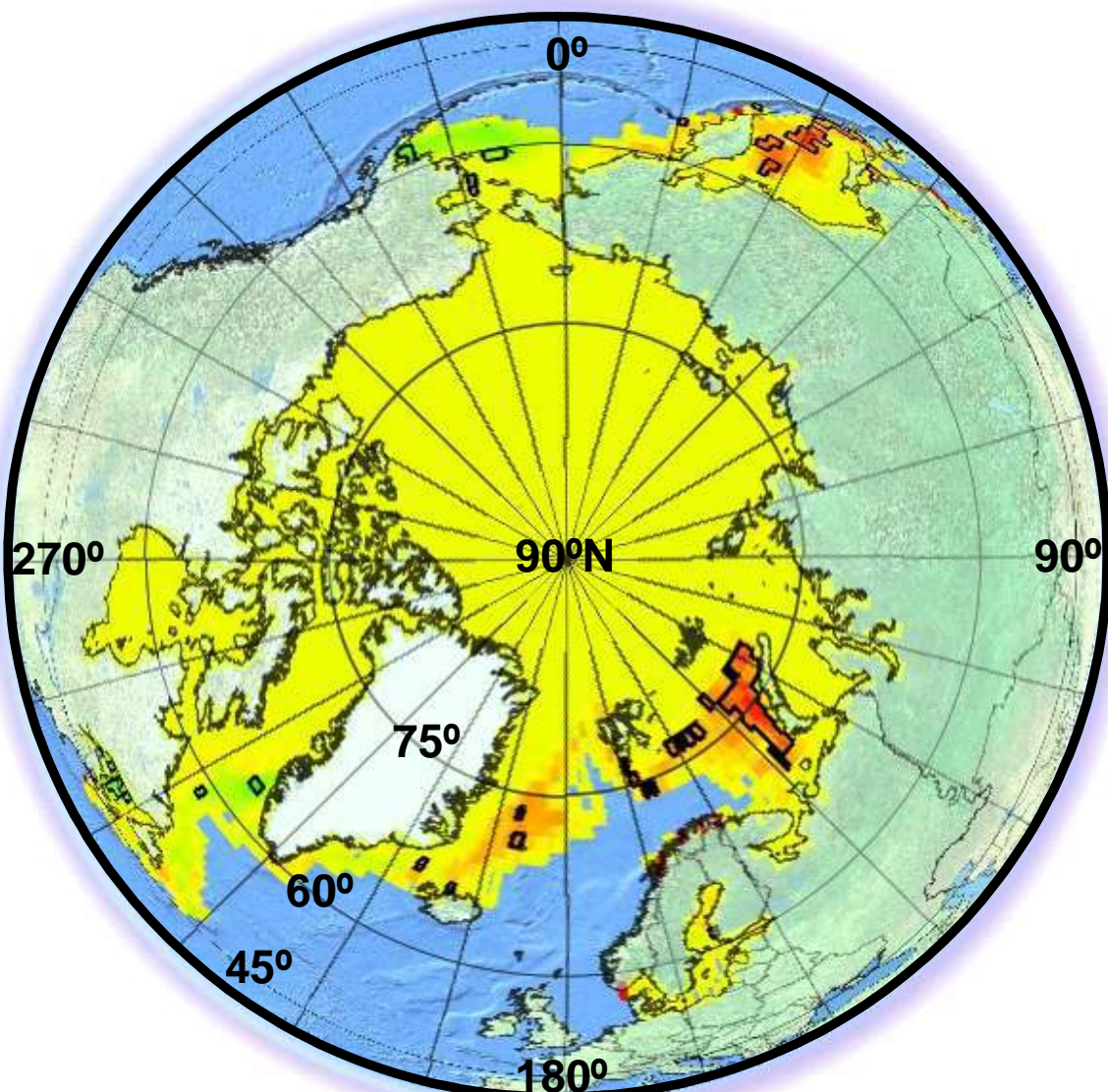


- The statistically weak positive trend is evident in the in the Bering Sea. The trends in the Okhotsk Sea are also weakly positive .
- In large parts of the Arctic, the ewak negative trend of January changeover to a weak positive trend in February.
- The trends in January were also statistically weak, however some of the areas starts showing significant trends from March onwards, which could be attributed to summer effect (see respective plates).



A-5

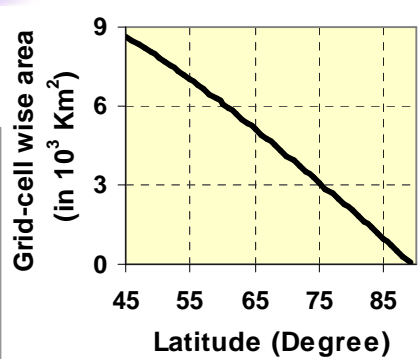
A-6: Month-wise Sea Ice Trends in the Arctic - March



Sea ice trend

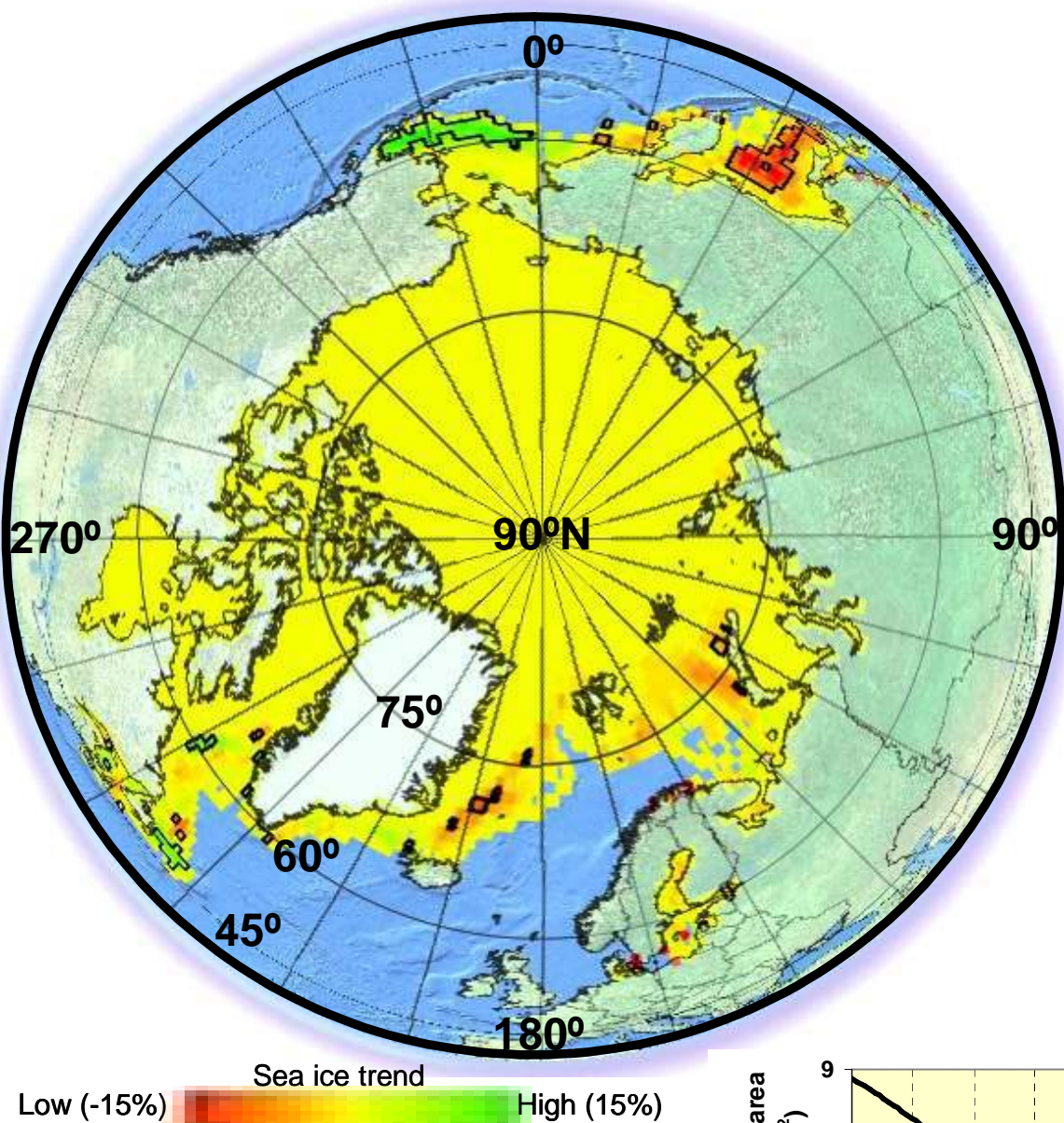
Low (-15%) High (15%)

- The positive trend in the Okhotsk Sea and negative in the Bering Sea as observed in February get strengthened in March. In these seas some of the areas show statistically significant trends.
- The large parts of the Arctic show a reversal of positive trend observed in February to a negative trend in the month of March.
- The statistically significant positive trend is visible in the Barents Sea, which was observed in the month of January (see respective plates).

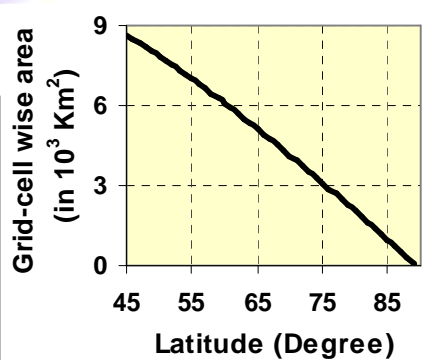


A-6

A-7: Month-wise Sea Ice Trends in the Arctic - April

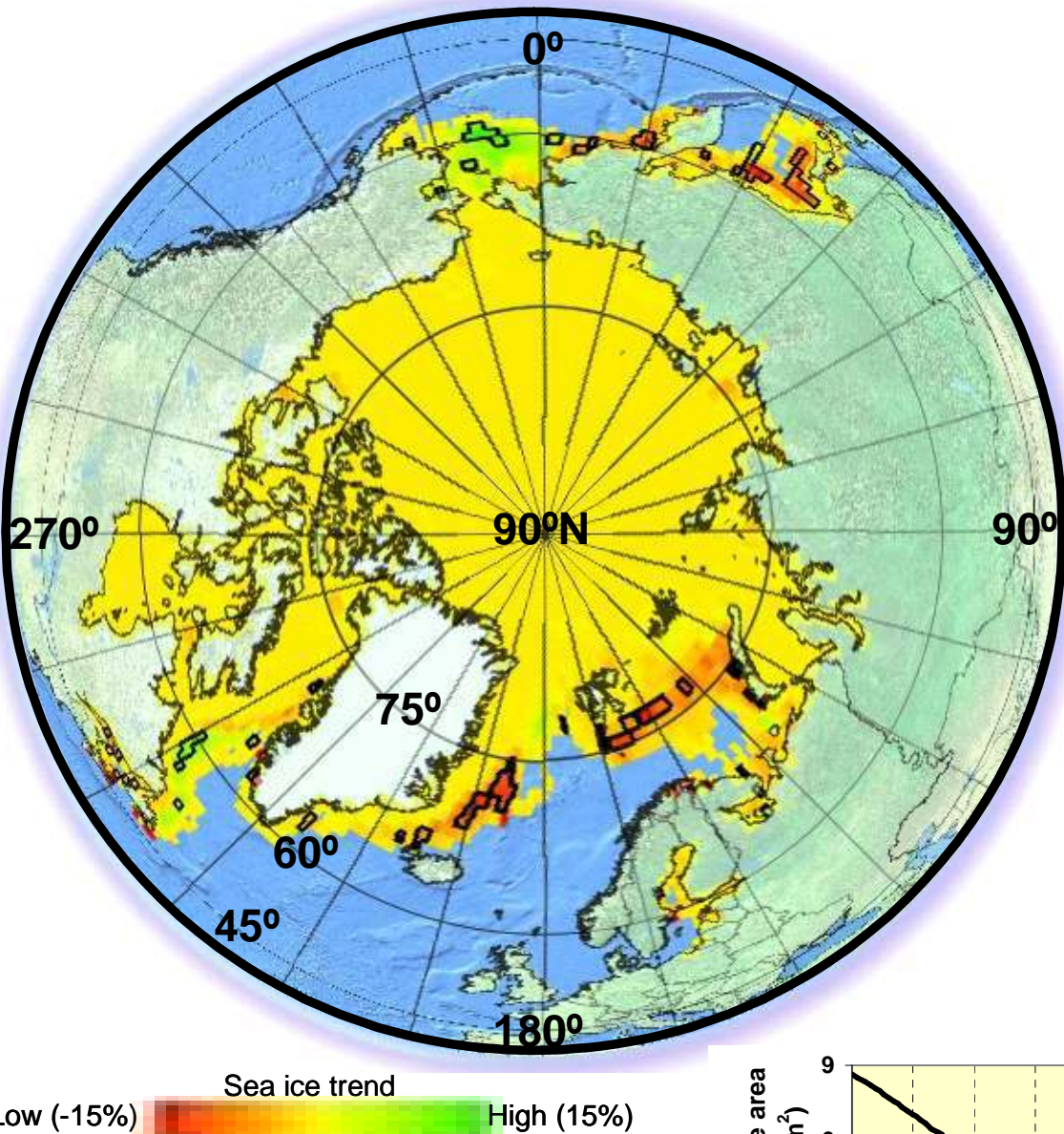


- The pattern of positive trend in the Okhotsk Sea and negative in the Bearing Sea, observed in previous two months is continued in April also. However, majority of areas in both the seas are showing statistically significant trend values.
- The weak negative trends are evident in the Barents and Greenland seas, these areas are showing statistically significant trends in the subsequent (May) month (see respective plates).
- The weak positive trend continue to exist as observed in the month of March.

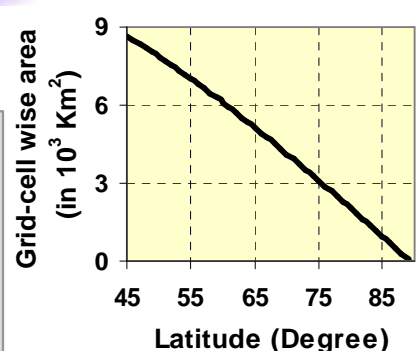


A-7

A-8: Month-wise Sea Ice Trends in the Arctic - May

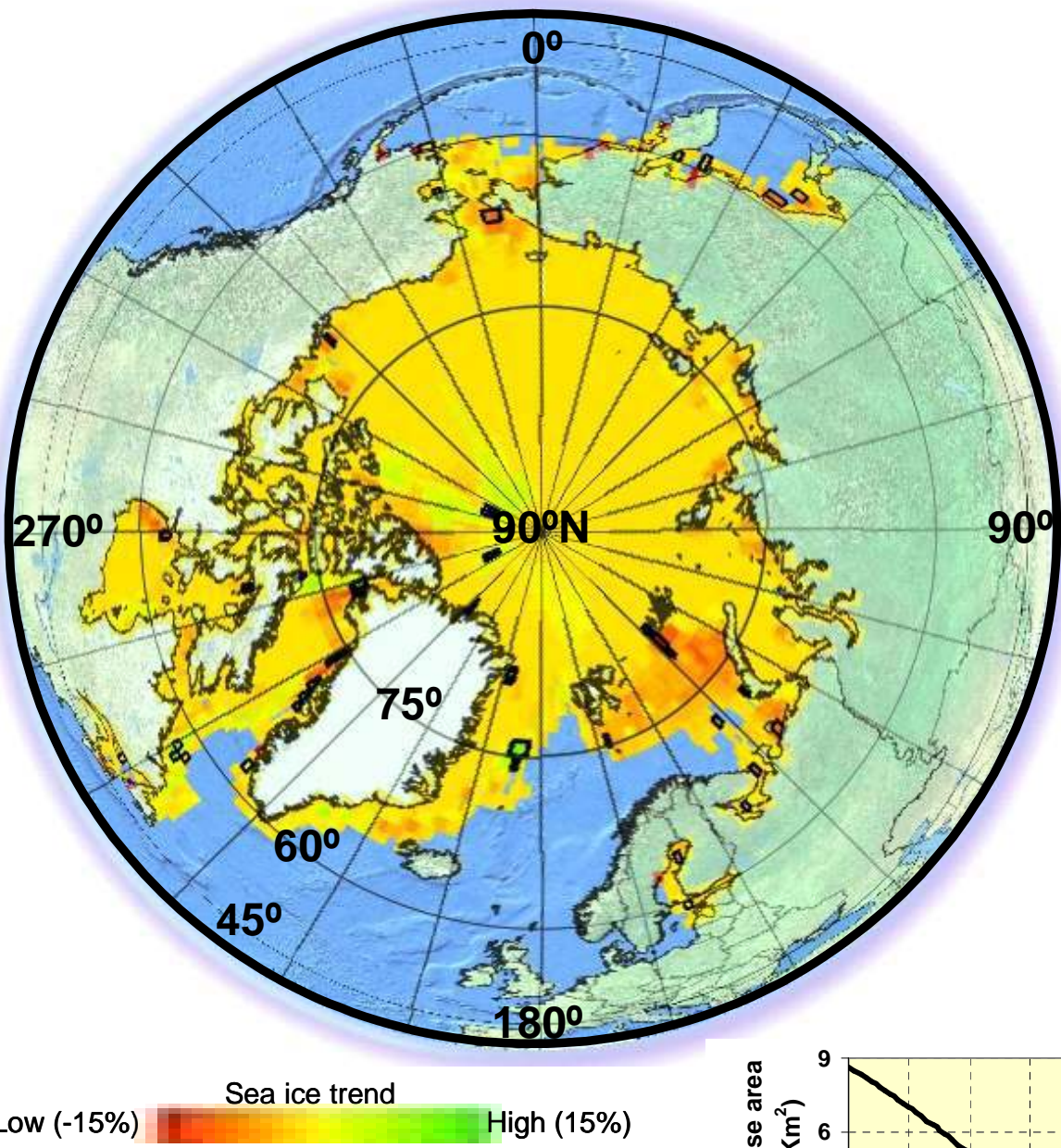


- The pattern of positive trend in the Okhotsk Sea and negative in the Bearing Sea, observed in previous months is also visible in May, however area showing these patterns has reduced from previous months.
- The statistically significant negative trend is evident in the Barents and Greenland seas. The trends in these areas in previous (April) or subsequent (June) are statistically weak (see respective plates).
- The weak positive trend of April changes over to a negative trend in May in the large parts of the Arctic.

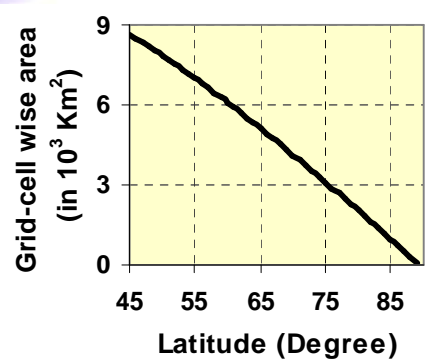


A-8

A-9: Month-wise Sea Ice Trends in the Arctic - June

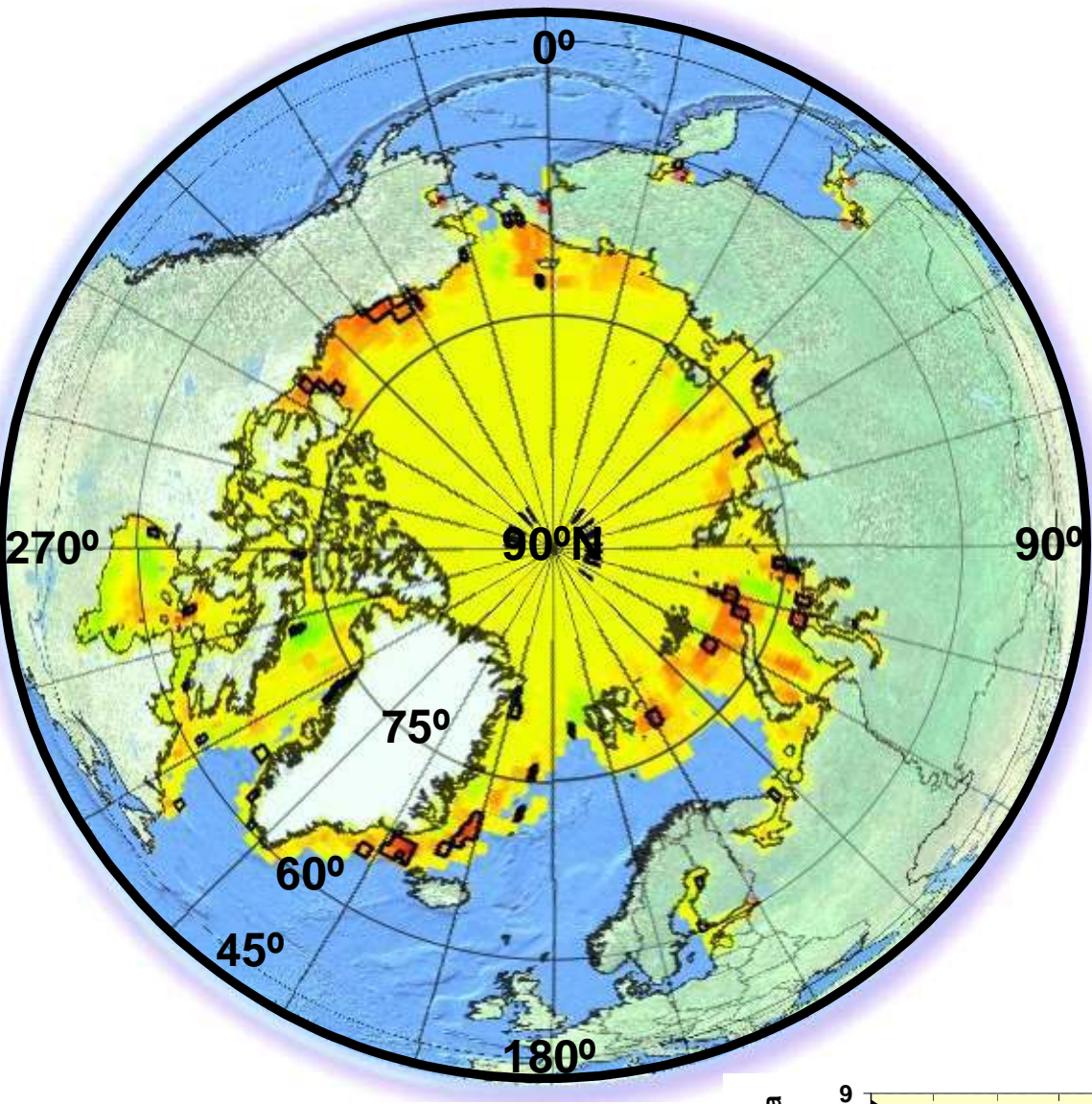


➤ Statistically weak negative trend is evident in the month of June, almost all over Arctic, except in a small region close to North Pole.



A-9

A-10: Month-wise Sea Ice Trends in the Arctic - July

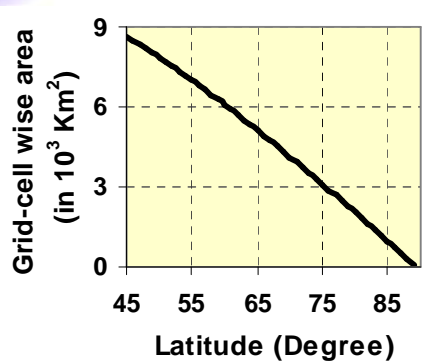


Sea ice trend

Low (-15%)

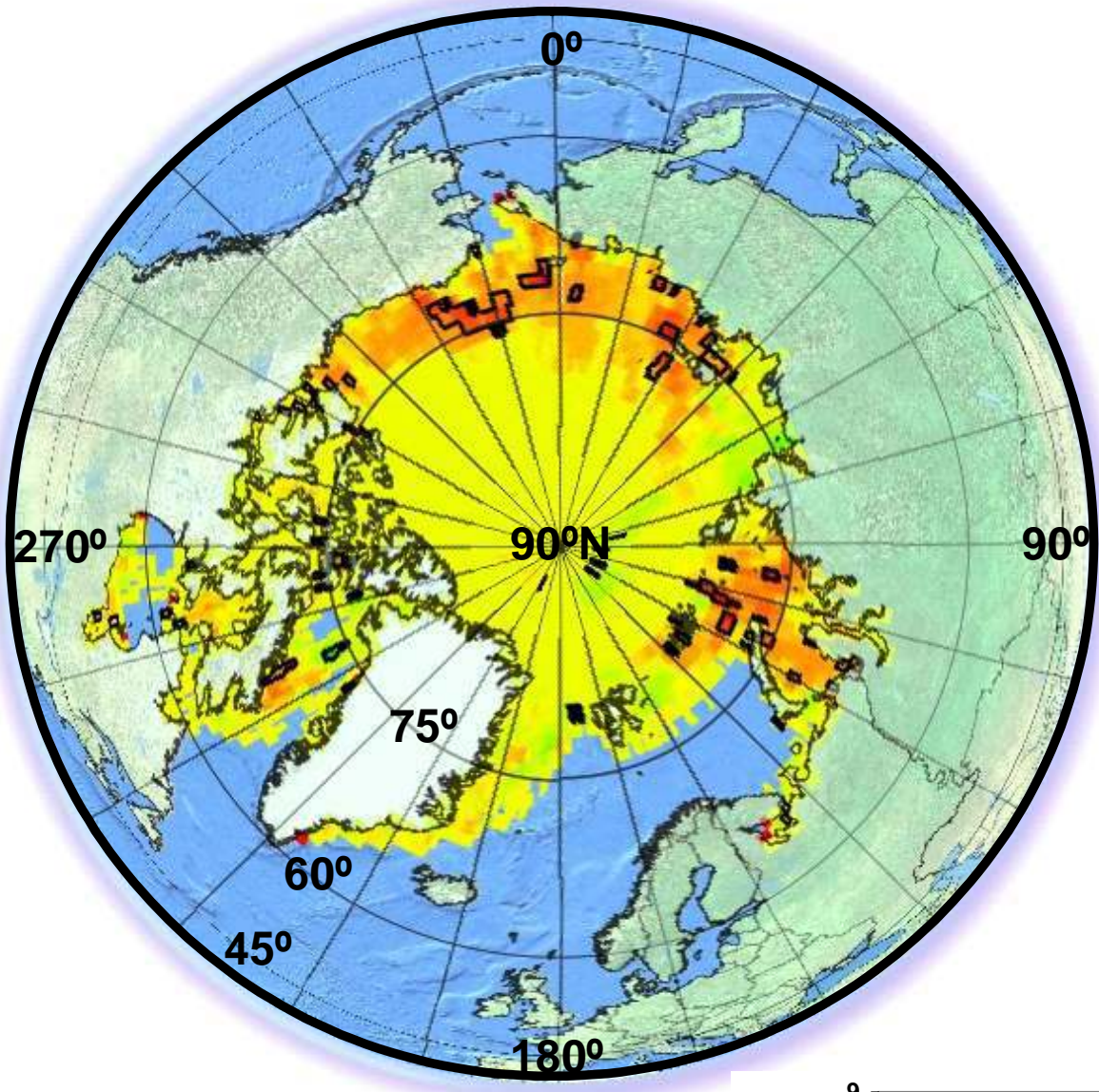
High (15%)

- Some of the area in the Beaufort, Chukchi and Barents Seas starts showing statistically significant negative trend from July, which were showing statistically weak trends in previous (June) month (see respective plates).
- Large parts of the Arctic show a weak positive trend.

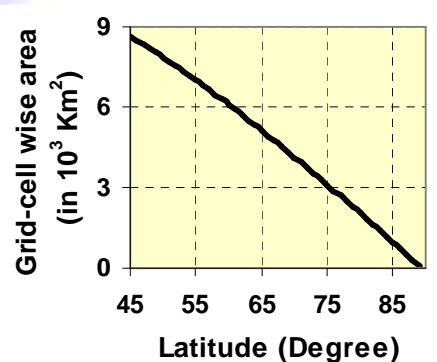


A-10

A-11: Month-wise Sea Ice Trends in the Arctic - August

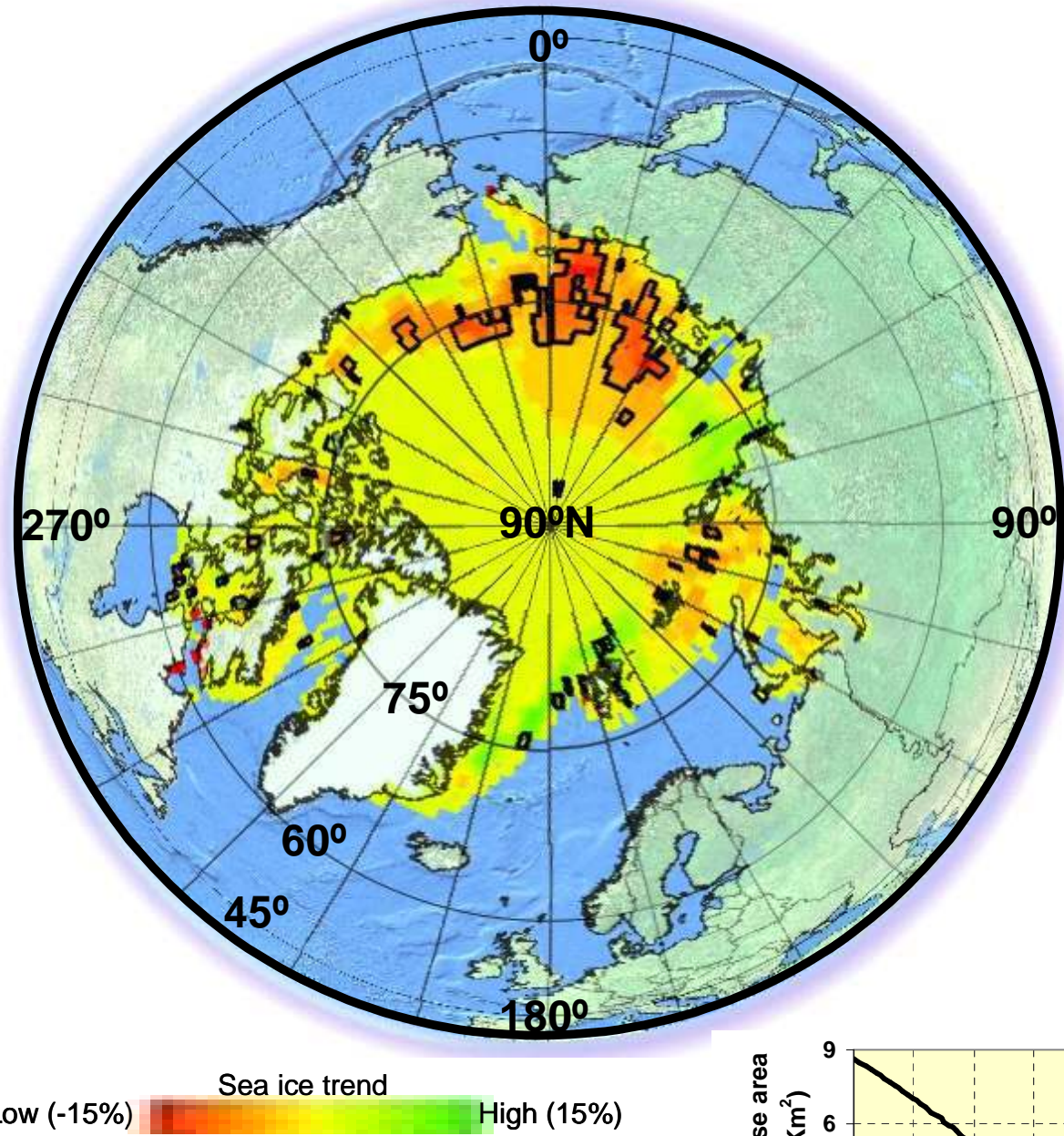


- Majority of the area in the Beaufort, Chukchi and Barents Seas starts showing statistically significant negative trend from July, which is in continuation of the trend from the previous (July) month (see respective plates).
- Some areas close to the pole and in Laptev Sea and near Svalbard show a positive trend. Rest of the Arctic also shows a weak positive trend.

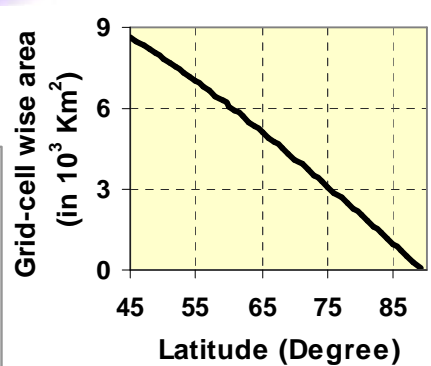


A-11

A-12: Month-wise Sea Ice Trends in the Arctic - September



- The area showing statistically significant negative trend is evident in the large area extending from Beaufort, Chukchi, East Siberian Seas, however negative trend is also visible from Kara to Greenland seas and also in some parts of Laptev Sea.
- Rest of the Arctic shows a weak positive trend.
- The area showing negative trend is higher than that observed in August and lower than that visible in October month. (see respective plates).



A-12

CHAPTER-4

4.0 ANTARCTIC SEA ICE TRENDS

4.1 Physiography of the Antarctic Polar region

Figure 4.1 shows the geographical extent of the Antarctic polar region and the surroundings. The Antarctic region of the southern ocean is surrounded by a circumpolar ocean current. Though the atmosphere in the Antarctic is colder than in the Arctic, the heat flux from the turbulent unprotected sea is much higher. This condition leads to the highly variable sea-ice cover that is 50% larger than the Antarctic continent in winter while it almost disappears in the summer. This leads to the prevalence of lower ice thickness and higher ice drift as compared to the arctic.

An ice cover of up to 20 M sq km extent girdles the Antarctic continent during winter (Eicken and Lemke, 2001). In the summer, patches of perennial ice, covering about 4 M sq km area, remain in the Weddell and Bellingshausen/Amundsen/Ross Sea sectors at 0-60°W and 70-180°W, respectively.

4.2 Analysis of inter-annual variations

The figure 4.2 shows the average SIE (figure 4.2a), for the extreme melting year and one normal year, as well as the average with one SD limits for the

study period (figure 4.2b) for the Antarctic. Inter-annual variations during summer period are also high, of the order of 1.5 M Sq. km in the Antarctic as in the case of the Arctic (2.0 M Sq km). Also, the minimum variability in the Antarctic is in the months of July and November and not in June and November as in the case of the Arctic.

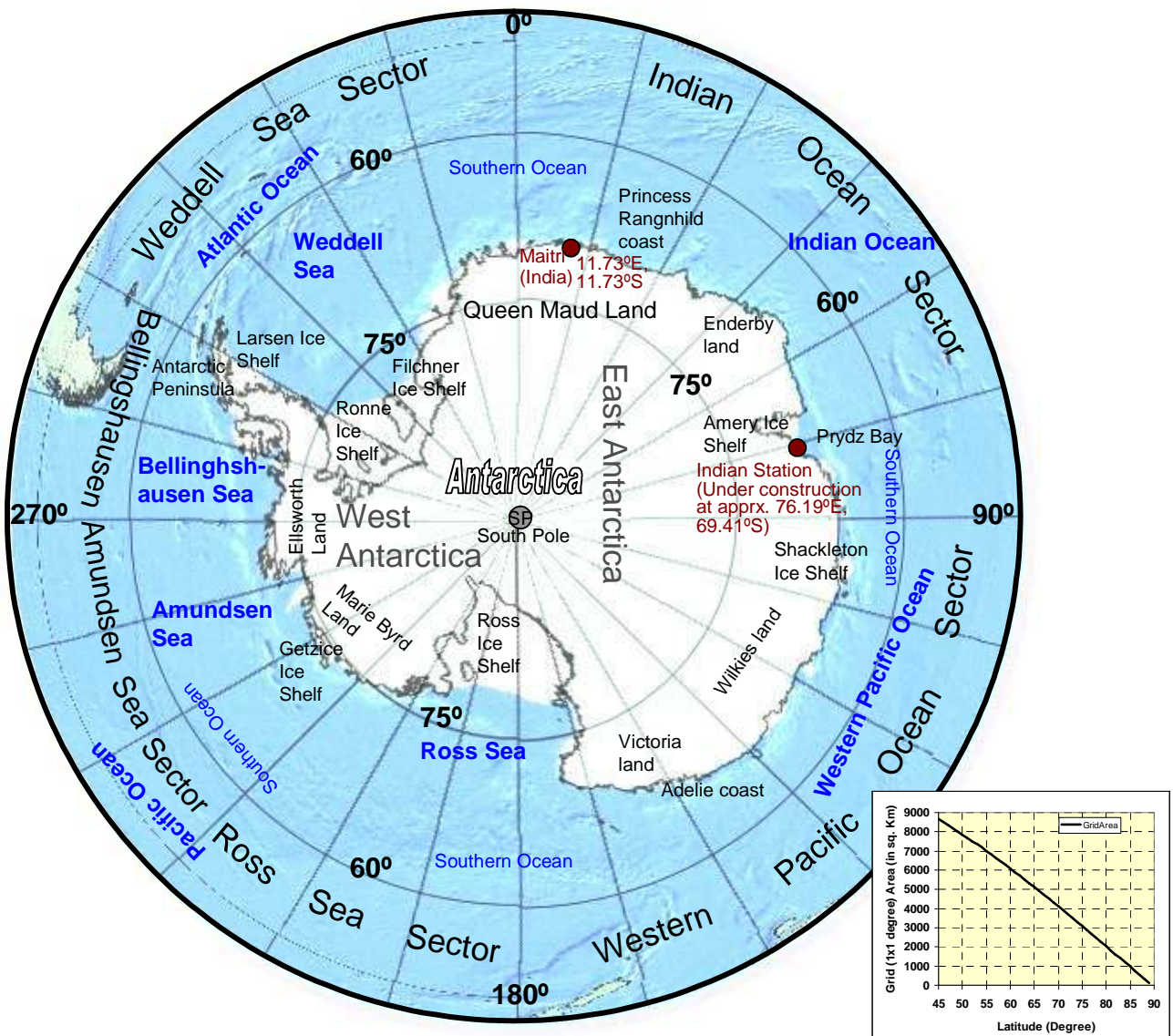


Figure. 4.1 Antarctic polar region and the surroundings

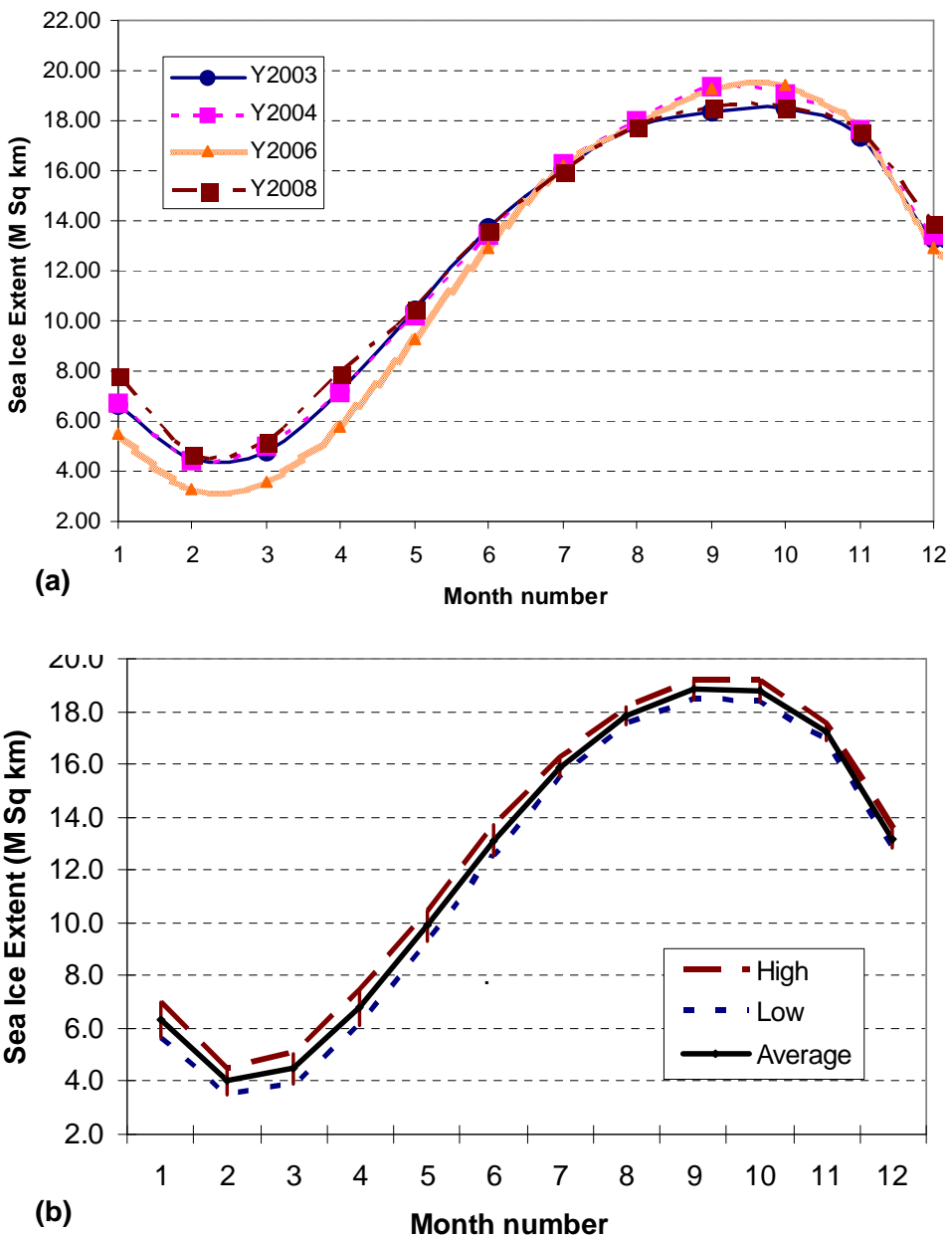


Figure 4.2: Monthly SIE statistics (2000-2008) of the Antarctic (a) Monthly SIE for some of the extreme melting years and one normal study year (b) Average monthly SIE for the entire study period with upper and lower limit of one SD. The following may be noted: (i) the larger variability of the summer minimum compared to winter maximum, (ii) minimum variability in June and November), (iii) summer variability (1.5 M km^2) less than Arctic (2.0 M km^2), and (iv) minimum variability in July and November.

4.3 Grid-wise sea ice trends of maximum and minimum sea ice cover

The grid-wise pattern of recent trends obtained from the derived 1x1 degree SIE data for the summer minimum and the winter maximum are shown in figure 4.3.

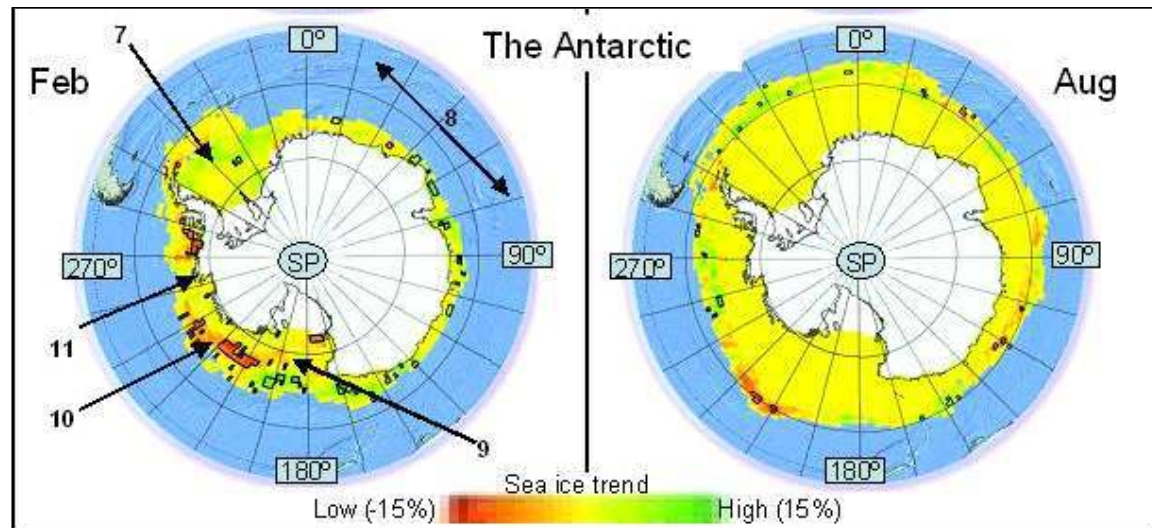


Figure 4.3: Trend observed in summer minimum and winter maximum SIE in the Antarctic. Locations identified with numbers are (7) Weddell, (8) Indian Ocean sector, (9) Ross, (10) Amundsen, (11) Bellingshausen

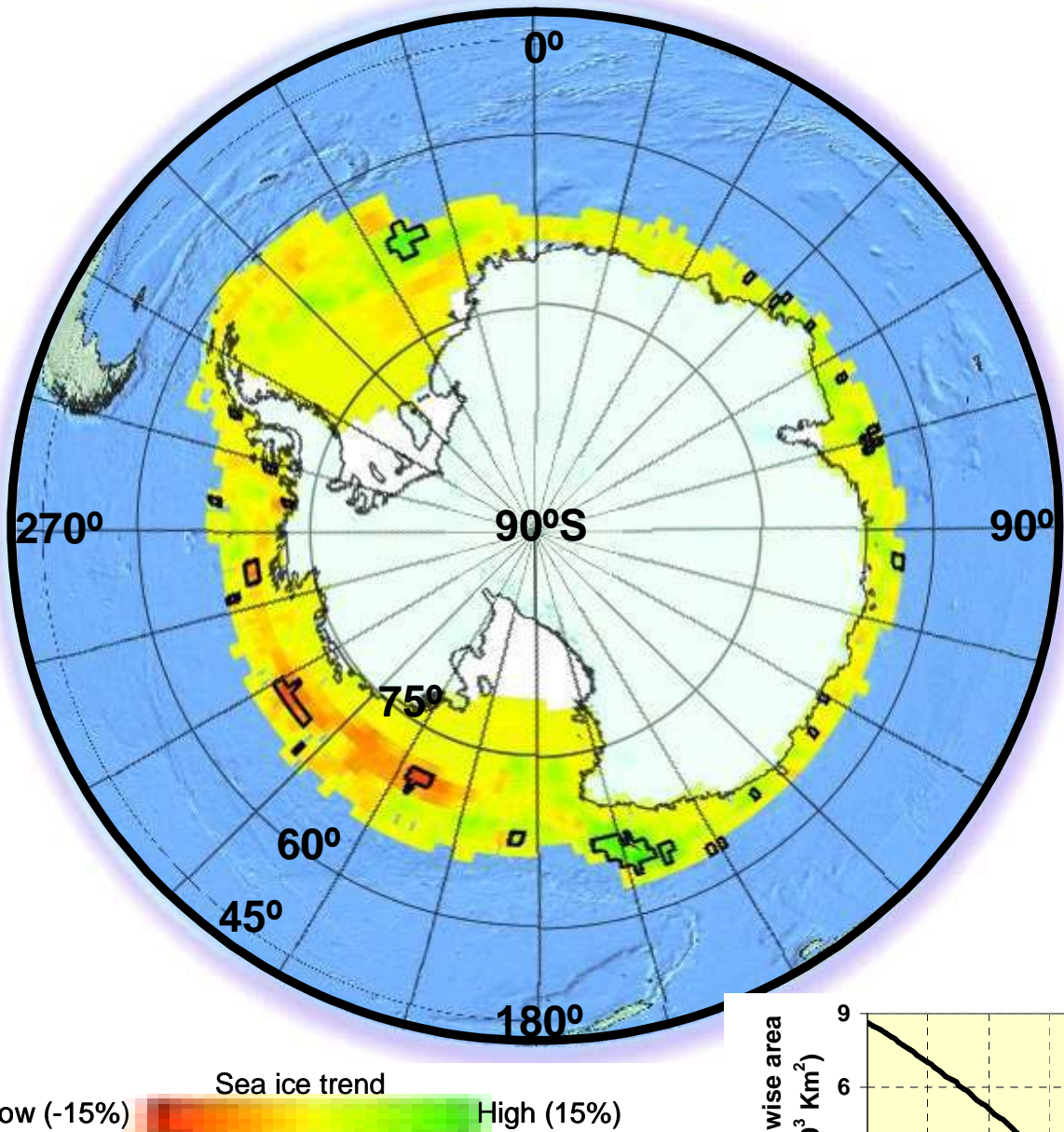
Month-wise trends observed in the Antarctic are shown in colour plate B1 to B12. Black colored Polygons in the sea ice region indicate grids showing statistically significant trends at 95% confidence interval. The sector-/region-wise summary of the trends observed in the Antarctic are shown in Table 4.1.

Table 4.1: Summary of the grid-wise trend observed in the Antarctic

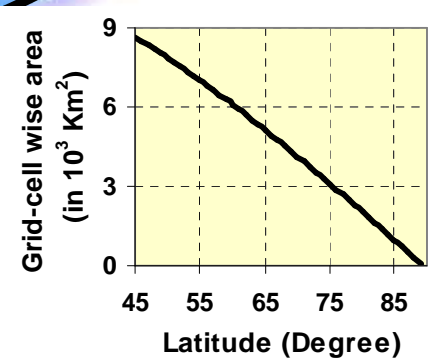
Region Name	Jan	Feb	Mar	Apr	May	Jun	Jul	Aug	Sep	Oct	Nov	Dec
Southern Ocean north of Indian Station Maitri (345 E – 30 E)	-/+S	+	-/+	- /+S	-/+S	-/+S	- /+S	+S	++S	++S	++S	-/+S
Southern Indian Ocean north of Enderby Land (30 E – 60 E)	-S	+S	-/+	+S	-/+S	-/+S	++	+S	-/+S	++S	++S	-/+
Southern Indian Ocean north of Amery Ice Shelf / Proposed Indian Station Bharati (60 E – 90 E)	-	++S	-/+	++ S	-S	-/+S	+	+	-/+S	+	+	-S
Western Pacific Ocean, North of Shackleton Ice Shelf (90 E – 105 E)	-	++S	-/+	+S	-/+S	-	+	+	++	+	++S	-
Western Pacific Ocean, North of Wilkies Land (105 – 135 E)	-S	+S	-	-/+	-	-S	+	-/+S	++	+S	+S	-
Western Pacific Ocean, North of Victoria Land (off Adelie Coast) (135- E 165 E)	-S	++S	++S	+	-	-	+	-/+S	++S	+S	++S	-/+S
Ross Sea Sector (165 E – 225 E)	-/+S	-/+S	-/+S	++ S	-S	-/+S	+S	-S	++	-/+S	-/+S	-/+S
Amundsen Sea Sector (225 E-270 E)	--S	-/+S	- -S	-/+	-/+S	-S	++ S	++S	++S	++S	-/+S	-S
Bellingshausen Sea Sector (270 E – 300 E)	--S	-S	-	-S	-/+S	-S	++ S	+S	-/+S	-/+S	-/+S	-
Weddell Sea Sector (300 E - 345 E)	-/+S	+S	++S	-/+	-/+S	-/+S	- /+S	++S	-/+S	-/+S	+	-/+S

Explanation of symbols used: Strong Negative trend (--), Weak Negative (-), No definite trend (.), Weak Positive (+), Strong Positive (++) , Statistically Significant (S).

B-1: Month-wise Sea Ice Trends in the Antarctic - March

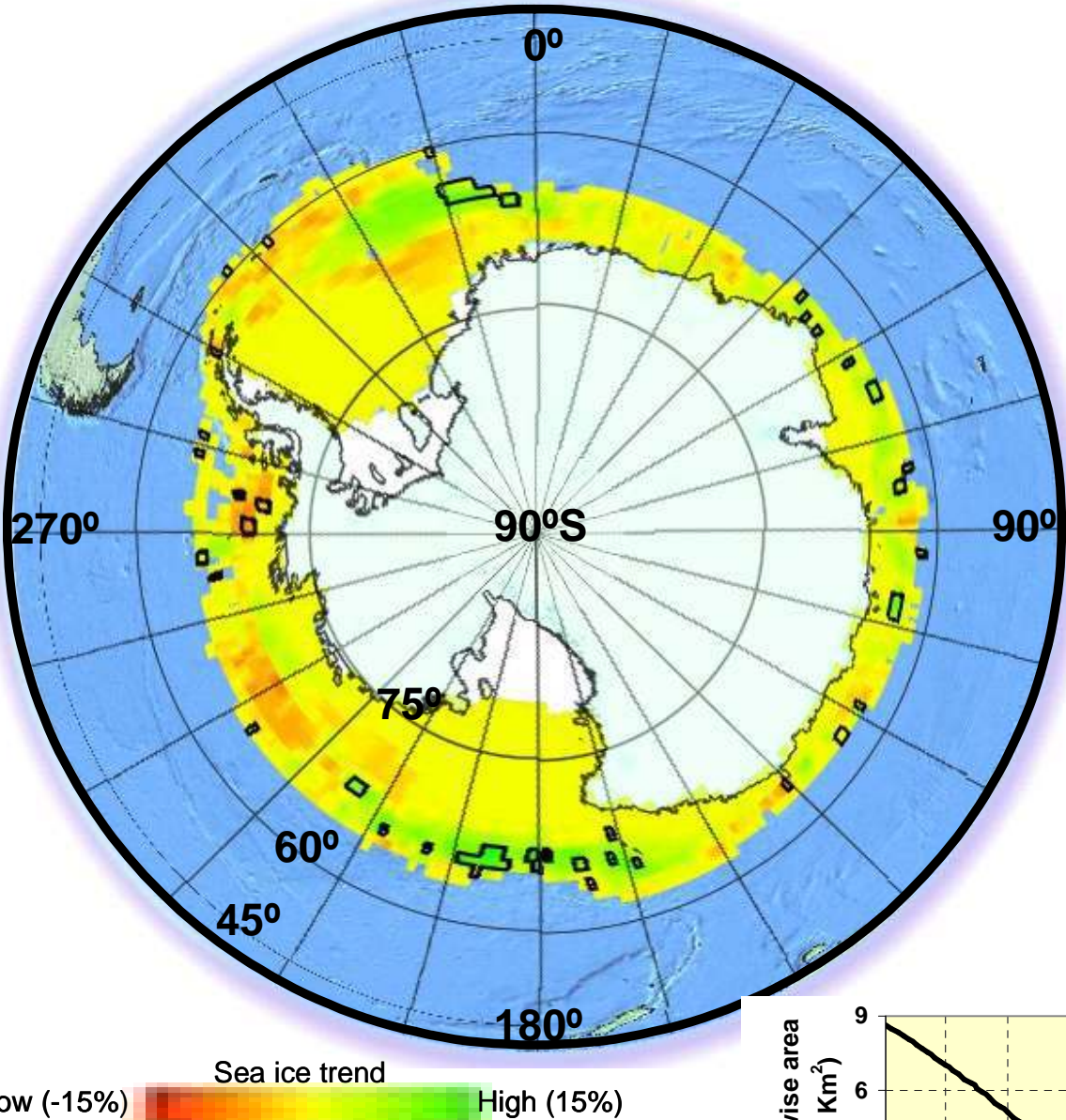


- Statistically significant positive trend is observed in Western Pacific Ocean Sector ($[\text{Long:Lat}]=[65^{\circ}:67.5^{\circ}]$) and Weddell Sea Sector ($[\text{Long:Lat}]=[337^{\circ}:67.5^{\circ}]$). This trend continues in subsequent April month also (see respective slide)
- Parts of Amundsen Sea show statistically significant negative trend.
- However, large parts of the Antarctic show statistically weak positive trend.

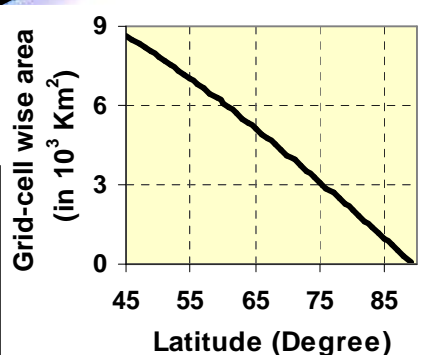


B-1

B-2: Month-wise Sea Ice Trends in the Antarctic - April

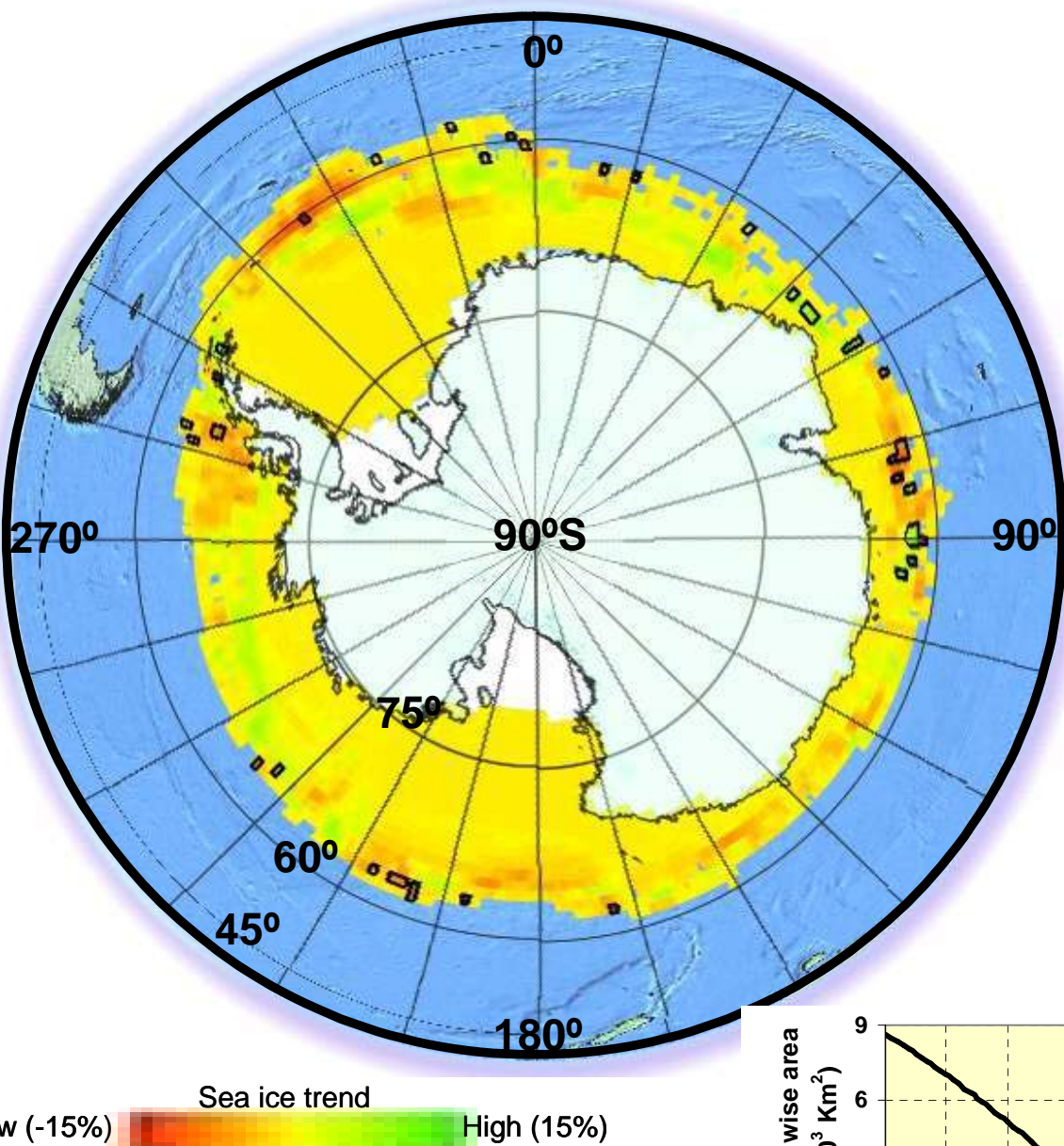


- Statistically significant positive trend is observed in Western Pacific Ocean Sector ([Long:Lat]=[65°:67.5°]) and Weddell Sea Sector ([Long:Lat]=[337°:67.5°]). This trend continues in subsequent April month also (see respective slide)
- Parts of Amundsen Sea show statistically weak negative trend as against statistically significant trend in previous month of March.
- The weak positive trend observed in the large parts of Antarctic in the month of March is reduced in April.

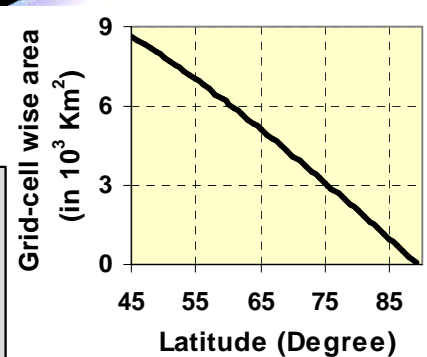


B-2

B-3: Month-wise Sea Ice Trends in the Antarctic - May

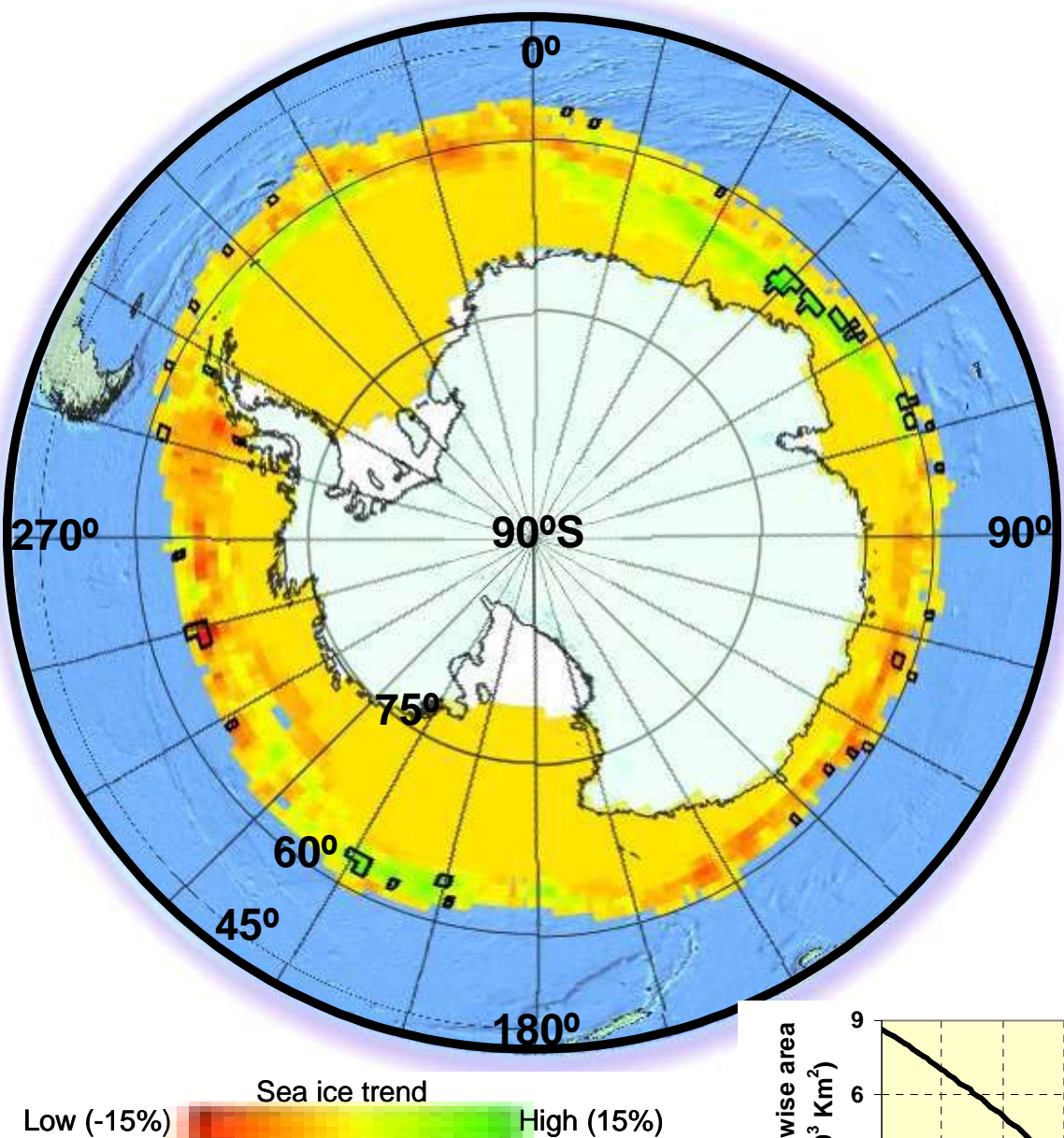


- The reduction in the areas with statistically weak positive trend from March to April is continued and large parts of the Antarctic changes over from positive to statistically weak negative trend in the month of May.
- However, parts of Amundsen Sea changes over from statistically weak negative trend to weak positive trend.

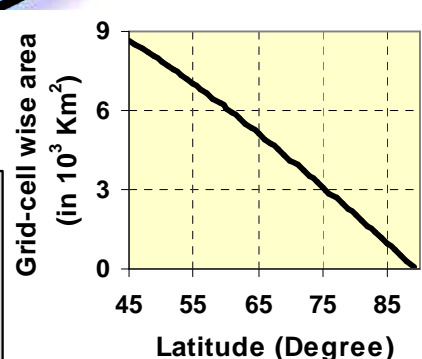


B-3

B-4: Month-wise Sea Ice Trends in the Antarctic - June

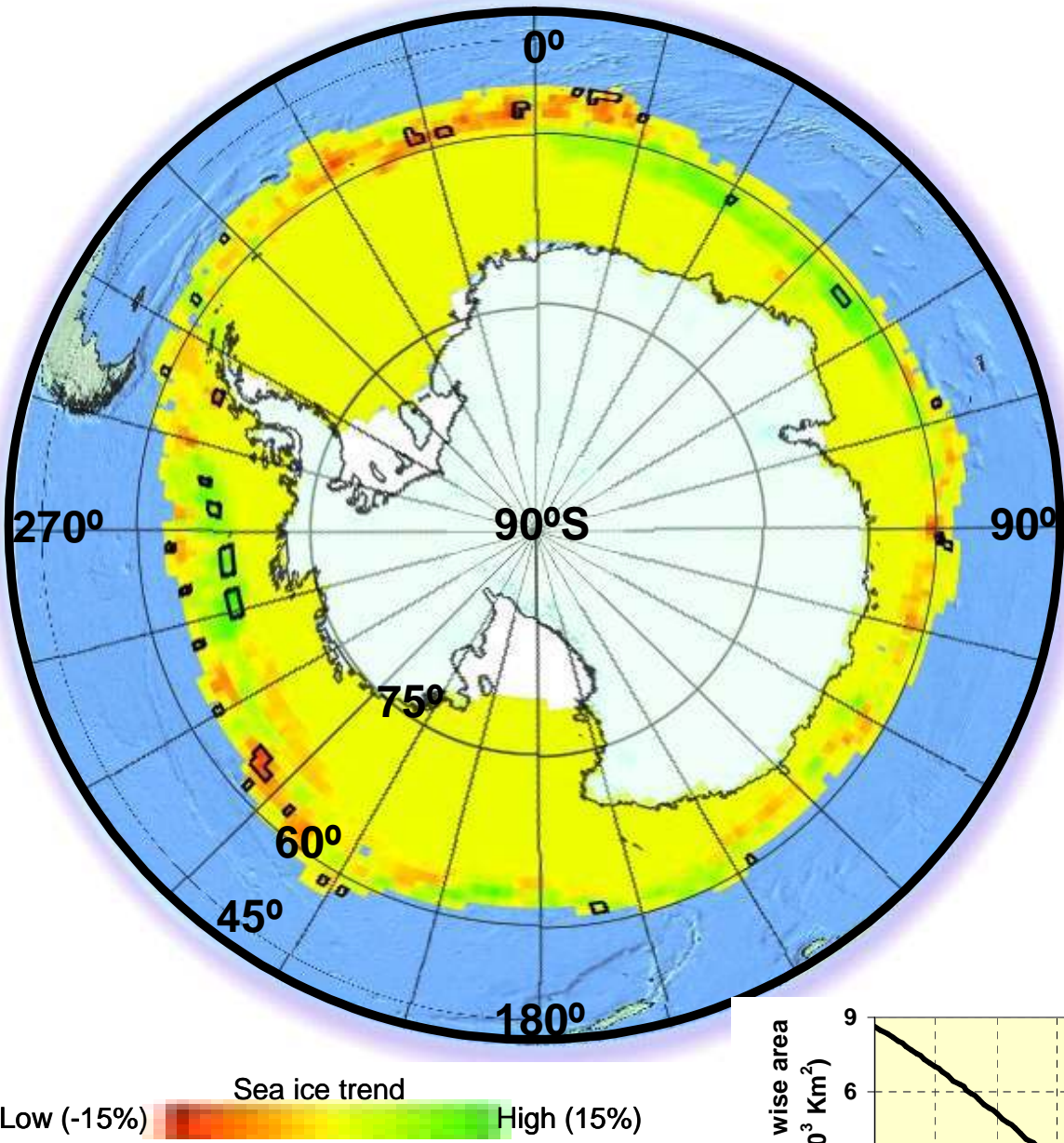


- The statistically significant positive trend is observed in the parts of Indian Ocean Sector and Ross Sea Sector.
- The change over (from May to June) of the trend from positive to negative in the parts of Amundsen Sea and from negative to positive in the Ross Sea are interesting observations.
- In rest of the Antarctic, statistically weak negative trend is observed.

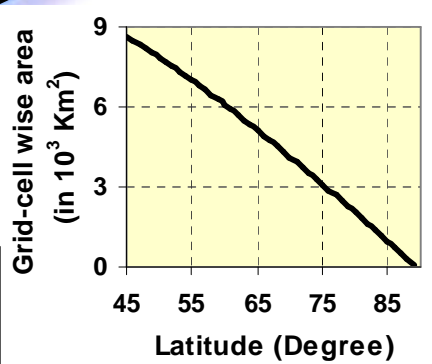


B-4

B-5: Month-wise Sea Ice Trends in the Antarctic - July

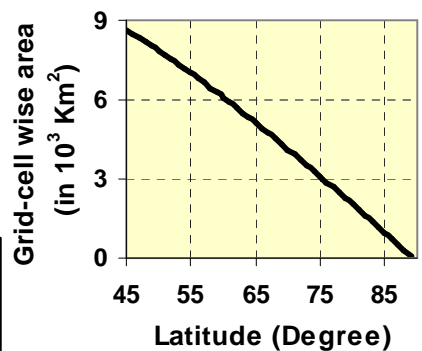
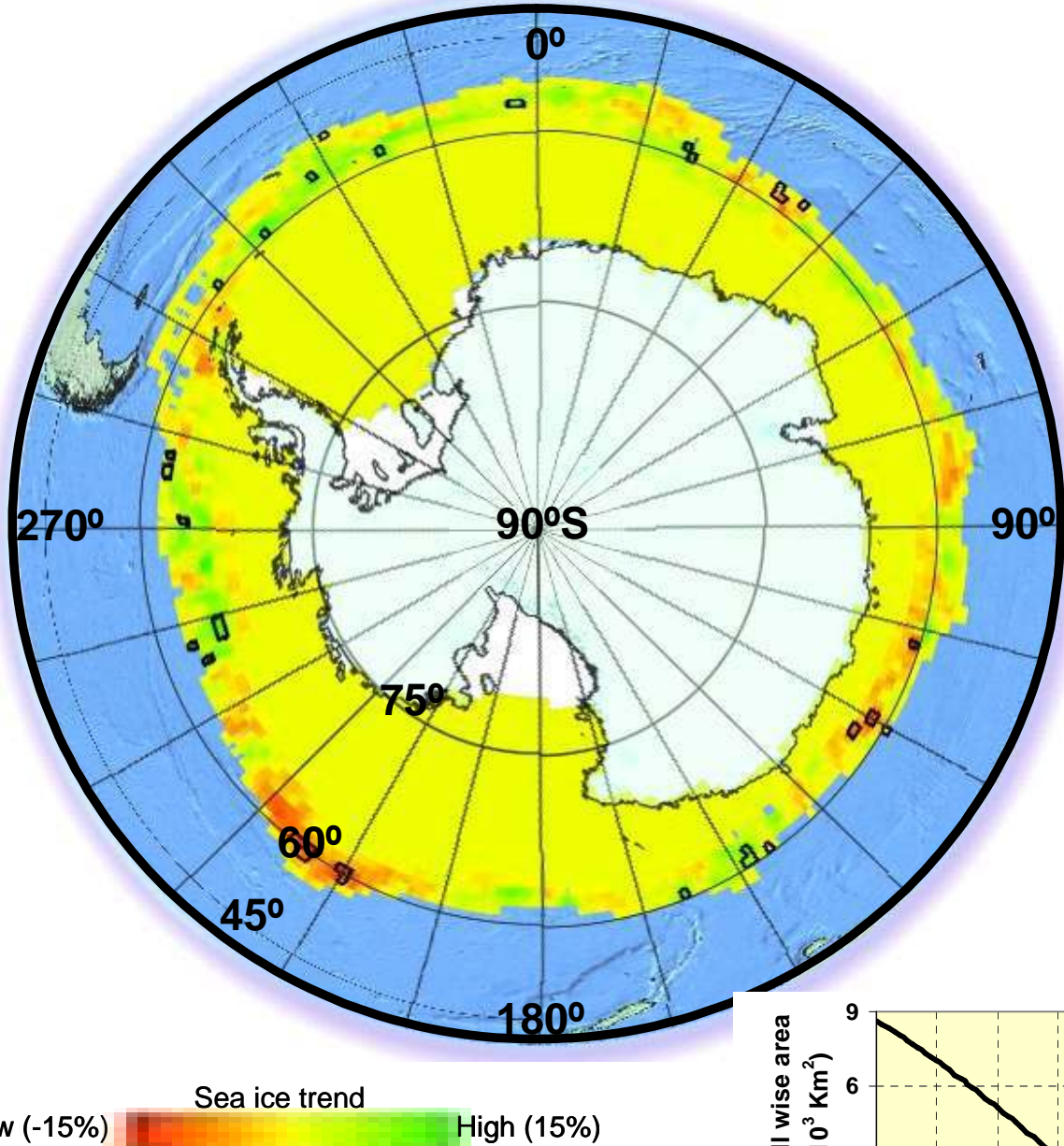


➤ The reversal of trend from weakly negative in the month of June to weakly positive trend in July month, in large parts of the Antarctic, is observed.



B-5

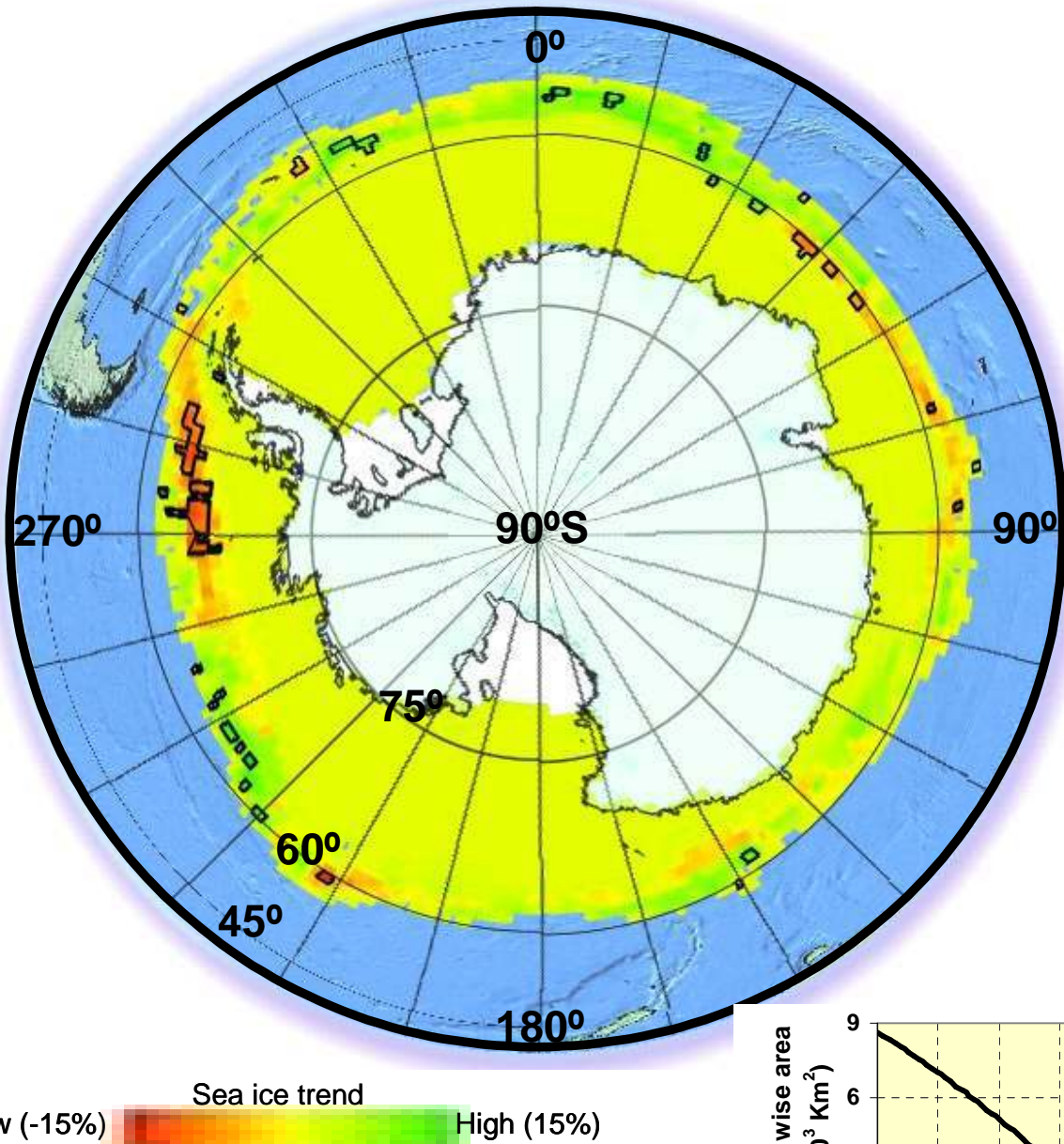
B-6: Month-wise Sea Ice Trends in the Antarctic - August



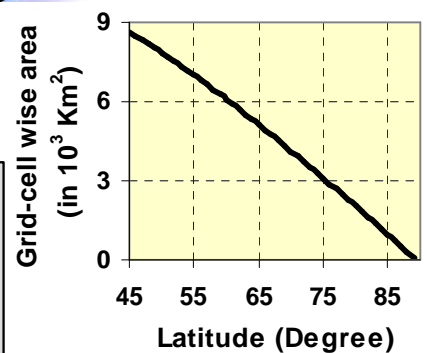
- As observed in the month of July, weakly positive trend is also observed in August month in large parts of the Antarctic.
- Statistically weak negative trend is also observed in the Ross Sea sector ($[\text{Long:Lat}] = [217^\circ:60^\circ]$)

B-6

B-7: Month-wise Sea Ice Trends in the Antarctic - September

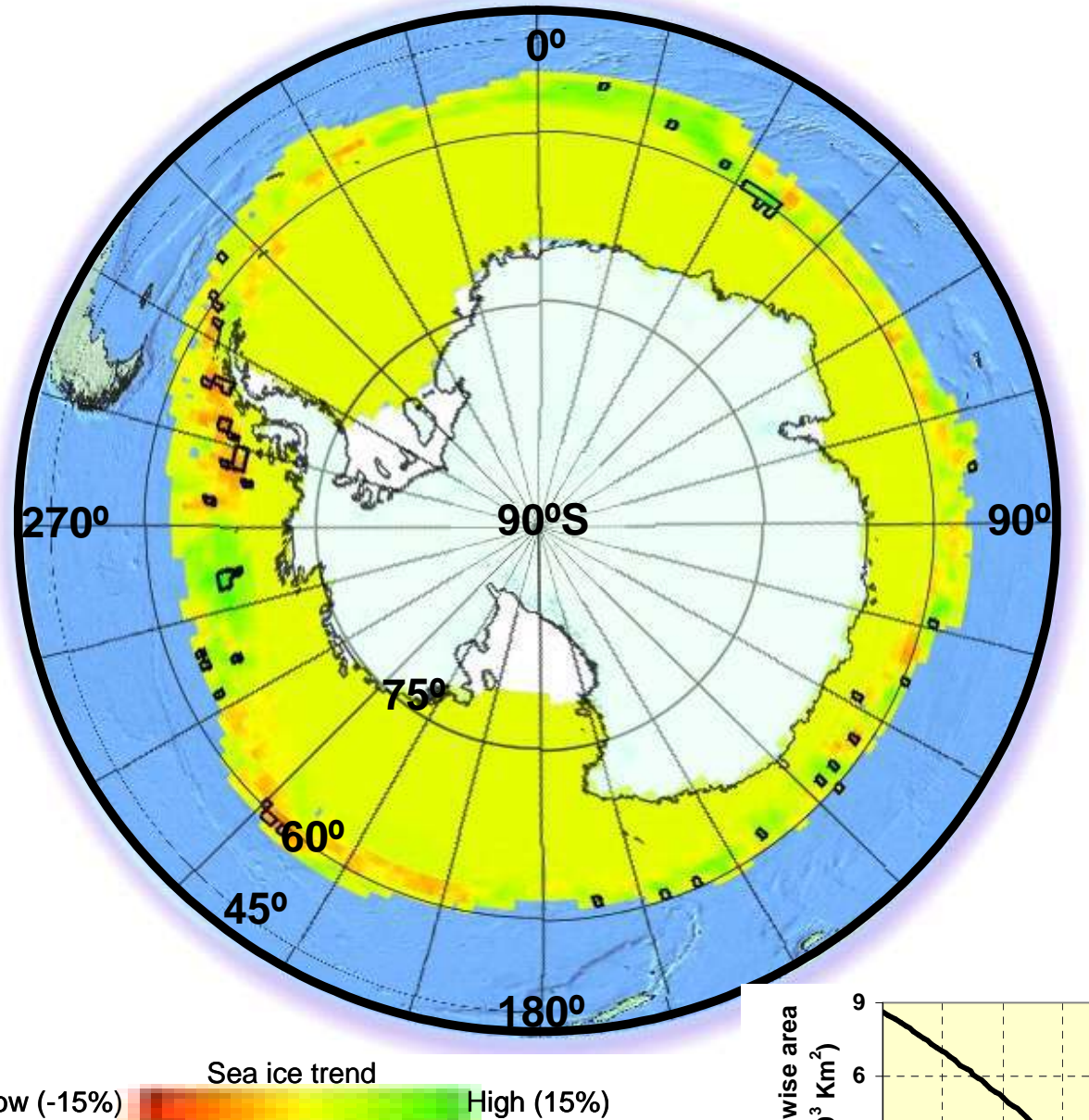


- As observed in the months of July and August, positive trend is dominant in the large parts of the Antarctic in September month.
- The reversal of trend from weakly positive in the month of August to statistically significant negative trend in Bellinghhausen Sea is observed in the month of September.

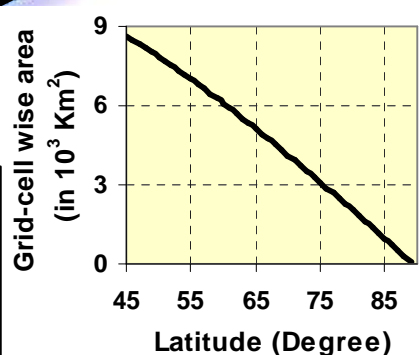


B-7

B-8: Month-wise Sea Ice Trends in the Antarctic - October

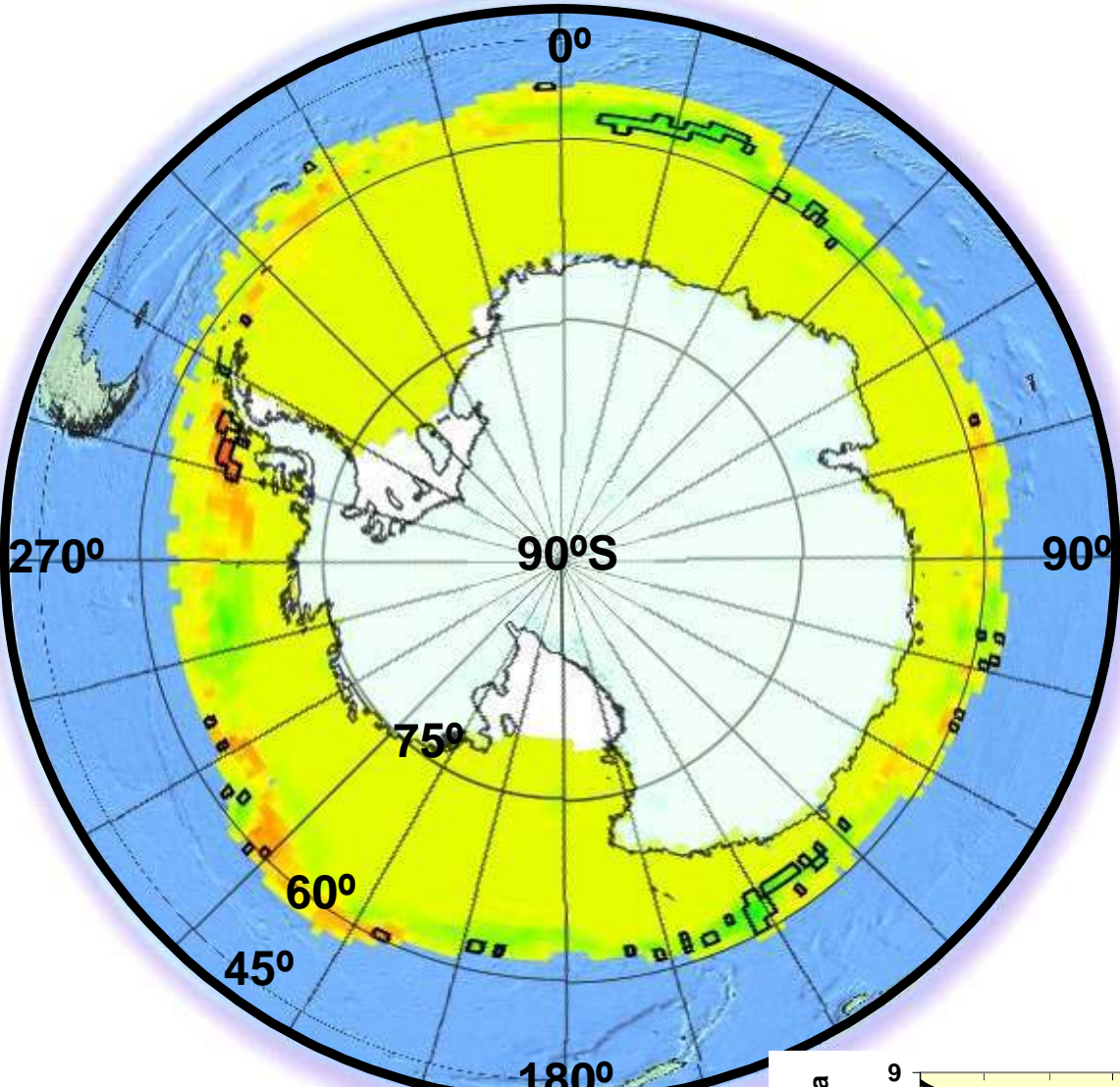


- As observed in the months of July to September, positive trend is dominant in the large parts of the Antarctic in October month.
- Parts of the Bellinghausen Sea, near the Antarctic Peninsula, are showing statistically weak negative trend, which were showing statistically significant trends in the previous September month (see respective slide).
- The areas showing negative trends are higher in Western side of the Antarctic as compared o the Indian Ocean and Western pacific sectors located in the Eastern side.

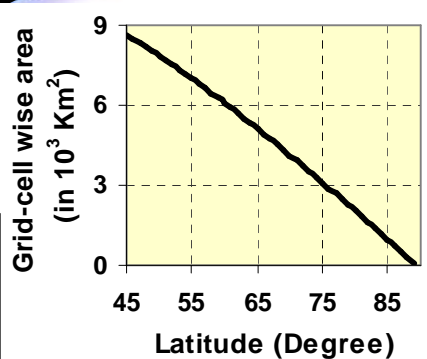


B-8

B-9: Month-wise Sea Ice Trends in the Antarctic - November

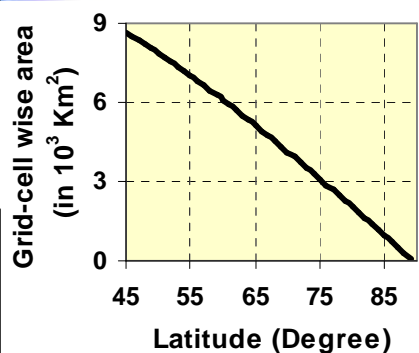
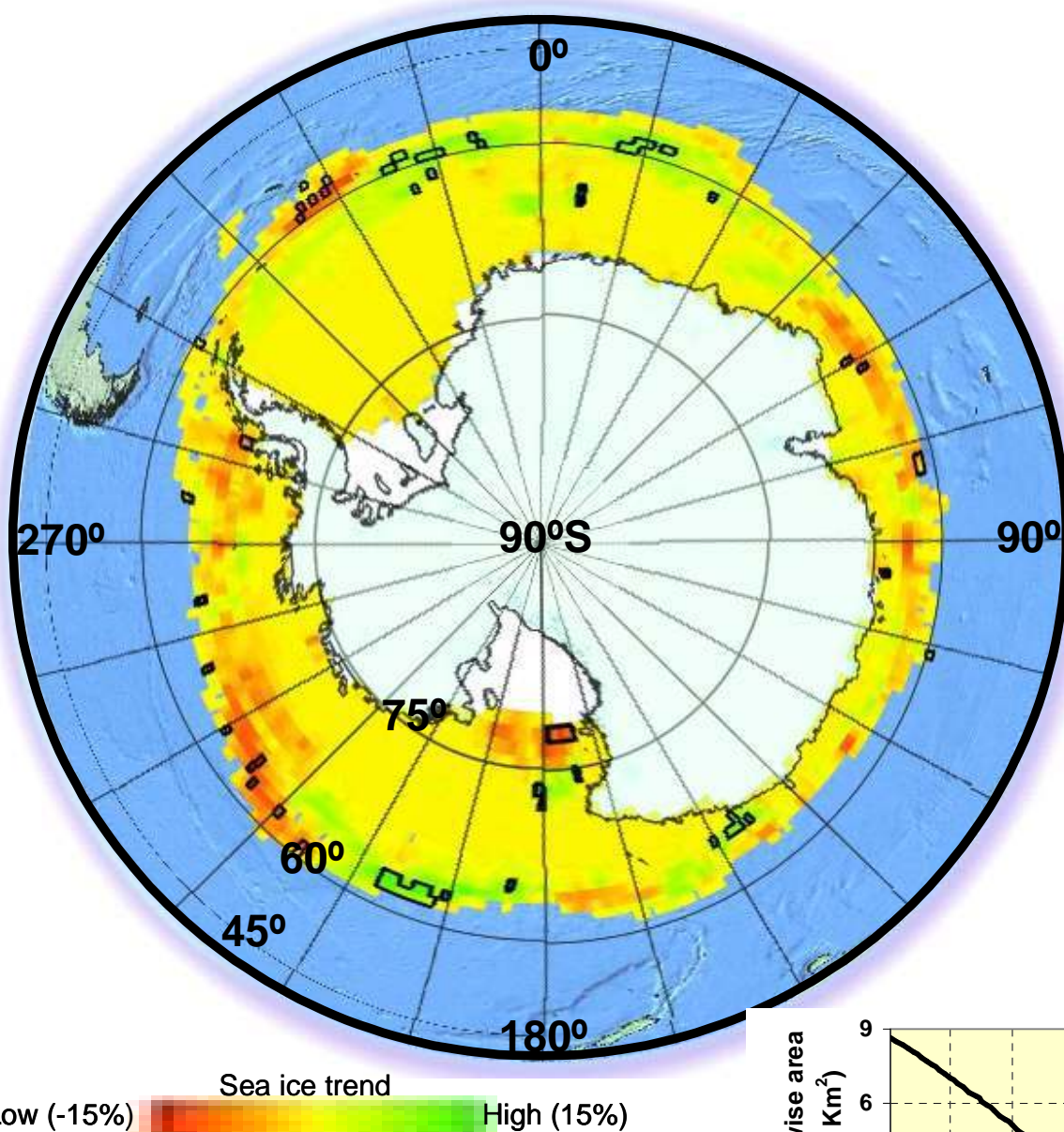


- Large area of the Antarctic is showing the positive trend, however weakly negative trend is also observed in the western side of the Antarctic.
- Large parts of the Indian ocean sector and western pacific sector are showing statistically significant positive trend, which were statistically weak in previous months (see respective slides).



B-9

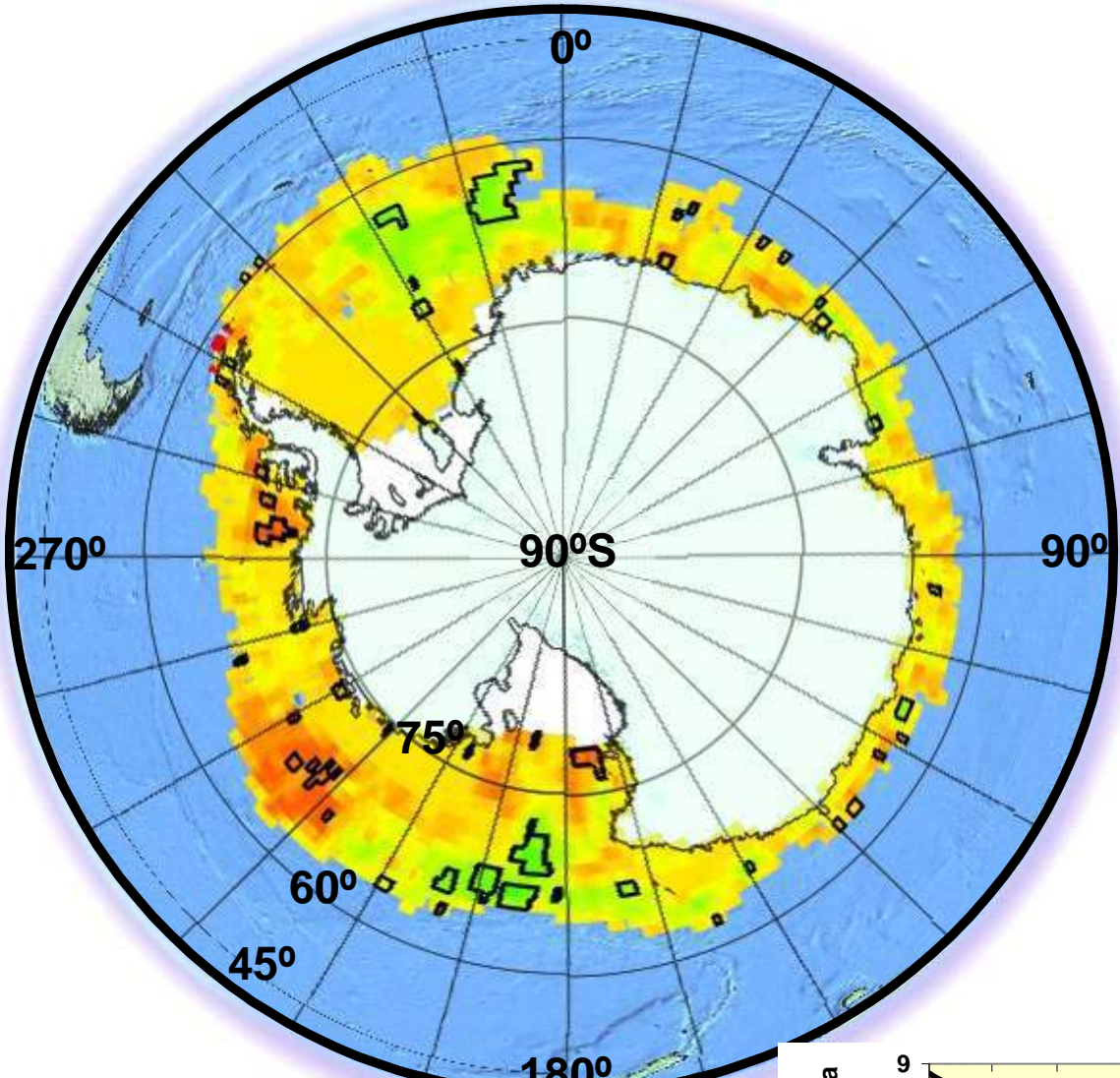
B-10: Month-wise Sea Ice Trends in the Antarctic - December



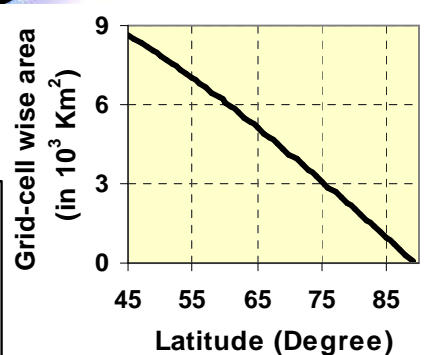
- The trend reversal from positive to negative trend (observed in the months of July-November) in the large parts of the Antarctic is observed in the month of December month.
- Some of the areas in Weddell Sea, Indian Ocean and Ross Sea sectors are showing positive trends.

B-10

B-11: Month-wise Sea Ice Trends in the Antarctic - January

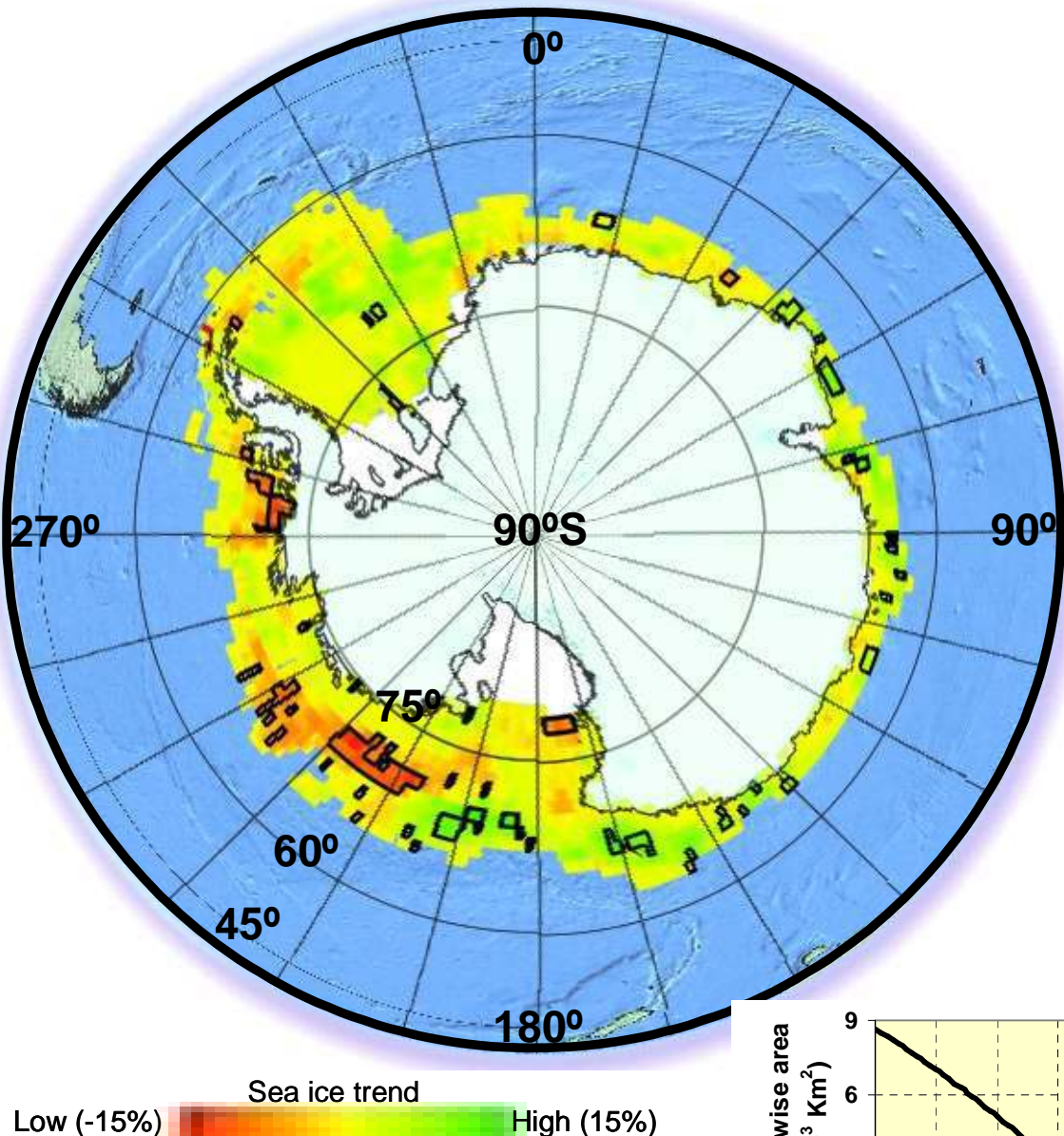


- The negative trend observed in large parts of the Antarctic in previous December month is continued in January month also.
- Some of the areas in Weddell Sea sector are showing positive trends.
- The parts of Ross Sea Sector nearer to Amundsen Sea are showing negative trend, whereas parts nearer to Western Pacific Sector shows statistically significant positive trend.

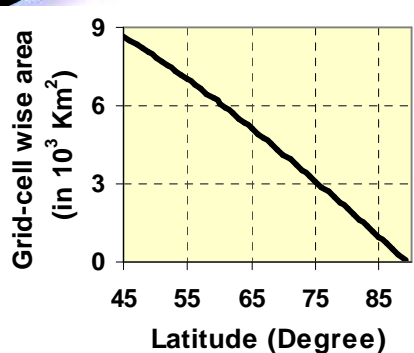


B-11

B-12: Month-wise Sea Ice Trends in the Antarctic - February



- The reversal of trend from negative (in January) to positive (in February) is observed in the large parts of the Antarctic.
- The parts of Ross Sea Sector nearer to Amundsen Sea are showing statistically significant negative trend, whereas parts nearer to Western Pacific Sector shows statistically significant positive trend (similar to previous month of January).



B-12

CHAPTER-5

5.0 INTER-COMPARISON OF HEMISPHERIC SEA-ICE PATTERNS

5.1 Inter-annual variations in sea ice extent

As observed in figure 5.1, the coefficient of variation (CV), which is indicative of standard deviation as a percentage of mean SIE, is almost 12% in summer months in both the hemispheres. The nearly constant (2%) CV during the period from August to November is a distinctive pattern in the Antarctic. In case of the Arctic, it shows marginal variations from 2 to 3 per cent during December to May.

A drastic drop in CV from October to November for the Arctic may be noticed from the figure, after which it remains around 2 to 3% only. The October month is the beginning of winter re-freezing in the Arctic. This indicates that re-freezing process is highly variable from year to year in the months of October and November. In contrast, the value of CV exhibits a sudden rise for the Antarctic from December to January, which are the months of predominant melting. This suggests that the melting process (not the freezing process) is highly variable from year to year in the southern polar ocean from December to next January.

The point of inflexion in the Antarctic is in the month of December and then again in July. After the month of December, melting process dominates till the month of July, with peak melting in the month of April. From the July month, re-freezing of sea ice dominates over the ice melting process.

5.2 Sea ice growth cycle

The monthly sea ice growth profile, from the onset of freezing to end of melting period is shown in figure 5.2. It is seen that in case of the Arctic, it takes longer time, seven months, for the melting process, whereas refreezing is faster, and takes only 5 months.

On the contrary, in case of the Antarctic, the melting of sea ice is taking much smaller time (5-months) as compared to refreezing (7-months). The reason for this kind of behavior in the Antarctic could be the influence of Antarctic circumpolar ocean current (with temperature gradient across its width) surrounding the Antarctic sea ice region. However, the landmass and the narrow outlets in to the Atlantic and the Pacific oceans isolate the Arctic region, from the influence of the oceans. This could be the reason for fast refreezing of sea ice due to the absence of direct interaction with relatively warmer ocean currents in majority of the areas.

5.3 Correlation between the Arctic and the Antarctic Sea Ice Extents

Figure 5.3 shows the scatter plot of monthly Arctic and Antarctic SIE. Both of these regions are in opposite hemispheres, hence the quantity of solar insolation and consequently, the SIE will be out of phase by six months. It is seen that the increase/decrease of monthly SIE in the Arctic is highly correlated with the corresponding decrease/increase of SIE in the Antarctic.

The behavior appears to be slightly nonlinear and therefore a second order polynomial fit was attempted, which is also shown in figure 4.7. The cause of non-linearity could be the difference between the geographic and the

oceanographic surroundings of the two regions that govern the pace of the melting and freezing processes occurring there.

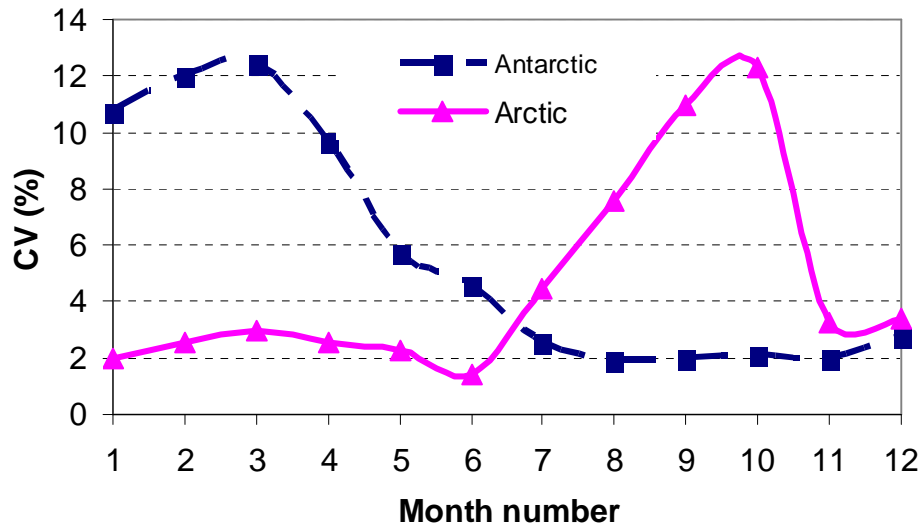


Figure 5.1: Month-wise Coefficient of variation observed in SIE during the period from 1999-2008. Low variability in winter and high variability in the summer months of corresponding summer months may be noted.

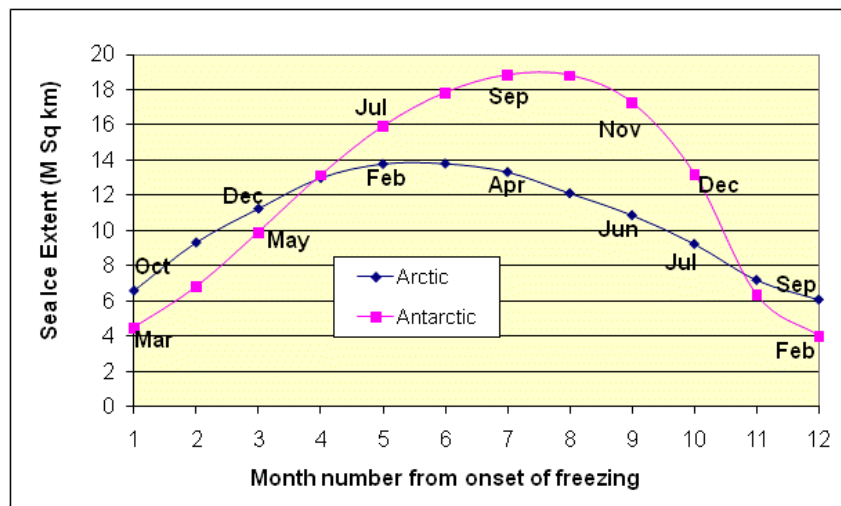


Figure 5.2: Sea Ice Growth profiles (Note that the build up of ice is fast and decay is slow in the Arctic. This is just the opposite in the Antarctic)

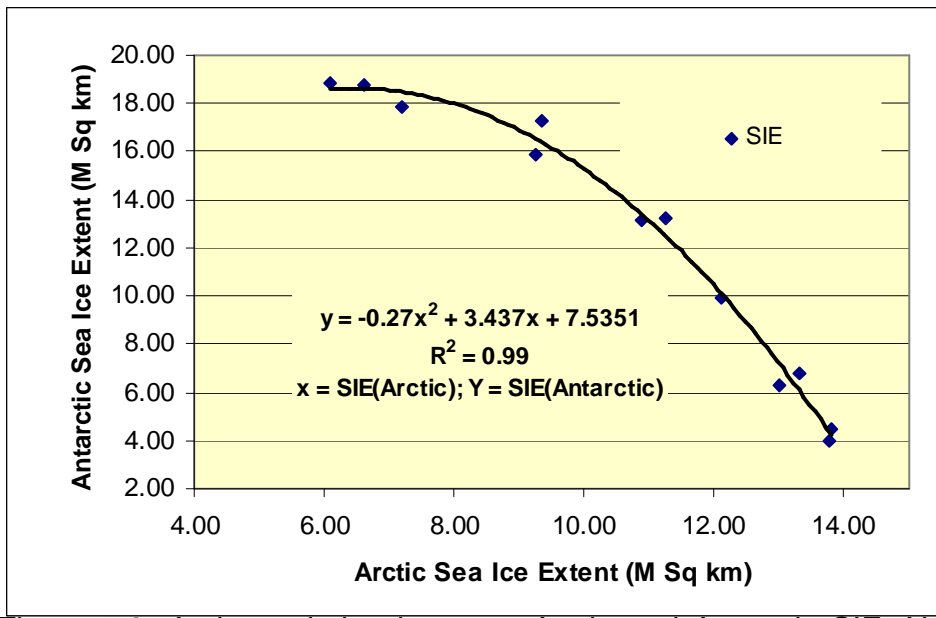


Figure 5.3: Anti-correlation between Arctic and Antarctic SIE. Note that the relationship is non-linear.

5.4 Trends of annual average sea ice extents

The 12-month running average SIE from 2001 to 2008 is shown in figure 5.4.

The total of both the hemispheres is also shown in the figure. It is seen that as observed in the September minimum (figure 3.2), decreasing trend is also visible for the Arctic 12-month running average SIE data. However, the weak increasing trend observed in the Antarctic has a distinct pattern of increase and decrease of SIE at time interval of three to four years.

The drastic increase of annual average SIE from 2007 to 2008 in both the hemispheres is an interesting observation. The 12-month running average Arctic SIE in 2007 is the lowest observed during the study period. The month-by-month interpretation of events was given in Zhang et al. (2008). They show that there was increased ice mass advection from the Pacific sector to the Atlantic sector of the Arctic Ocean and into the Greenland Sea, caused primarily by anomalous winds in July, August and September. This increase in

advection loss increased the open-water area and set the stage for increased absorption of solar flux and consequently increased melt of ice volume.

This increase in the advection of ice from the Pacific sector to the Atlantic sector may be amplified by two dynamic feedbacks (i) thinner (and hence weaker) ice is more easily compacted (Maslanik et al., 2007) and (ii) thinner ice responds more readily to wind forcing that resulted in higher ice drift speeds (Rampal et al., 2007). The thinner ice is more easily compacted and is flushed out of the basin more quickly. In addition, winds favorable for sequestering multi-year ice within the basin have been rare since 1980s (Lindsay et al., 2009).

The year 2006 is the second minimum and 2005 is the third minimum. However, as seen in the figure, SIE in 2008 is higher than that observed in 2005. This means that the decrease observed in three years has recovered in one year. This is an important observation in the present climate change scenario.

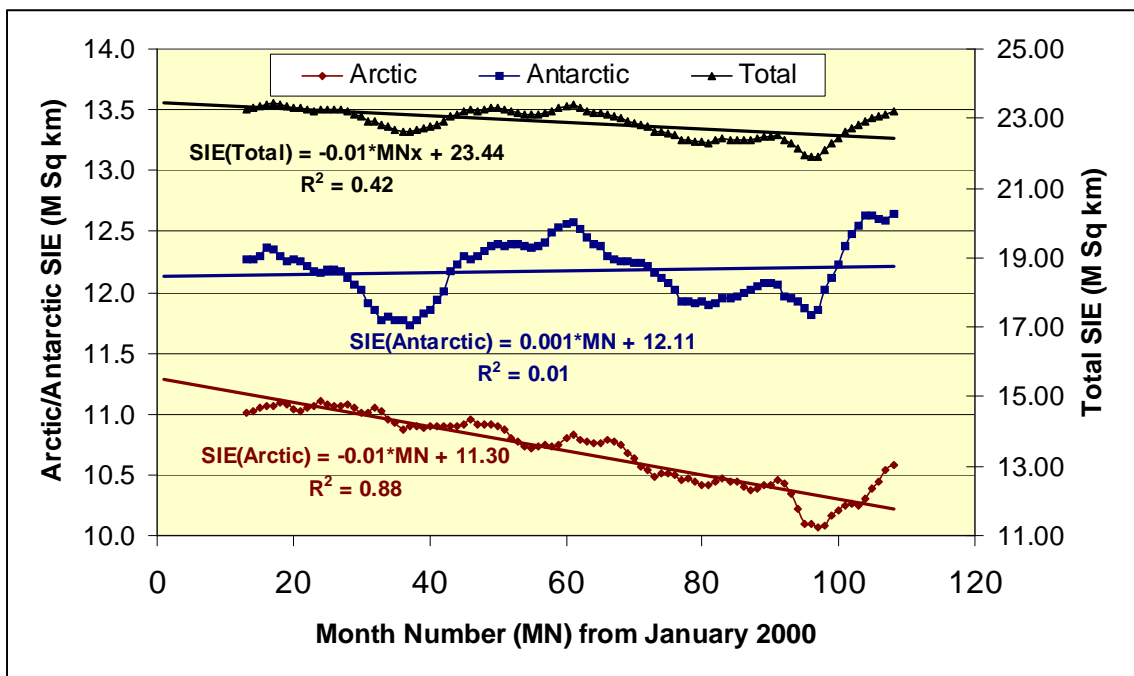


Figure 5.4: 12-month running average sea ice extent. Note that the slope of the curve for the Antarctic is an order of magnitude smaller compared to the Arctic, although the signs are opposite.

CHAPTER-6

6.0 SUMMARY OF FINDINGS AND FUTURE SCOPE

6.1 Important findings

The present report describes the important findings from the decadal analysis of sea ice extent carried out using QuikSCAT 0.2° resolution data (1999-2008). The important findings are summarized below.

- i. It has been observed that the recent decline in summer sea ice extent in the Arctic is of the order of 2.54% (0.16 M Sq km) per year with reference to the average summer sea ice extent between 1999 to 2008. For the same period the decline as per Passive Microwave Radiometer (PMR) based NSIDC data is of the order of 3.52 % (0.20 M Sq km) per year. However, in the Antarctic, increasing and decreasing behavior is observed at an interval of 3 to 4 years, with an overall statistically insignificant marginal positive trend. The lower sea ice extent obtained from PMR sensors can be explained as discussed below in point number (ii).
- ii. Scatterometer is expected to give more accurate sea ice extent information in the marginal sea ice zone as compared to passive microwave radiometers due to its higher sensitivity to sea surface roughness, which is caused by the melting of ice-floes at the sea ice-water interface. Also the sensitivity of passive sensors is low in such regions due to very low concentration of sea ice.

- iii. A drastic increase of 12-months running average SIE from 2007 to 2008 can be noticed in both the hemispheres. It is an interesting observation. Due to this phenomenon the total of both the hemispheres is also showing a drastic increase in 2008 from the all time low of 2007. This is in contrast to the gradual reduction of sea ice cover with small fluctuations in the previous years.
- iv. It is observed that the year-to-year variations are higher during the summer period as compared to the winter period in both the hemispheres. In case of the Arctic, it is the re-freezing process which is highly variable from year to year in the months of October and November. However, in the case of Antarctic it is not the freezing but the melting process, which is highly variable and takes place from December to January.
- v. The rate of the melting and the freezing processes in the two hemispheres are also opposite to each other. The melting process in the Arctic takes seven months whereas refreezing is faster, and takes only 5 months. In the Antarctic, melting of sea ice is taking much smaller time (5-months) as compared to refreezing (7-months). The reason for this could be the difference between the geography of the two regions. The Arctic is encompassed by land masses with narrow openings to open oceans, whereas the Antarctic is surrounded by the circumpolar ocean on the outer side and continental land mass on inner side.

- vi. The average monthly SIE, at decadal scale, is showing high anti-correlation between the two polar regions as expected due to the out of phase relationship between the solar insolation received by the two.
- vii. The grid level analysis brought out that in the Arctic, a significant negative trend up to 15% per year is observed in the Chukchi and East Siberian seas in the summer minimum extent of sea ice cover. However, a negative trend in the winter-maximum is observed in Barents Sea, which is a distinct pattern. The positive trend in the Bering Sea and a negative trend in Okhotsk Sea are also visible in the winter-maximum image. In contrast to the dominant negative trend in the Arctic, a mix of positive and negative trends is visible in different regions of the Antarctic during the southern summer.
- viii. A weak negative trend is visible during the months of May and June in the Arctic. However, positive trend in the months of February and September is a distinct pattern. In case of the Antarctic, a statistically significant positive trend during January to April (end of summer to the beginning of the winter) is an interesting outcome of the present analysis.
- ix. An interesting observation (from space) is the recent (2008-2009) increase in SIE over both the hemispheres. The decrease observed in previous 3 years has recovered in a single year. This emphasizes the need of close monitoring of the hemispheric sea ice extent in the future years.

6.2 Future Scope of work:

Till early 1980's, the Arctic sea-ice cover was considered to be static. However, it is now no longer valid so, as found by the satellite observations available since 1978. The decrease in the Arctic summer ice cover, particularly evident in the western Arctic, is a strong indication of changing climate conditions. Over the past several decades, numerous studies have documented decreasing trends in sea-ice characteristics such as the ice extent, area, age, and thickness (e.g., Belchansky et al., 2004; Comiso, 2002; Meier, 2005; Rigor and Wallace, 2004; Stroeve et al., 2005).

The present atlas also shows significant changes in sea ice cover in various parts of the Arctic and the Antarctic observed in the recent decade (1999-2009), that confirm the continuation of the previous trend of sea ice decline till 2007. The large export of freshwater and sea ice during summer could increase the salinity of the upper ocean and lead to development of the mixed layer suppression of sea-ice growth during the subsequent winter (Inoue and Kikuchi, 2007). Although the exact mechanisms responsible for this sea ice decline are not fully understood, recent evidence suggests that combinations of oceanic and atmospheric conditions are driving the observed changes (e.g., Maslanik et al., 2007; Shimada et al., 2006). The anomalies in the sea ice seasonality, concentration and thickness distribution have again implications on oceanic and atmospheric circulation, and their role, as a climate change indicator which need to be pursued further.

Indian Space Research Organisation (ISRO) is having a long term plan for monitoring the climate through its satellite missions. The Oceansat-2 satellite launch by ISRO in September 2009 carries a Ku-band scatterometer

OSCAT with specifications almost similar to that of QuikSCAT. The changes that concern the applications are mainly (i) daily composite σ_0 product resolution of 50 km as against 25 km of QuikSCAT and (ii) incidence angles of H-pol. and V-pol. are respectively 49° and 58° , whereas the corresponding angles for the QuikSCAT were 46° and 54° .

The period of November 2009 to March 2010 is the summer melting period in the southern hemisphere. The sea ice cover observed by the OSCAT data during summer melting period in the Antarctic is shown in figure 6.1.

It shows the potential of OSCAT daily composite σ_0 product for sea ice application. For the comparison of the derived sea ice edge, it is overlaid on the OSCAT-2 Sigma-0 data, reconstructed at 25km enhanced resolution in polar stereographic projection system. In the figure 6.1, Red-Green-Blue image planes represent H-, V-, V-Sigma-0 data. The significant decay of sea ice cover from November to January due to melting, which is a typical pattern of the Antarctic, is clearly visible. It is also observed that the difference from the climatic maximum (1979-2002) sea ice extent is higher on the western side of the Antarctic as compared to that observed on the eastern side.

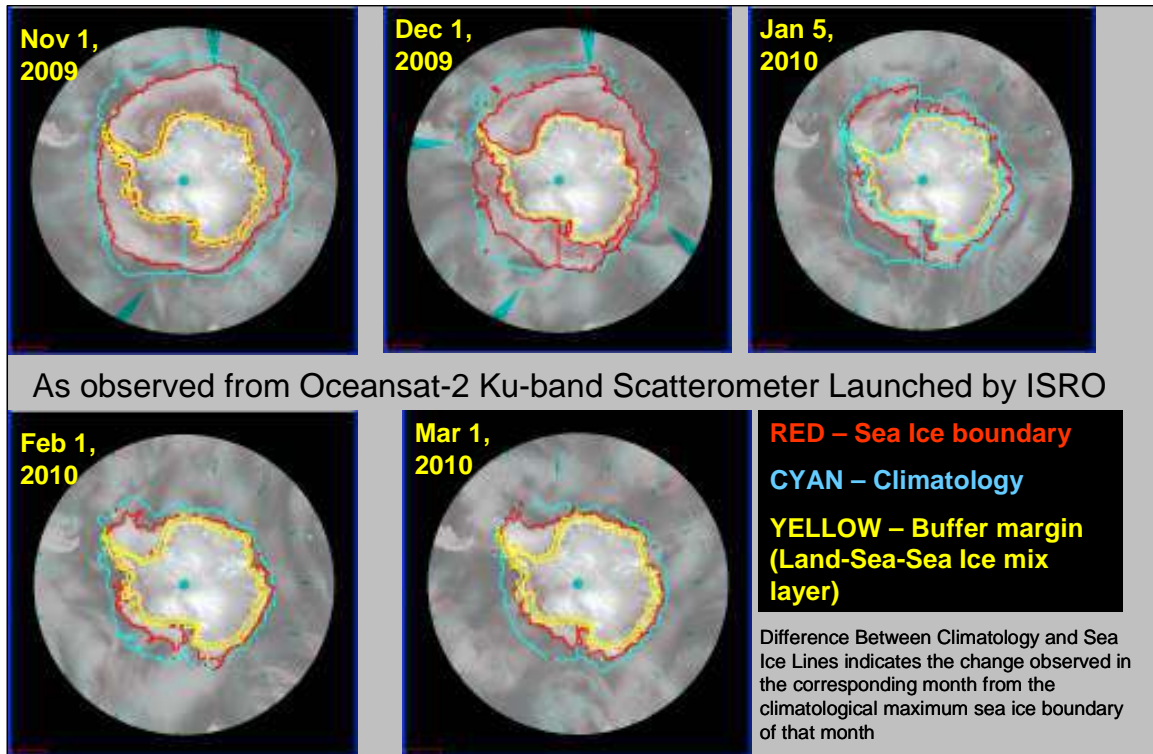


Figure 6.1: The sea ice decay observed from OCEANSAT-2 OSCAT in the Antarctic from November to March due to summer melting of sea ice cover

Availability of additional data from forthcoming SARAL-Altika altimeter (Ku-band) and RISAT-SAR (C-band) active microwave sensors along with available passive microwave radiometers is expected to play a significant role in providing the useful information on sea ice parameters that significantly influence the climate.

REFERENCES

- Belchansky, G. I., Douglas, D. C. and Platonov, N. G., 2004. Duration of the arctic sea ice melt season: Regional and Interannual Variability 1979– 2001. *Journal of Climate*, 17:67–80.
- Bhandari, S. M. and Khare, N., 2009. Investigations of the seasonality oscillating sea-ice edge over the Southern Ocean based on Oceansat-1 MSMR and QuikSCAT observations. *Indian Journal of Geoscience*, 63:221-228.
- Bhandari, S. M., Dash, M. K., Vyas, N. K., Khare, N. And Pandey, P. C., 2002. Microwave remote sensing of sea ice in the Antarctic region from Oceansat-1 MSMR, in Advances in marine and polar science, Eds. D. Sahoo and P. C. Pandey, A. P. H. Publishing Corporation, New Delhi, India.
- Bhandari, S. M., Vyas, N. K., Dash, M., Khanolkar, A., Sharma, N., Khare, N. and Pandey, P. C., 2005. Simultaneous MSMR and SSM/I observations and analysis of sea-ice characteristics over the Antarctic region. *Int. J. Remote Sens.*, 26:3123-3136.
- Bhandari, S. M., Vyas, N. K., Dash, M., Sharma, N. and Khare, N., 2006. A novel QuikSCAT dual-polarization sigma-zero based algorithm for delineation of sea ice and ice-edge over the Southern Ocean. SCAR – Open Science Conference, July 12-14, 2006, Hobart, Australia.
- Bhattacharya, B. B., and Majumdar, T. J., 1987, Bedrock elevation studies in Queen Maud Land, Antarctica: Technical Publication No. 4. Scientific Report: Fourth Indian Scientific Expedition to Antarctica. Department of Ocean Development, Govt. of India, New Delhi, 1987, pp. 35-41.
- Bhattacharya, S., Majumdar, T. J., and Bhattacharya, A. K., 2006, Generation of DEMs over parts of Antarctica using SEASAT altimeter data and their probable implications in studying ice sheet/glacier movements. *Geocarto International*, V. 21, No. 1, pp. 27-32.
- Campbell, W. J., 1973. NASA remote sensing of sea ice AIDJEX, Proceedings of the World Meteorological Organization Technical Conference, Tokyo, Japan, WMO No. 350, 55–56.
- Cavalieri, D. J., Crawford, J. P., Drinkwater, M. R., Eppler, D. T., Farmer, L. D., Jentz, R. R. and Wackerman, C. C., 1991. Aircraft active and passive microwave validations of sea ice concentrations from the DMSPSSM/I. *J. Geophys. Res.*, 96:21 989–22 008.
- Cavalieri, D. J., Gloersen, P. and Campbell, W. J., 1984. Determination of sea-ice parameters with the NIMBUS-7 SMMR, *J. Geophys. Res.*, 89, 5355–5369.
- Comiso, J. C., 2002. A rapidly declining perennial sea ice cover in the Arctic. *Geophysical Research Letters*, 29, 1956. doi:10.1029/2002GL015650
- Curry, J. A., Schramm, J. L. and Ebert, E. E., 1995. Sea ice-albedo climate feedback mechanism. *Journal of Climate*, 8:240-247.

- Dash, M. K., Bhandari, S. M., Vyas, N. K., Khare, N., Mitra, A. And Pandey, P. C., 2001. Oceansat- MSMR imaging of the Antarctic and the Southern Polar Ocean, *Int. J. Rem., Sensing*, 22:3253-3259.
- Draper, D. W. and Long, D. G., 2004. Evaluating the effect of rain on SeaWinds scatterometer measurements. *J. Geophys. Res.*, 109, C02005, doi:10.1029/2002JC001741.
- Early, D. S. and Long, D. G., 1997. Azimuthal modulation of C-band scatterometer σO over southern ocean sea ice. *IEEE Trans. Geosci. Remote Sensing*, 35:1201-1209.
- Eicken, H. and Lemke, P., 2001. The response of polar sea ice to climate variability and change. In: Lozan et al., Climate of the 21st century: Changes and risks. GEO, Hamburg/Germany, pp. 206-211.
- Gohil, B. S, Sarkar, Abhijit and Agarwal, V. K., 2008. A New Algorithm for Wind-Vector Retrieval From Scatterometers, *IEEE Geoscience and Remote Sensing Letters*, 5:387-391.
- Gohil, B. S, Sharma, P., Sikhakolli, R. and Sarkar, Abhijit, 2010. Directional Stability and Conservation of Scattering (DiSCS)-Based Directional-Ambiguity Removal Algorithm for Improving Wind Fields From Scatterometer: A QuikSCAT Example. *IEEE Geoscience and Remote Sensing Letters*, 7:592-595.
- Gohil, B. S. and Pandey P. C., 1985. An algorithm for retrieval of oceanic wind vectors from the simulated SASS normalized RADAR cross-section measurements. *Journal of Geophysical Research*, 90 (C4):7307-7311.
- Gohil, B. S., 1992. Extraction of ocean surface wind field from simulated ERS-1 scatterometer data. *Int. J. Remote Sensing*, 13:3311-3327.
- Haarpaintner, J., Tonboe, R. T. and Long, D. G., 2004. Automatic Detection and Validity of the Sea-Ice Edge: An application of Enhanced-Resolution QuikSCAT/ Sea Winds Data. *IEEE Trans. Geosci. and Rem. Sensing*, 42:1433-1443.
- Hallikainen, M. and Winebrenner, D. P., 1992. The physical basis for sea ice remote sensing. Chapter 3. pages 29-46 in *Microwave Remote Sensing of Sea Ice*, Ed. F. Carsey. AGU Geophysical Monograph, American Geophysical Union, Washington, D. C.
- Inoue, J. and Kikuchi, T., 2007. Outflow of summertime Arctic sea ice observed by ice drifting buoys and its linkage with ice reduction and atmospheric circulation patterns. *Journal of the Meteorological Society of Japan*, 85:881-887.
- Jones, W. L., Schroeder, L. C., Boggs, D. H., Bracalente, M., Brown, R. A., Dome, G. J., Pierson, J. and Wentz, F. J., 1982. The Seasat-A satellite scatterometer: The geophysical evaluation of remotely sensed wind vectors over the ocean. *Journal of Geophysical Research*, 87: 3297-3317.
- Jones, W. L., Wentz, F. J. and Schroeder, L. C., 1978. Algorithm for inferring wind stress from SEASAT-A. *J. Spacecraft and Rockets*, 15:368-374.

- Kumar, V., 2005. Study of polar cryosphere using remote sensing data and GIS. M.Tech. Thesis, Department of Remote Sensing, Birla Institute of Technology, Mesra, Ranchi, India.
- Laxon, S. W., Peacock, N. and Smith, D., 2003. High Inter-Annual Variability of Sea Ice Thickness in the Arctic Region. *Nature*, 425:947–950.
- Lindsay, R. W., Zhang J., Schweigner, A., Steele, M. And Stern H., 2009. *Journal of Climate*, doi: 10.1175/2008JCLI2521.1.
- Long, D. G., 2000. A QuikSCAT/SeaWinds Sigma-0 Browse Product, Version 2.0, Brigham Young University, Provo, UT.
- Long, D. G., Drinkwater, M. R., Holt, B., Saatchi, S. and Betoria, C., 2001. Global Ice and Land Climate Studies Using Scatterometer Image Data. *EOS, Transaction of the Americal Geophysical Union*, 82: 503.
- Majumdar, T. J., and Mohanty, K. K., 2000, Detection of areal snow cover changes over Antarctica using SSM/I passive microwave data. *Current Science*, V. 79, No. 5, 10 Sept. 2000, pp. 648-651.
- Manjul, S. S., Narayananbabu, P. and Samudraiah, D. R., 2010. Design and development of field radiometers for ground truth data collection at Antarctica. *Journal of Indian Society of Remote Sensing*, 38:193-202.
- Maslanik, J. A., Drobot, S. D., Fowler, C., Emery, W. and Barry, R., 2007. On the Arctic Climate Paradox and the Continuing Role of Atmospheric Circulation in Affecting Sea Ice Conditions. *Geophysical Research Letters*, 44, L03711. doi:10.1029/2006GL028269.
- Maslanik, J. A., Fowler, C., Stroeve, J., Drobot, S., Zwally, J., Yi, D. and Emery, W., 2007. A younger, thinner Arctic ice cover: Increased potential for rapid, extensive sea ice loss. *Geophysical Research Letter*, 34, L24501, doi:10.1029/2007GL032043.
- Meier, W. N., 2005. Comparison of Passive Microwave Ice Concentration Algorithm Retrievals With AVHRR Imagery in Arctic Peripheral Seas, *IEEE Transactions on geoscience and remote sensing*, 43:1324:1337.
- Oza S. R., Singh, R. K. K., Vyas, N. K. and Sarkar, Abhijit, 2010.. Recent trends of arctic and antarctic summer sea-ice cover observed from space-borne scatterometer. *Journal of Indian Society of Remote Sensing*. 38:611-616.
- Oza S. R., Singh, R. K. K., Vyas, N. K. and Sarkar, Abhijit, 2011a. Spatio-temporal analysis of melting onset dates of sea-ice in the Arctic. *Indian Journal of Marine Sciences*, 40:497-501.
- Oza, S. R., Singh, R. K. K, Vyas, N. K. and Sarkar, Abhijit, 2011b. Study of inter-annual variations in surface melting over Amery Ice Shelf, East Antarctica using space-borne scatterometer data. *Journal: Journal of Earth System Science*, 120:329-336.
- Oza, S. R., Singh, R. K. K., Vyas, N. K., Gohil, B. S. and Sarkar, Abhijit, 2011c. Spatio-temporal coherence based technique for near-real time sea-ice identification from

- scatterometer data. Submitted to the Journal of Indian Society of Remote Sensing. 39:147-152.
- Pandey, P. C., 1987. Measurements of global oceanic winds from Seasat SMMR and its comparison with Seasat SASS and ALT derived winds. IEEE Trans. On Geosci. And Remote Sensing, 25:670-676.
- Rampal, P., Weiss, J., and Marsan, D., 2007. Evidence for significant acceleration of arctic sea ice drift over 25 years. Eos, Trans. Amer. Geophys. Union, 88 (Fall Meeting Suppl.), Abstract C11B-0438.
- Rees, W. G., 2006. Remote Sensing of Snow and Ice. CRC Press, Taylor & Francis Group, New York, p. 16.
- Remund, Q. P. and Long, D. G., 1999. Sea ice extent mapping using Ku band scatterometer data. J. Geophys. Res. 104:11515-11527.
- Rigor, I. G. and Wallace, J. M., 2004. Variations in the age of arctic sea ice and summer ice extent. Geophysical Research Letters, 31: L09401. DOI:10.1029/2004GL019492.
- Sarkar, Abhijit and Kumar, R., 1985. A study on the sensitivity of the radar scattering coefficient to oceanic winds. Proc. Indian Acad. Sci. (Earth Planet. Sci.), 94:249-259.
- Sarkar, Abhijit and Kumar, R., 1986. A new semi-empirical sea spectrum for estimating the scattering coefficient, Int. J. Rem. Sen., 7:1369-1375.
- Sarkar, Abhijit, 2003. Space based techniques for remote sensing of oceanic winds: A review. MAUSAM, 54:111-120.
- Sehra, P.M., 1976a. Atmospheric circulation: Exploration over Antarctica and seasonal variations. Geophys. Res. Lett., 3: 669-672.
- Sehra, P.M., 1976b. Antarctic Atmosphere: Temperature Exploration and Seasonal Variations. Journal of Geophysical Res., 81: 3715-3718.
- Sharma, N., Dash, M. K., Pandey, P. C. and Vyas, N. K., 2009. Hemispheric sea ice extent dynamics as observed from MSMR. MAUSAM, 60:295-308.
- Shimada, K., Kamoshida, T., Itoh, M., Nishino, S., Carmack, E., McLaughlin, F., et al., 2006. Pacific Ocean inflow: Influence on catastrophic reduction of sea ice cover in the Arctic Ocean. Geophysical Research Letters, 33, L08605. doi:10.1029/2005GL025624
- Singh, R. K. K., Oza, S. R., Vyas, N. K., and Sarkar, Abhijit (2011). Estimation of Thin Ice Thickness from the Advanced Microwave Scanning Radiometer-EOS (AMSR-E) for a Coastal Polynya in the Chukchi and Beaufort Seas. IEEE Transactions on Geoscience and Remote Sensing (Accepted).
- Smirnov, A. V. and Zavorotny, V. U., 1995. Study of polarization differences in Ku-band ocean radar imagery," J. Phys. Oceanog., 25:2215–2228.
- Smith, D. M., 1996. Extraction of winter total sea-ice concentration in the Greenland and Barents Seas from SSM/I data. Int. J. Remote Sens., 17:2625-2646.

- Spreen, G., Kaleschke, L. and Heygster, G., 2007. Sea Ice Remote Sensing AMSR-E 89 GHz Channels, *J. of Geophys. Res.*, doi:10.1029/2007.
- Sreenivasan, G., and Majumdar, T. J., 2006, Mapping of Antarctic sea ice in the depletion phase : an indicator of climatic change? *Current Science*, V. 19, No. 6, 25th March, 2006, pp. 851-857 (Cover Page Publication).
- Stoffelen, A. and Portabella, M. 2006. On Bayesian scatterometer wind inversion, *IEEE Trans. Geosci. Remote Sens.*, vol. 44, no. 6, pp. 1523–1533, Jun. 2006.
- Stroeve, J. C., Serreze, M. C., Fetterer, F., Arbetter, T., Meier, W., Maslanik, J. and Knowles, K., 2005. Tracking the Arctic's shrinking ice cover: Another extreme September minimum in 2004. *Geophysical Research Letters*, 32, L04501, doi:10.1029/2004GL021810.
- Tedesco, M., Serreze, M. and Fettweis, X., 2008. Diagnosing the extreme surface melt event over southwestern Greenland in 2007. *The Cryosphere*, 2, pp.159–166.
- Thomas D. N. and Dieckmann, G. S., 1995. *Sea Ice, An Introduction to its Physics, Chemistry, Biology and Geology*. Blackwell Science Ltd., Oxford, UK.
- Tucker, W. B., Perovich, D. K., Gow, A. J. and Weeks, W. F., 1992. Physical properties of sea ice relevant to remote sensing, in *Microwave Remote Sensing of Sea Ice*, Ed. F. Carsey, American Geophysical Union, Washington, DC.
- Turner, J., Overland, J. E. and Walsh, J. E., 2007. An Arctic and Antarctic perspective on recent climate change. *Int. J. Climatology*, 27:277-293.
- Ulaby, F. T., Moore, R. K. and Fung, A. K., 1986a. Radar remote sensing and surface scattering and emmision theory, . *Microwave Remote Sensing Active and Passive*, Vol II, Artech House, Norwood.
- Ulaby, F. T., Moore, R. K. and Fung, A. K., 1986b. From theory to applications, *Microwave Remote Sensing Active and Passive*, Vol III, Artech House, Norwood.
- Vyas N. K., Bhandari, S. M., Dash, M. K., Pandey, P. C., Khare, N., Khanolkar, A. and Sharma, N., 2004. An Atlas of Antarctic Sea Ice from OCEANSAT-1 MSMRSAC-NCAOR-01-2004, National Centre for Antarctic and Ocean Research (DOD), Goa, India.
- Vyas, N. K. and Dash, M. K., 2000. Oceansat-MSMR observes interesting features on the frozen continent and surrounding sea. *Journal of Indian Society of Remote Sensing*, 28: 67.
- Vyas, N. K., Dash, M. K., Bhandari, S. M., Khare, N., Mitra, A. And Pandey, P. C. 2001. Large scale Antarctic features captured by Multi-Frequency Scanning Microwave Radiometer onboard Oceansat-1. *Current Science*, 80:1319-1322.
- Vyas, N. K., Dash, M. K., Bhandari, S. M., Khare, N., Mitra, A. and Pandey, P. C., 2003. On the secular trend in sea ice extent over the Antarctic region based on Oceansat-1 MSMR observations, *Int. J. Rem. Sensing*, 24:2277-2287.

- Wu, C., Graf, J., Freilich, M., Long D. G., Spencer, M., Tsai, W., Lisman, D. and Winn, C., 1994. The SeaWinds scatterometer instrument. International Geoscience and Remote Sensing Symposium, Pasadena, CA, 1994 Aug 8-12.
- Young, N. W. and Hyland, G., 1998. Directional anisotropy of C- and Ku-band MW backscatter from the East Antarctic snow cover: Differences and Similarities. ESA SP-424 : Workshop Proceedings, ESA Publications Division, Nov. 1998.
- Yueh, S. H., Kwok, R., Lou, S. and Tsai W., 1997. Sea ice identification using dual polarized Ku-band scatterometer data. IEEE transaction on Geoscience and Remote Sensing, 35:560-569.
- Zhang, J., Lindsay, R., Steele, M. and Schweiger, A., 2008. What drove the dramatic retreat of Arctic sea ice during summer 2007? Geophysical Research Letter, 35, L11505, doi:10.1029/2008GL034005.

ANNEXTURE-1 ACRONYMS

ADEOS	Advanced Earth Observing Satellite of NASA
AMI	Active Microwave Instrument Onboard ERS-1/2
AMSR-E	Advanced Microwave Scanning Radiometer for EOS
AOSG	Atmospheric and Oceanic Group of EPSA/SAC
APR	Active Polarization Ration
APR _o	Upper Threshold value of APR for sea ice identification
CV	Coefficient of Variation
DMSP	Defense Meteorological Satellite Program of NASA
EOS	Earth Observing System program of NASA
EPSA	Earth, Ocean, Atmosphere, Planetary Sciences and Applications Area of SAC/ISRO
ERS	European Remote Sensing Satellite
FBV	Fractional Brine Volume
FY ice	First Year sea ice
ISRO	Indian Space Research Organisation (India)
MSMR	Multi-frequency Scanning Microwave Radiometer
MY ice	Multi-Year sea ice
NASA	National Aeronautics and Space Administration (USA)
NCAOR	National Centre of Antarctic and Oceanic Research (India)
NSCAT	NASA Scatterometer onboard ADEOS
NSIDC	National Snow and Ice Data Centre
OSCAT	Ku-band scatterometer onboard ISRO's Oceansat-2
OSD	Oceanic Sciences Division of AOSG/EPSA/SAC
PMR	Passive Microwave Radiometer
QuikSCAT	SeaWinds Ku-band scatterometer on board NASA's QuikSCAT
SAC	Space Application Centre of ISRO
SAR	Synthetic Aperture RADAR
SASS	SEASAT-A Scatterometer System
SD	Standard Deviation
SIA	Sea Ice Area
SIE	Sea Ice Extent
SIF	Sea Ice Fraction
SSM/I	Special Sensor Microwave Imager onboard DMSP
STD	Spatio-Temporal Detection technique for sea ice identification

ANNEXURE-2 : SEA ICE GLOSSARY

ABLATION: Disintegration of an ice sheet or glacier through the processes of melting, evaporation or breaking into icebergs; has a meaning opposite to that of accumulation.

ABLATION ZONE: Region of glacier where more ice is lost through melting or evaporation than gained through snowfall.

ACCUMULATION: Addition of ice to glaciers through snowfall/rainfall and material brought in by winds and avalanches; has meaning opposite to that of ablation.

ACCUMULATION ZONE: Region of the glacier where there is net gain of ice through snowfall or rainfall. Generally, this region lies at high altitudes near the origin of the glacier.

ALBEDO: A quantity (non-dimensional as well as unit-less) describing the ability of a surface to reflect solar radiation; fractional value within 0 to 1. Perfect absorber has albedo of 0 while a perfect reflector has a value of 1.

ANTARCTIC CONVERGENCE: Also known as the Antarctic Polar Front, it is a permanent feature of circumpolar strip of sea around the southernmost point of the Atlantic, Indian and Pacific Oceans, extending between 48° and 61° S; sea surface temperature decreases by about 2-3° C around this belt.

ANTARCTIC CIRCUMPOLAR CURRENT: The only ocean current flowing around the globe; flows from west to east thereby, getting the name West Wind Drift.

ARCTIC OCEAN: Ocean in the North Polar region located north of the Arctic Circle (66.5° N), considered to be the smallest of the five major world oceans.

BACKSCATTERING COEFFICIENT: Also known as the normalized radar cross section, it gives the average reflectivity of ground cell per unit area

BLIZZARD: A cold storm having wind speed of more than 56 km/hr and temperature less than -6.7°C. The strong winds carries snow from the ground taking it around and the visibility becomes very poor.

BRIGHTNESS TEMPERATURE: Temperature of a blackbody, in thermal equilibrium with its surrounding that would be needed to radiate the same intensity of a gray body at a given wavelength.

BRINE: Water saturated with salt, as in seawater.

CRYOSPHERE: A word used to include all the frozen places of the earth where water is found in its solid phase. Sea ice, glaciers, ice caps, permafrost etc are included.

DOWNTWELLING: Sinking of surface water due to increased density; arises either due to change in temperature or increase in salinity. It brings oxygen rich waters from the surface to the bottom.

EMISSIVITY: Ability of a material to radiate energy; given by the ratio of energy radiated by a gray body to that of a black body at the same temperature.

FAST ICE: Sea ice fastened to the coast or ice front extending toward the sea; may be attached between grounded icebergs. It may be over 20 m in extent.

FIRN: An extremely hard, dense ice transitional between snow and glacial ice found underneath the snow.

FIRST YEAR ICE (FYI): Sea ice of not more than one winter's growth, having a thickness of 30 cm to 3 m.

FRAZIL ICE: Early in the formation of sea ice, needle-shaped crystals or fine spicules of ice suspending in seawater.

GALE: Strong wind having speed of 62 to 74 km/hr. They are common in Antarctica.

GLACIER: A slowly moving large mass of ice and snow; it moves from higher to lower ground and is the largest reservoir of freshwater on the earth. Friction plays a major role in determining its speed of flow.

GRAY ICE/GRAY-WHITE ICE: Young ice of thickness ~ 10-15 cm; less elastic than nilas breaking on swell. When gray ice becomes thicker (~ 15-30 cm) and lighter in colour, it becomes gray-white ice.

GREASE ICE: During the formation of sea ice after frazil ice is formed, coagulated form of a soupy layer on the surface; reflects little light giving the sea a matt appearance.

GROUNDING LINE: When a glacier flows into the sea it starts floating over the sea from some point onward and forms an ice-shelf thereafter. The edge formed by all such points is called the grounding line.

ICE CAP: Mass of ice covering less than 50,000 km² of land area.

ICE CRYSTALS: Small particles of ice growing on surfaces when the air gets supersaturated with water.

ICE FLOE: Sheet of sea ice floating in open seawater.

ICE SHEET: Mass of glacial ice covering more than 50,000 km² of land, bigger than ice shelves.

ICE SHELF: A thick, floating ice sheet extending from a glacier or an ice sheet toward the ocean (ice front); usually of great horizontal extent; thickness of 2-50 m above sea level.

ICE STREAM: A fast moving current of ice in an ice sheet or ice cap. They move faster than the surrounding; speed may be about 1 km/yr.

ICE TONGUE: A long, narrow, projection of ice flowing out from the coast; origin similar to that of ice shelf; generally formed where a valley glacier flows out in to a sea or a lake.

ICEBERG: A huge piece of ice of varying shapes more than 5 m above sea level which has broken away from a glacier; may be floating or grounded.

KATABATIC WINDS: Strong winds generated by down slope gravitational flow of high density air largely confined to the places where relatively steep slopes in orography are present.

LENSES AND PIPES: Refrozen melt structures within snowpack, generally, in percolation zones where melt water percolation occurs; exhibits intensive microwave backscattering; horizontal features are called lenses while the vertical ones are the pipes.

MICROWAVE BACKSCATTER: The amount of microwave energy that is directed backward to the microwave sensor from a distributed surface target having a roughness of the order of microwave wavelength.

MULTI YEAR ICE (MYI): Sea ice that has survived at least two summers' melts, having thickness of 2 m or more.

NEW ICE: A general type of sea ice; represents the earliest stages of the growth of sea ice.

NILAS: A weakly consolidated continuous layer of elastic sheet of thin ice, generally up to 10 cm thick; gives a matte appearance to the surface.

OKTA: A dimensionless unit in which the cloud-cover over the sky is expressed. It is always expressed as an integral value and not a fraction, each value representing one-eighth of the sky covered by clouds. 0 okta means completely clear sky while an overcast sky has 8 oktas.

PACK ICE: Frozen sea that formed somewhere else and has floated to its present position through wind, tides and currents.

PANCAKE ICE: In the formation of sea ice, circular discs of sea ice with raised rims formed from frazil ice due to the pieces striking one another; diameter of ~ 30 cm – 3 m with a thickness of about 20 cm.

POLARIZATION RATIO: Ratio between the vertical and the horizontal components (of brightness temperature) at a given frequency (channel). Or in terms of backscattering coefficients, the normalized difference between the polarizations.

POLYNYA: Non-linearly shaped opening of water enclosed in sea ice region; consists of thin ice up to a thickness of about 30 cm. If the opening is linear in shape, it is called a lead.

PRECIPITATION: Moisture falling from clouds to the surface of the Earth, e.g., rain, snow, hail, sleet etc. Even if the precipitation is in the solid form, it is always measured as water or rain

RADIOMETER: An instrument that measures the radiant flux of an electromagnetic radiation.

RAFTING: A process in which one piece of ice overriding another, generally occurring in new and young ice but is common in all ice thickness too.

RIDGING: Physical process of deforming sea ice into ridges.

SALINITY: Amount of salt dissolved in sea water. Seawater has an average salinity of 35 parts per thousand.

SCATTEROMETER: Microwave radar sensor used to measure the reflection or scattering effect produced while scanning the surface of the earth from an aircraft or a satellite.

SEA ICE AREA: A portion of a grid cell covered by sea ice, expressed in km².

SEA ICE CONCENTRATION: Relative amount of sea ice area actually covered by sea ice in total sea ice extent; generally, expressed in percentage.

SEA ICE EXTENT: A region / a grid cell in ocean area having ice concentration greater than a given threshold (typically, 15%); it is different from ice area: extent classifies a region as sea ice if a particular threshold of concentration is achieved in it, however, area gives how much of the region is covered by sea ice.

SEA ICE: Ice found at sea which has originated from the freezing of sea water below around -1.8°C.

SHUGA: An accumulation of spongy white ice lumps formed from grease ice or slush.

SLUSH: Saturated snow mixed with water on land or ice surfaces; viscous mass floating in water after snowfall.

SOUTHERN OCEAN: Ocean extending from the coast of Antarctica northward to 60°S (the Antarctic Convergence); affects the meteorological pattern of the entire globe.

THERMOHALINE CIRCULATION: Currents that are driven by density difference of water caused by differences in temperature and salinity.

UPWELLING: Rising of bottom/deeper waters to the surface. It brings nutrient rich waters to the surface.

YOUNG ICE: Type of sea ice less than one year old having thickness of about 10 to 30 centimeters.